Università degli Studi di Parma

Dipartimento di Chimica Organica ed Industriale

Ph.D. in Science and Technology of Innovative Materials
XX° Cycle

H-Bonding in Supramolecular Sensing and Ion-Channels Self-Assembly

Monica Melegari

Coordinator: **Prof. Manfredo Manfredi**

Supervisor: **Prof. Enrico Dalcanale**

Author: **Monica Melegari**

Contents

CHAPTER 3

Mixed bridged thio-phosphonate cavitands

CHAPTER 4

New techniques of cavitand layers deposition and their influence on the QCM sensing performances

CHAPTER 5

Rational design of water clusters with phosphonate cavitands

CHAPTER 6

Large and stable synthetic ion channels from lipophilic guanosine

General introduction: weak interactions and chemical sensors

1

1.1 Interactions involved in supramolecular chemistry

Supramolecular chemistry may be defined as “chemistry beyond the molecule”, bearing on the organized entities of higher complexity that result from the association of two or more chemical species held together by intermolecular forces. The possible interactions involved in this self-association are reported in Table 1.1.

Interaction	Energy range [kJ/mol]	Type of interaction
Covalent bond	120-800	Chemical reaction
Ion-Ion	100-400	Only between ions
Coordination, Complexation	8-200	Weak chemical interaction
Hydrogen-bond	5-180	Hydrogen bond A-H···B
Ion-dipole	10-20	Between ions and dipoles
Dipole-Dipole	1-5	Between polar molecules
London Forces \ Induced Dipole	0.1 - 2	Physical interaction

Table 1.1. Different types of interactions.

Non covalent forces plays an important role in supramolecular assembly and molecular recognition, and in regulating biochemical processes. Specificity and efficiency of the chemical processes are achieved by intricate combinations of weak intermolecular interactions of various sort.
In particular, in this work we draw the attention only to the supramolecular "aggregates" created by weak, non-covalent interactions, mainly H-bonding, CH-π and π-π interactions.

1.1.1 The H-bonding interactions

Hydrogen bonds play an important role in determining the three-dimensional structure of chemical and biological systems as a consequence of their specificity and directionality.
In the first edition of *The Nature of the Chemical Bond* written in 1939 Pauling reported for the first time the concept of hydrogen bonding as a major cohesive force between molecules containing hydroxyl and amino groups, with carbonyl and hydroxyl groups as the major hydrogen bond acceptors and donors respectively. In the following period 1939-1953, the crucial presence of hydrogen bonds in subunits of biological structures like amino acids, carbohydrates, pyrimidines and purines was investigated by the early crystal structure analyses. In particular, the 1953 was a fundamental year of the DNA double helix discovery by Watson and Crick, where it was realized that hydrogen bond is the most important intra and intermolecular cohesive force, determining geometry and mode of recognition and association of biological molecules.
The formation of one or multiple hydrogen bonds, especially in combination with other noncovalent forces, such as ionic or hydrophobic interactions, can lead to a dramatic change in the micro- and macroscopic properties of the resulting supramolecular assemblies.[1]
In contrast to covalent bonds, which once formed are stable under normal conditions and can only be broken by providing sufficient energy, the formation of hydrogen bonds is reversible and their strength depends on the chemical environment, such as the solvent or temperature. Through a variation of the external parameters, this reversibility allows for the direct control of those physical properties of supramolecular assemblies[2] which are determined by the hydrogen bonds. The main drawback of hydrogen bonds is their limited strength, because the more polar the solvent, the weaker are the hydrogen

bonds; the reason is the increasing competitive solvation of donor and acceptor sites by solvent molecules. Therefore, a single hydrogen bond possesses a considerable binding energy only in apolar, aprotic solvents . However, stable supramolecular assemblies can also be obtained in slightly polar solvents, such as chloroform or acetonitrile, by a combination of several such weak interactions in binding motifs with multiple hydrogen bonds.

Hydrogen bonding is generally considered with a geometry, D (donor)-H····A (acceptor). Some of the commonly used functions involve the modified Lennard- Jones potentials with D-H····A angle dependent term like:[3]

$$E_{H-bond}(R) = \varepsilon\left[A\left(\frac{R_0}{R}\right)^{12} - B\left(\frac{R_0}{R}\right)^{10}\right](\cos\theta_{D-H\cdots A})^4$$

where *R* is the distance between the D and A, R_0 is the equilibrium distance, ε is the depth of the potential and A and B are the adjustable parameters. The angular term ensures that the strength of the H-bonding interaction maximizes for linear D-H····A bonds.[4]

We know of hydrogen bonds that are so strong that they resemble covalent bonds in most of their properties, and we know of others that are so weak that they can hardly be distinguished from van der Waals interactions. Indeed, the phenomenon has continuous transition regions to such different effects as the covalent bond, the purely ionic, the cation-π, and the van der Waals interaction. The electrostatic dominance of the hydrogen bond is true only for some of the occurring configurations, whereas for others it is not. The H····A distance is not in all hydrogen bonds shorter than the sum of the van der Waals radii.

For an X-H group to be able to form hydrogen bonds, X does not need to be "very electronegative", it is only necessary that X-H is at least slightly polar. This requirement includes groups such as C-H, P-H, and some metal hydrides. X-H groups of reverse polarity, $X^{\delta+}$-$H^{\delta-}$, can form directional interactions that parallel hydrogen bonds. Also, the counterpart A does not need to be a particularly electronegative atom or an anion, but only has to supply a sterically accessible concentration of negative charge.

The energy range for dissociation of hydrogen bonds covers more than two factors of ten, about 0.2 to 40 kcal/mol, and the possible functions of a particular type of hydrogen bond depend on its location on this scale.

As we have seen, hydrogen bonds exist with a continuum of strengths. Nevertheless, it can be useful for practical reasons to introduce a classification, such as “weak”, “strong”, and possibly also “in between”. The system described by Jeffrey is followed,[5] who called hydrogen bonds *moderate* if they resemble those between water molecules or in carbohydrates (one could also call them “normal”), and are associated with energies in the range 4-15 kcal/mol. Hydrogen bonds with energies above and below this range are termed *strong* and *weak*, respectively. Some general properties of these categories are listed in Table 1.2.

	Strong	**Moderate**	**Weak**
Interaction type	strongly covalent	mostly electrostatic	electrostatic/ dispersive
Length of H···A [Å]	1.2-1.5	1.5-2.2	> 2.2
Length of X-H [Å]	0.08-0.25	0.02-0.08	< 0.02
X-H *versus* H···A	X-H ≈ H···A	X-H < H···A	X-H « H···A
X···A [Å]	2.2-2.5	2.5-3.2	> 3.2
directionality	strong	moderate	weak
Bond angles [°]	170-180	> 130	> 90
Bond energy [Kcal/mol]	15-40	4-15	< 4

Table 1.2. Hydrogen bonding categories following the classification of Jeffrey.

It must be stressed that there are no “natural” borderlines between these categories, and that there is no point in using this or any related system in too stringent a way.

1.1.2 The CH-π interactions

In the past few decades, evidence has gradually accumulated that forces weaker than the ordinary hydrogen-bonds, such as CH-O, CH-N, OH-π and NH-π interactions, are also important. Among these, the CH-π interaction has been found to play a central role in the fine tuning of organic-biochemical reactions and molecular recognition, influencing also biochemical processes.
Experimental methods included X-ray, NMR, IR, circular dichroism and dipole moment measurements indicated clearly that an extra attractive interaction, different from the traditional dispersion forces, is present between alkyl and phenyl groups. In general, attractive interactions are present between C-H groups and π-electron systems: a suggestion for the presence of such an interaction, called CH-π interactions, has come from studies on conformational problems of a series of compounds bearing an aliphatic group on one side of the molecule and a phenyl group at the other terminus.[6]
The CH-π interaction is characterized by a relatively large contribution from delocalization (charge transfer from π to σ^*) and dispersive interaction as compared to the normal H-bonding, while the electrostatic contribution has been shown to be unimportant. A relevant observation is that the CH-π interaction plays a role either in polar or in non-polar media, unlike in the typical hydrogen bond between a hard acid and a hard base, where the presence (or absence) of water changes completely the final effect. The enthalpy for CH-π bond has been estimated to be at most 9 kJ/mol for intermolecular interacting CH-donor/aromatic π-base systems by temperature dependence measurements of the NMR chemical shifts. Moreover, many CH groups can participate simultaneously and in a cooperative way, without considerable loss of entropy.

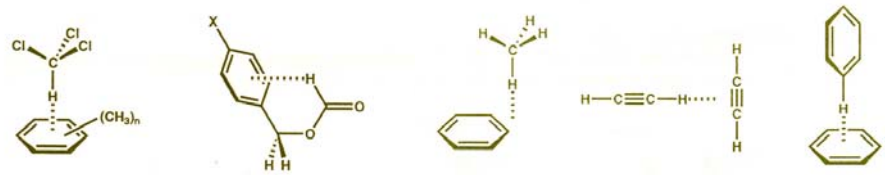

Figure 1.3. Examples of CH-π interactions.

The extent of CH-π interactions becomes greater if the π-electron density of the aromatic ring involved increases, and at the same time the hydrogens of the

guest molecule become more acidic (for example trimethyl ammonium chloride binds stronger than t-butyl alcohol).

1.1.3 The π-π interactions

Attractive interactions between π-systems have been known for over half a century. The π-π interactions are non-covalent interactions caused by intermolecular overlapping of p-orbital in π conjugated systems, so they become stronger as the number of π-electrons increases.[7]

The aromatic groups implicated in these interactions, behave in one of the several geometries, depending on the nature of the rings involved. Nevertheless, aromatic interactions are intriguing molecular recognition elements since they are expected to be strong in water (because the hydrophobic component of the interaction), and at the same time, should be selective if the electrostatic component is significant, thus providing the best features of both hydrophobic interactions and hydrogen bonding.

The electrostatic component has been proposed to arise from interactions of the quadrupole moments of the aromatic rings. Although benzene has no net dipole, it has an uneven distribution of charge, with greater electron-density on the face of the ring and reduced electron-density on the edge, which gives rise to the quadrupole moment.

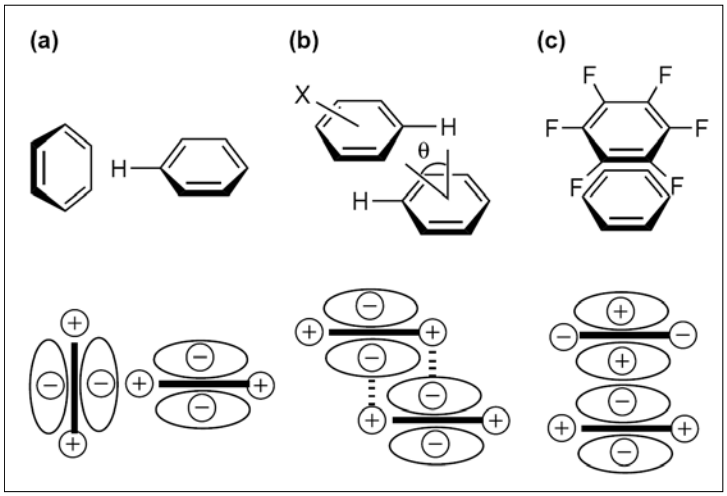

Figure 1.4. Geometries of π-aromatic interactions.

The edge-to-face geometry (Figure 1.4a), which can be considered a CH-π interaction, is found in benzene in the solid state, and is commonly observed between aromatic residues in proteins.[8] The offset stacked orientation (Figure 1.4b) is also commonly found in porphyrin,[7] in proteins and is the geometry of base stacking in DNA. In this geometry, more surface area is buried, and the van der Waals and hydrophobic interactions are increased. This orientation appears to be more common when the electron density on the face of one or both rings is reduced. A third possible geometry is the face-to-face stacked orientation (Figure 1.4c). This is commonly observed with donor-acceptor pairs and compounds that have opposite quadrupole moments, such that the interaction between the faces of the rings is attractive. The benzene-perfluorobenzene interaction is an excellent example of this type of aromatic interaction, and has been calculated to provide 15.5 kJ/mol in stability.[9]

1.2 Chemical sensors

"A chemical sensor is a device that transforms chemical informations, ranging from the concentration of a specific sample component to total composition analysis, into an analytically useful signal".[16]
Chemical sensing is part of an acquisition process in which some informations on the chemical composition of a system are obtained in real time. The acquisition process consist of two distinct steps: *recognition* and *amplification*. The *recognition* is supplied by a material capable of interacting with the desired analyte, while the *amplification* is provided by a transducer on which the material is deposited (Figure 1.5). The transducer is a device which transforms a chemical information in a readable signal.

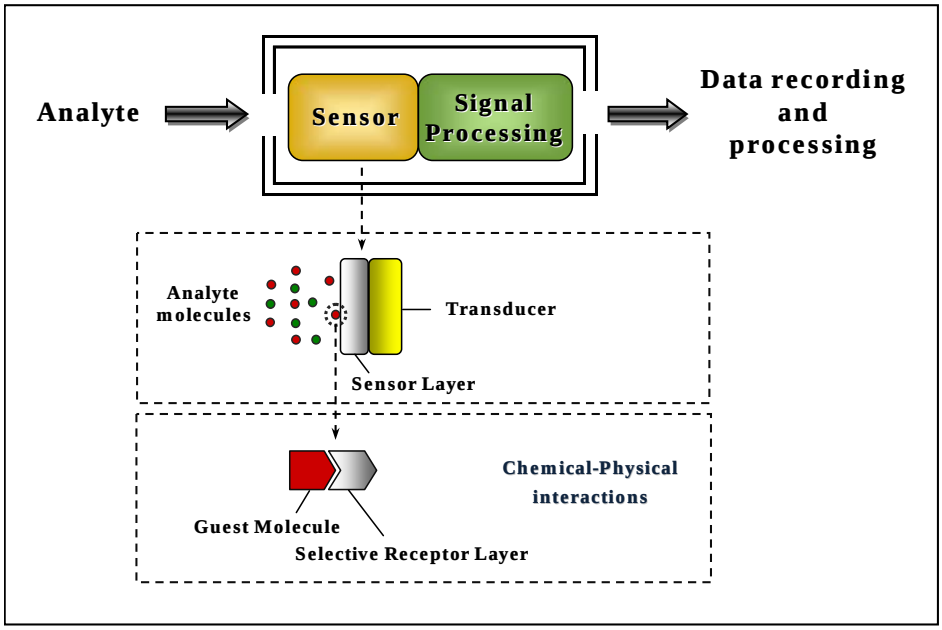

Figure 1.5. The chemical sensing process.

Sensors are typically characterised by three properties: *sensitivity*, *selectivity* and *reversibility*.
Sensitivity can be generally defined as the slope of the analytical calibration curve, that is correlated with the magnitude of the change in the sensor signal upon a certain change in the analyte concentration.[10] "Cross sensitivity" hence

refers to the contributions of other than the desired compound to the overall sensor response.

Selectivity is instead the ability of a sensor to respond primarily to only one chemical species in the presence of other species (usually denoted interferents).

The quest for better selectivity remains the cornerstone of the chemical sensing research:[11] it can be achieved by using biosensors (e.g. biologically derived selectivity by appropriate enzymes, structure-binding relationship in antibody-antigen complexes,) or by synthesizing materials containing specific binding sites.

Reversibility describes the sensor's ability to return to its initial state after it has been exposed to chemical species. The reversibility requires the involvement of weak interactions, since the formation of covalent or ionic bonds would result in an irreversible saturation of the layer.[12]

We want to highlight, that the primary interest in "real sensors" is a reversible behaviour. Rapid reversibility place constraints on desired interactions between chemical sensor coating materials and analytes: a limit of reversibility at room temperature can be considered up to an energy level of 20 kJ/mol.

An interaction mechanism in chemical sensing implies different types of chemical interactions, ranging from very weak physisorption (where only dispersion forces with aspecific or directional interactions are present) through rather strong chemisorption to charge transfer and chemical reaction.

On the other hand, chemical sensors using specific covalent bond formation between the analyte and sensor coating should be defined as dosimeter-type devices, because then they can not be regenerated for repetitive or continuous use.

Conventional approaches for selective chemical sensors have traditionally made using a "lock-and-key" design (a steric fit concept enunciated for the first time by Emil Fischer in 1894),[13] wherein a specific receptor is synthesized in order to bind selectively the analyte of interest.[14] Indeed, to achieve this specificity, biological systems exploit molecular recognition between two species that complement one another in size, shape and functionality. As for biological systems, the concepts of shape recognition and binding site complementarity are central for effective molecular recognition in artificial host-guest systems. This selectivity mechanism is particularly useful in the development of chemical sensors, whereas the recognition process can be translated into an analytical signal.

The negative facet of the lock and key approach, so successful in the liquid phase, is that can not be automatically transferred to vapour and gas sensing due to two major hurdles:

- in moving from the vapour to the condensed phase the analyte experiences a dramatic increase in aspecific dispersion interactions, negligible in liquid to solid transfer;[15]
- the entropic cost for binding to the receptor is not alleviated by solvent release in the bulk liquid phase.[16]

For these reasons achieving effective molecular recognition at the gas-solid interface is a demanding task, which requires a fresh approach, both in terms of receptor design and characterization tools.

1.2.1 Acoustic wave devices in supramolecular gas sensing

Acoustic wave (AW) transducers are the workhorse of supramolecular sensing of gases, because they do not require receptor derivatization for their operation modes, like fluorescent probes for optical sensing. They measure the mass uptake of a sensing layer when exposed to vapours. Usually AW sensors consist of a piezoelectric quartz crystal with electrodes affixed to each side of the plate. When an oscillating potential is applied at a frequency near the resonant frequency of the piezoelectric crystal, a stable oscillating circuit is formed. The key feature of AW sensors is that the frequency and the amplitude of the acoustic wave is affected by a mass change of the system. The Sauerbrey equation describes the resonant frequency shift of an acoustic resonator upon mass increase on its surface.[14]

$$\Delta f = -2 f_0^2 \cdot \Delta m \cdot A^{-1} \cdot \sqrt{c/\rho}$$

In the equation f_0 (Hz) is the fundamental frequency of the quartz crystal, Δf (Hz) is the frequency shift proportional to the deposited mass Δm (g), A (m^2) is the area of quartz plate or electrode surface, c (s^2m/g) is the elastic coefficient of the system and ρ (g/m^3) represents the crystal density.
The Sauerbrey Equation expresses in an adequate manner the real trend for a material in which the frequency shift induced by the coating deposition is lower than 3% of the quartz crystal fundamental frequency. Moreover, it does not

work for thick films, viscous liquid, elastic solids and viscoelastic bodies for which special theoretical models have to be applied to account for the observed frequency shift and impedance spectra.[17]

On the other hand, it implies the assumption that the deposited coating film has an uniform thickness across the entire active region of the resonator and that the frequency shift, resulting from a mass deposited at some radial distance from the centre of the crystal, will be the same regardless of the radial distance.

The more widely applied mass sensors based on this principle are quartz crystal microbalance (QCM) and surface acoustic wave (SAW) resonators (Figure 1.6). In the former one, the acoustic wave propagates through the bulk of the system in a direction normal to the surface. Therefore thickness and permeability of the layer are critical features. The higher the frequency of the resonator, the less coating most be applied to avoid a quenching of the oscillation: in this sense a resonant frequency of 30 MHz is usually the limit for a typical QCM resonator. The maximum layer thickness depends on the transducer design, the operating frequency of the device, the applied analyte concentrations and the coating nature. As a rule of thumb, the upper limit for the thickness, d, of viscoelastic acoustically thin films was given as $d << (G/f\upsilon\rho)$ where G is the shear modulus of the coating layer, υ is the SAW velocity (3.16 Km/s for quartz material), ρ is the film density and f is the fundamental oscillation frequency.[18]

The acoustic wave produces surface particle displacements that are parallel to the surface. In the SAW device, motion occurs only at the surface, penetrating to a depth of approximately one acoustic wavelength into the crystal; here the direction of propagation is parallel to the surface itself. The waves generated are Rayleigh waves. These have one particle displacement component that is normal to the surface, in contrast with QCM devices. Since in SAW resonators the acoustic energy is trapped near the surface, they are potentially much more sensitive than bulk wave devices. On the other hand the influence of small temperature fluctuations and mechanical stresses is higher, and therefore their handling and interpretation of experimental results is not as straightforward as the case of QCM. In polymer coatings for instance, all volume changes of the layer associated either to vapour sorption (swelling) or thermal expansion perturb the viscoelastic properties of the coating and this significantly contributes to the observed response.

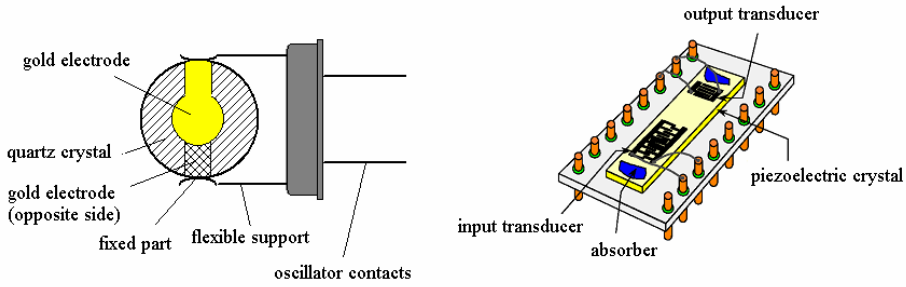

Figure 1.6. QCM (left) and SAW (right) transducers.

By integrating an AW measurement platform with a selective sensing layer, a chemical sensor is constructed, in which molecular recognition events are converted into an electric signal. An important feature of AW sensors is that mass transduction disregards the electronic properties of the sensing layer since the electric read-out does not rely on the conductivity of the organic material but only on the frequency shift of the piezoelectric crystal. This allows to overcome the limitation due to the restricted number of conductive organic materials, making it possible to exploit each molecule endowed with molecular recognition as sensing material.

Göpel and co-workers investigated arrays of QCM resonators with both polymer and non-polymer coating material in 1991,[19] noting an interesting correlation between ln$K$ and T_b/T.

$$\ln K_b \approx \frac{T_b}{T}$$

where K is the polymer-gas partition coefficient, T_b is the analyte's boiling point and T is the temperature at which response measurements are detected.

The presence of molecular recognition event, perturb this linear relationship, which is not any more satisfied.

The calculation of the partition coefficient can be derived from the definition of Gibbs free energy, considering that analyte sorption from gas into a polymeric phase split into two steps (model): condensation of analyte into liquid state and mixing of liquid with polymer.

$$\ln K = -\frac{\Delta H^o}{R}\left(\frac{1}{T}\right) + \frac{\Delta S^o}{R}$$

where R is the molar gas constant, T is the temperature, ΔH^o is the molar sorption enthalpy and ΔS^o is the molar sorption entropy. To clarify better the means of the term "sorption" it can be said that when a gas or vapor is brought into contact with a solid, part of it is taken up by the solid. The molecules that disappear from the gas either enter inside of the solid, or remain on the outside, attached to the surface. The sorption behaviour of an amorphous sorbent layer towards different analytes can be inferred using the linear sorption energy relationship equation (LSER).[20] According to this model and under the hypothesis of weak non-covalent interactions, the logarithm of the coefficient partition of a sorbent layer with respect to a given volatile species is the linear combination of five terms expressing the intensity of five basic interaction mechanisms: polarizability, dipolarity, H-bond acidity and basicity and the solubility term related to dispersion interactions. The relation can be written as follows:

$$\log K_p = c + r \cdot R_2 + s \cdot \pi_2^H + a \cdot \alpha_2^H + b \cdot \beta_2^H + l \cdot \log L^{16}$$

where K_p is the layer coefficient partition, c is a constant arises from the method of multiple linear regression, R_2 provides a quantitative indication of polarizable n and p electrons, π_2^H measure the ability of a molecule to stabilize a neighbouring charge or dipole, α_2^H and β_2^H measure effective hydrogen bond acidity-basicity, and $\log L^{16}$ is the liquid/gas partition coefficient of the solute on hexadecane at 298 K (determined by gas-liquid chromatography). Moreover the $\log L^{16}$ parameter is a combined measure of enthalpically favourable dispersion interactions (that increase $\log L^{16}$) and the enthapically unfavourable cost of creating a cavity in hexadecane (that decrease $\log L^{16}$). The coefficients r, s, a, b, and l are related to the properties of the absorbing material which are complementary to the vapour properties (thus characterize the solubility properties of the absorbing material). For molecular receptors the last term $\log L^{16}$ must be minimized or, even better, eliminated to fully exploit its complexation properties. In other words, one or more of the material coefficients relative to specific binding modes (r, s, a, b) must be maximized with respect to the l coefficient, expression of dispersion interactions.

To conclude, the facets involved in the chemical sensors performance are several, indeed thickness, morphology, permeability, mechanical and chemical aspects of the sensing material thin layer can influence both the interaction mechanism and sensor responses.

1.3. References

[1] a) G.M. Whitesides, J.P. Mathias, C.T. Seto, *Science* **1991**, *254*, 1312; b) N.B. Bowden, M. Weck, I.S. Choi, G.M. Whitesides, *Acc. Chem. Res.* **2001**, *34*, 231.

[2] a) F. Vögtle, *Supramolecular Chemistry,* Wiley, Chichester, **1991**; b) J.-M. Lehn, *Supramolecular Chemistry; Concept and Perspectives,* VCH, Weinheim, **1995**; c) J.W. Steed, J.L. Atwood, *Supramolecular Chemistry,* Wiley, Chichester, **2000**.

[3] F. Jensen, *Introduction to Computational Chemistry*, Wiley, Chichester, **1999**.

[4] T. Steiner, *Angew. Chem. Int. Ed. Engl.* **2002**, *41*, 48.

[5] G.A. Jeffrey, *An Introduction to Hydrogen Bonding*, Oxford University Press, Oxford, **1997**.

[6] M. Nishio, M. Hirota, Y. Umezawa, *The CH-π Interactions*, Wiley-VCH, New York, **1998**; M. Nishio, Y. Umezawa, M. Hirota, Y. Takeuchi, *Tetrahedron* **1995**, *51*, 8665.

[7] C.A. Hunter, K.R. Lawson, J. Perkins, C.J. Urch, *J. Chem. Soc., Perkin Trans. 2* **2001**, 651.

[8] E.A. Meyer, R.K. Castellano, F. Diedrich *Angew. Chem. Int. Ed. Engl.* **2003**, *42*, 1210.

[9] J. West, S. Mecozzi, D.A. Dougherty, *J. Phys. Org. Chem.* **1997**, *10*, 347.

[10] A. D'Amico, C. Di Natale, *IEEE Sensors Journal* **2001**, *1*, 183.

[11] J.Janata, M. Josowicz, *Anal. Chem.* **1998**, *70*, 179.

[12] A. Hierlemann, A. J. Ricco, K. Bodenhöfer, W. Göpel, *Anal. Chem.* **1999**, *71*, 3022.

[13] E. Fischer, *Ber. Dtsch. Chem. Ges.* **1894**, *27*, 2985.

[14] R. Elghanian, J.J. Storhoff, R.C. Mucic, R.L. Letsinger, C.A. Mirkin, *Science* **1997**, *277*, 1078.

[15] J.W. Grate and G.C. Frye, in *Sensors Update*, (eds. H. Baltes, W. Göpel and J. Hesse), WILEY-VCH, Weinheim, **1996**, Vol. 2, 37.

[16] J. Janata, in Principles of Chemical Sensors, Plenum press, New York, USA, **1989**.

[17] H.L. Bandey, S.J. Martin, R. Cernosek, *Anal. Chem.* **1999**, *71*, 2205.

[18] A. Ricco, *J. Electrochem. Soc.Interface* **1994**, *3*, 38.

[19] R. Lucklum, B. Henning, P. Hauptmann, K.D. Schierbaum, S. Vaihinger, W. Göpel, *Sens. Actuators A* **1991**, *25-27*, 705.

[20] R.W. McGill, M.H. Abraham, J.W. Grate, CHEMTECH, **1994**, 27.

Molecular recognition properties of tetraphosphonate cavitands

2

2.1 Introduction

Cavitands, as originally defined by Cram,[1] "are synthetic organic compounds with enforced cavities large enough to complex complementary organic molecules or ions." These compounds are extremely interesting and versatile molecular receptors, whose complexation properties have been extensively studied in the solid state,[2] in solution[3] and in the gas phase.[4]

Resorcin[4]arenes are convenient molecular platforms for the construction of cavitands. They can be easily prepared in high yield by the acid-catalyzed condensation between resorcinol and either aliphatic or aromatic aldehydes (Scheme 2.1).

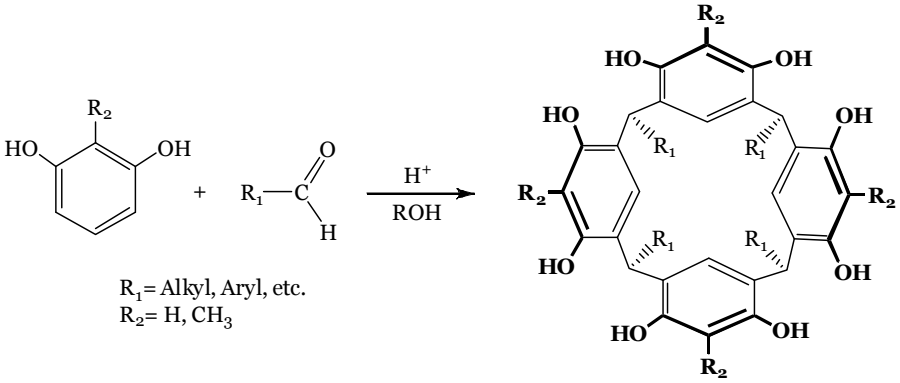

Scheme 2.1. Synthesis of resorcin[4]arenes.

The flexible macrocycles formed can be rigidified by reacting its four couples of adjacent phenolic oxygens with different bridging groups. In particular, in the design of cavitands, the choice of the bridging groups is pivotal since it determines shape, dimensions and complexation properties of the resulting cavity.

Phosphorous groups play an important role in host-guest chemistry and the properties of the phosphoryl (P=O) and thiophosphoryl (P=S) moieties to bind neutral and cationic species have been investigated. Because of their binding capabilities, these groups have been included in preorganized structures to enhance the complexation properties of cavitands. Many references in the literature concerned phosphorous macrocycles containing (thio)phosphorylated moieties,[5] phosphorous cryptands[6] and phosphahemispherands.[7]

In particular, much attention is currently devoted to the phosphorous derivative of resorcin[4]arenes, which have opened the route to promising preorganized hosts.[8] The main specific interactions responsible for recognition evidenced by these studies are H-bonding, CH-π, and cation-dipole interactions.

In this chapter, we report different types of methylene and phosphorous-bridged cavitands, as a case study to pinpoint the main interactions responsible of molecular recognition toward alcohols at the gas solid interface. The specific interactions operating at each single phase level are analyzed and their potentials for the generation of highly selective mass sensors are explored.

2.2 Phosphorous-bridged cavitands

The first attempt to synthesize phosphorous-bridged cavitands was carried out in Cram's group in the 1980s by reacting a methyl-footed resorcin[4]arene[9] with dichlorophenylphosphonate.[10] The complex mixture obtained was not investigated further, due to the difficulties to isolate the different diasteromers obtained. The field got a new start in the 1984 when Dalcanale and Mann reported synthesis and stereochemical elucidation of tetraphosphate cavitands.[11] In fact, the presence of four stereogenic centers in the tetrabridged phosphocavitands gives rise to six possible diasteromeric cavitands. The inward (i) and outward (o) configurations are defined relative to the different orientation of the P=O moieties. The proposed nomenclature,[12] summarized in Scheme 2.2, showed the tetrabridged phosphonatecavitands discussed in this chapter with their acronym below.

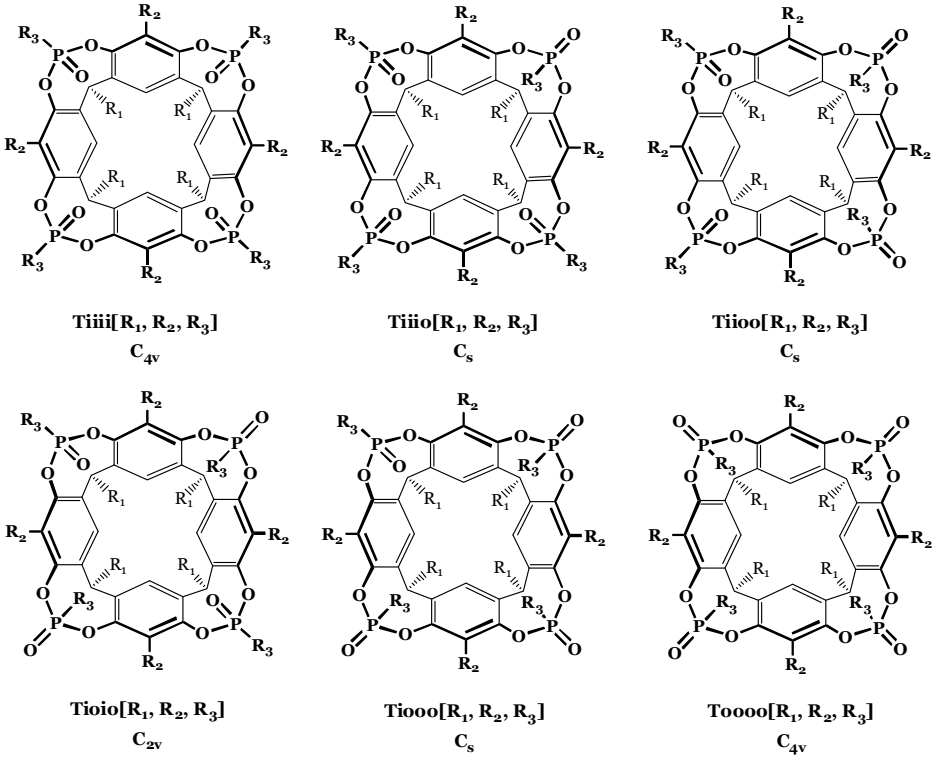

Scheme 2.2. Isomers of tetraphosphonate bridged cavitands.

The capital letter, defines number and nature of bridges, the lower case letters define the in-out stereochemistry, and R_1, R_2 and R_3 in brackets define the substituents at the lower rim, in the apical positions and on the phosphorous stereocenters respectively.

To ensure strong binding, the cavity should contain binding sites preorganized for interaction with guest, and the Tiiii stereoisomer appears to have a prerequisite for good recognition properties toward cationic and neutral species.

In the early 1990s, studies on the design of phosphorous cavitands and investigation of their structures were started in several laboratories independently of each other. At first on the topic was investigated by R. J. Puddephatt *et al.*,[13] who prepared phosphonite cavitands and studied its transition metal complexation properties. The used phosphorous bridging reaction was performed with dichlorophenylphosphine and pyridine as base, to give the new $4P^{(III)}$ derivative. Molecular mechanics calculations and NMR resonance indicated that of the six possible isomers was preferred only the isomeric forms with all lone pairs directed inwards the cavity.

With a similar way Nifant'ev *et al.*[14] synthesized the first thiophosphorylated cavitands from resorcinarene and $P(NMe_2)_3$ or $P(NEt_2)_3$ followed by addition of sulphur.

At the same time, new cavitands with phosphonate bridging moieties have been obtained by J.-P. Dutasta and co-workers.[15] This new stereoselective sinthesis involved dichlorophenylphosphine oxide ($P^{(V)}$) instead $P^{(III)}$ in the presence of an amine. In detailed this reaction was performed in refluxing toluene and N-methylpyrrolidine as amine, to provide the Tiiii with only a minor amount of Tiiio isomer present.

The results showed that solvent/amine pair plays a crucial role in the formation of the tetraphosphonate inward stereoisomer. Indeed in our group we tried to perform the same reaction in acetone or THF in the presence of triethylamine as base,[16] but in all cases we obtained the formation of a mixture consisting especially of the Tioio, Tiioo and Tiooo, without traces of Tiiii and Tiiio. Moreover the presence of substituents different from hydrogen in the apical positions of the resorcinarene skeleton (R_2 groups) and of bulky groups on phosphorus (R_3 groups) did not affect significantly the stereochemical course of reaction.

It is tempting to suggest that the origin of the reaction selectivity has been attributed to the template effect of the N-methylpyrrolidinium salt formed in situ; therefore in the first stage of the reaction, after the entrance of the first

P=O bridge, the host-guest complex between resorcin[4]arene and ammonium cation, directed the incoming PO groups inward via H-bonding and electrostatic interactions. Secondly, the formation of the Tiiii isomer is solvent dependent, since the ammonium ion interaction with the PO groups is effective only in weakly solvating agents, such as toluene.

Later, Dutasta's group, drew on Puddephatt work's, developed a different procedure to obtain Tiiii via direct oxidation of TSiiii.[17] This reaction proceeds with retention of configuration at the phosphorous centre, and gives only the inward isomer.

Going by these results our group has recently performed a new method to achieve only pure Tiiii with high yields.[18] Reaction of resorcin[4]arene with dichlorophenylphosphine in the presence of pyridine afford exclusively the $4P^{(III)}$iiii cavitand. Its subsequent *in situ* oxidation with H_2O_2, proceeds with retention of configuration at the phosphorous centre and lets have, in only one step, the Tiiii without need of purification. Unfortunately this method does not work well if the substituent on the phosphorous stereocentre (R_3) is a methyl instead phenyl group. Therefore in this chapter we follow two different synthetic routes (Scheme 2.3): the first one that employ the $P^{(V)}$ strategy in the case of tetramethylphosphonate cavitands, Tiiii[R_1, R_2, CH_3], and the second one that employ the $P^{(III)}$ strategy in the case of tetraphenylphosphonate cavitands Tiiii[R_1, R_2, Ph].

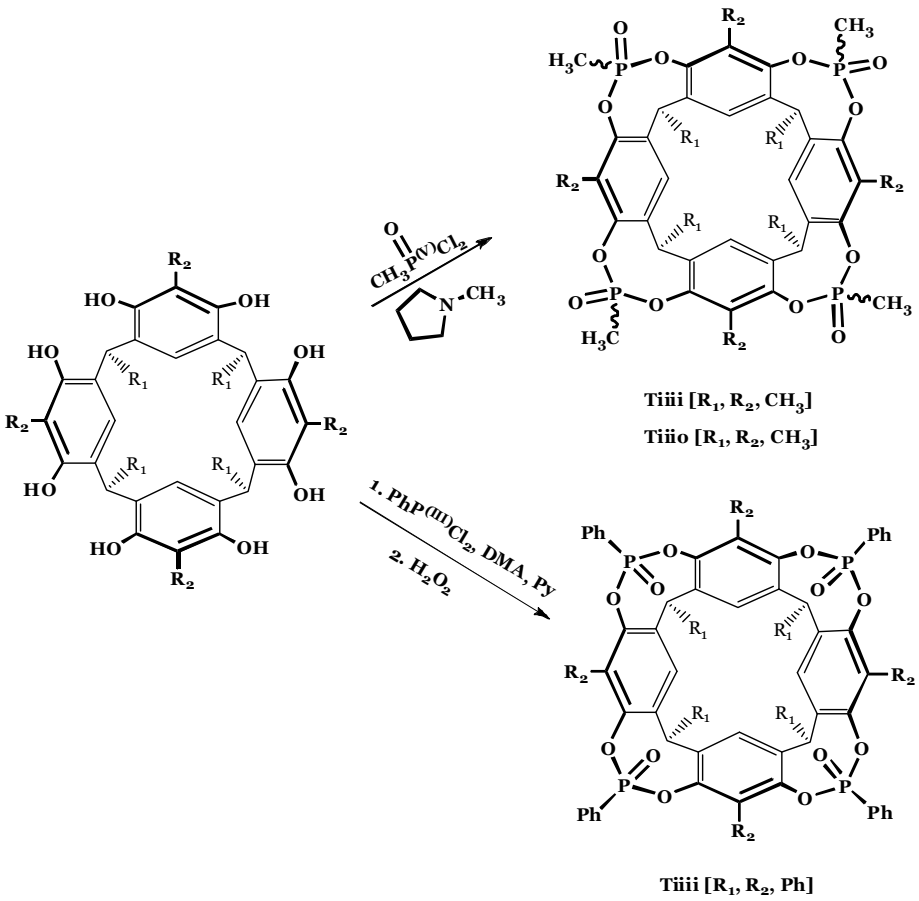

Scheme 2.3. Two different synthetic routes performed.

2.3 Probing the molecular recognition properties of phosphonate cavitands

We have started to study the complexation properties of phosphonate cavitands, from the point of view of molecular recognition, long ago.[19]

Here we report an effective methodology for probing the molecular recognition properties of a given receptor at the gas-solid interface. It relies on the combined use of ESI-MS, X-ray crystallography and Quartz Crystal Microbalance (QCM)[20] measurements. ESI-MS and X-ray crystallography were employed for the evaluation of the complexation properties of the receptors at the gas phase and in the solid state respectively. They provide precise information on the type, number, strength and geometry of the weak interactions responsible of host-guest associations.

The predictive value of such information for gas-solid interactions is validated by coating QCM transducers with the receptors and by exposing them to the analytes.

The compounds used in previous studies are the phosphonate cavitands reported in Scheme 2.4. They present an open, conformationally rigid cavity, delimited by one (Mi),[21] two (ABii)[22] and four (Tiiii) inward oriented phosphonate bridging groups at the upper rim.

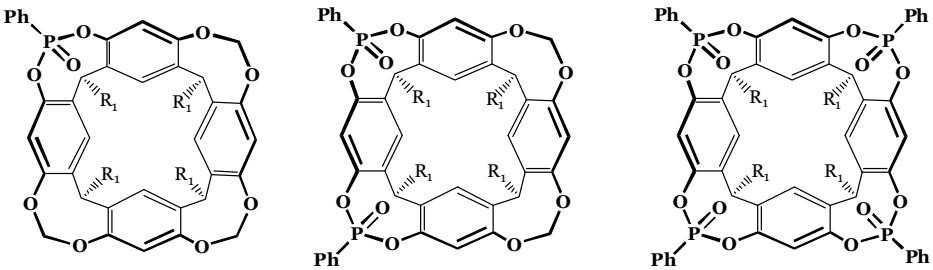

Scheme 2.4. Mono, di and tetra phosphonate cavitands.

Significant is also focused the attention at the lower rim, because in this case all receptors have long alkyl chains (R_1=$C_{11}H_{23}$). The reason of this choice is the need to obtain a suitable permeability of the cavitand layer.
Since QCM transducers measure analyte adsorption across the entire layer, a suitable morphology of the deposited layer is essential to achieve the reversibility of the responses. Analytes diffusion in the layer, increase with permeability that is highly enhanced in amorphous layer with respect to the microcrystalline ones. Long chains at the lower rim prevent the crystallization, therefore enhance the diffusion process.
The key factors that we found to affect the sensing performances of mono and diphosphonate cavitands toward alcohols are:

- simultaneous presence of H-bonding with one of the PO groups and CH-π interactions with the π-basic cavity;[21]
- a rigid cavity which provides a permanent free volume for the analyte around the inward facing PO groups, pivotal for effective H-bonding;[23]
- presence, in the diphosphonate cavitands, of two energetically equivalent H-bonding options available to the analyte.[22]

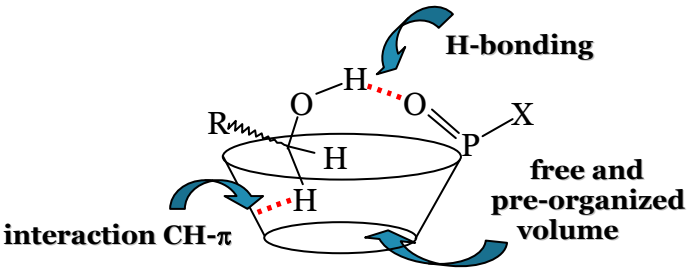

Figure 2.5. Representation of key factors affecting sensing performances.

The last factor suggests that increasing the number of convergent P=O groups in the cavitand, should enhance alcohol complexation at the gas-solid interface.
This hypothesis was confirmed at the gas phase with ESI-MS competition studies. With this technique, relatively weak non-covalent complexes formed in solution can be transferred to the gas phase and their intrinsic properties can be studied without solvent interference. The competition experiments, among Mi, ABii and Tiiii, were performed to estimate the relative affinity of these cavitands toward EtOH. The results shows (Figure 2.6) that the thermodynamic stability

of the complexes strongly depends on the number of P=O groups directed inward the cavity, since the formation of tetraphosphonate cavitand complex with EtOH is clearly preferred over that of the complex of diphosphonate or monophosphonate cavitands with the same alcohol.

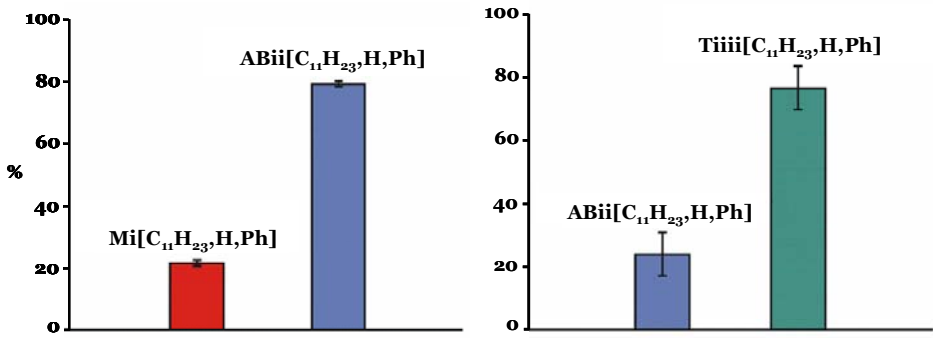

Figure 2.6. Mean intensities of ethanol complexes obtained in competition experiments for the pairs Mi (red)/ABii (blu) and 2POii/Tiiii (green).

Different competition tests were assessed via CID (Collision Induced Dissociation) MS-MS experiment.[24] In this case, the ethanol complexes of the three cavitands dissociated producing protonated cavitands $[M+H]^+$ as product ion. No protonated ethanol was observed, confirming that the proton affinities of cavitands are greater than those of alcohols.[25] The relative kinetic stability indicate that the ethanol complex of tetraphosphonate cavitands is more stable than the other ones, confirming once again the advantage of four convergent P=O moieties in the cavitand (see Figure 2.7).

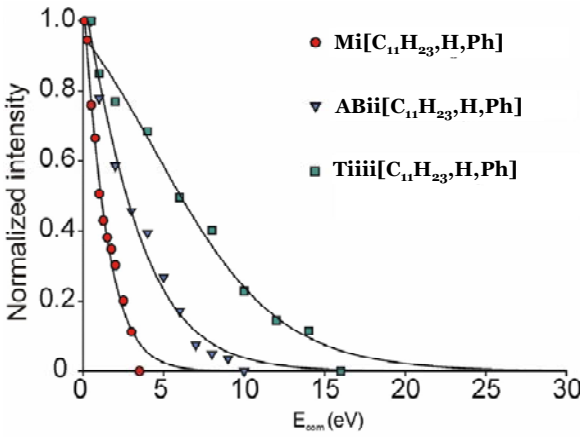

Figure 2.7. Dissociation (CID) of the ethanol complexes of Mi (red), ABii (blue) and Tiiii (green).

The same trend was obtained at the gas solid interface by QCM measurements. PECH (reference polymer) and cavitands Mi [$C_{11}H_{23}$, H, Ph], ABii [$C_{11}H_{23}$, H, Ph] and Tiiii [$C_{11}H_{23}$, H, Ph] were deposited by spray coating on both sides of a QCM transducer and exposed to vapours of methanol (1500 ppm). These tests (Figure 2.8) clearly indicates the positive effect of the number of inward facing P=O moieties on the sensor performances.

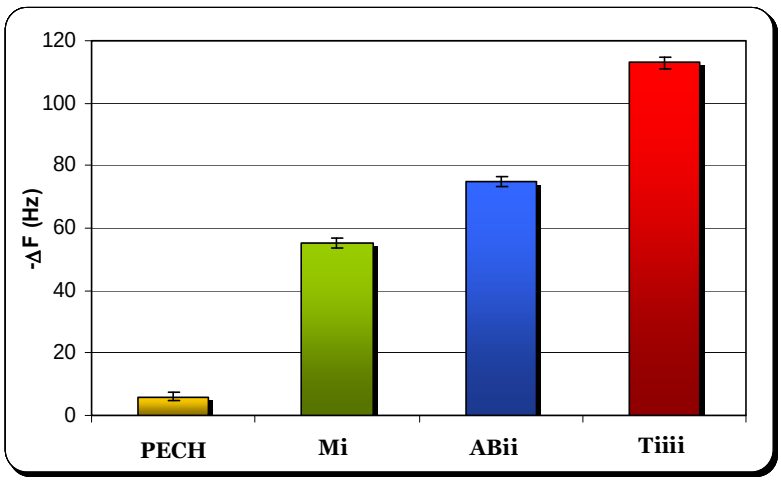

Figure 2.8. Selectivity pattern of PECH, Mi [$C_{11}H_{23}$, H, Ph], ABii [$C_{11}H_{23}$, H, Ph], Tiiii [$C_{11}H_{23}$, H, Ph] to methanol at 1500 ppm.

So far all QCM responses of cavitands have been compared to those of PECH (poly epichlorohydrine) under the same conditions. PECH is a totally unspecific layer, in which only polarity is the discriminating parameter.
However, PECH suffers of two drawback: a mismatch in both polarity and morphology with respect to any cavitand employed. Therefore we chose an unspecific layer, the tetrathiophosphonate cavitand (TSiiii), structurally identical to the other ones except for the presence of four P=S instead of four P=O.

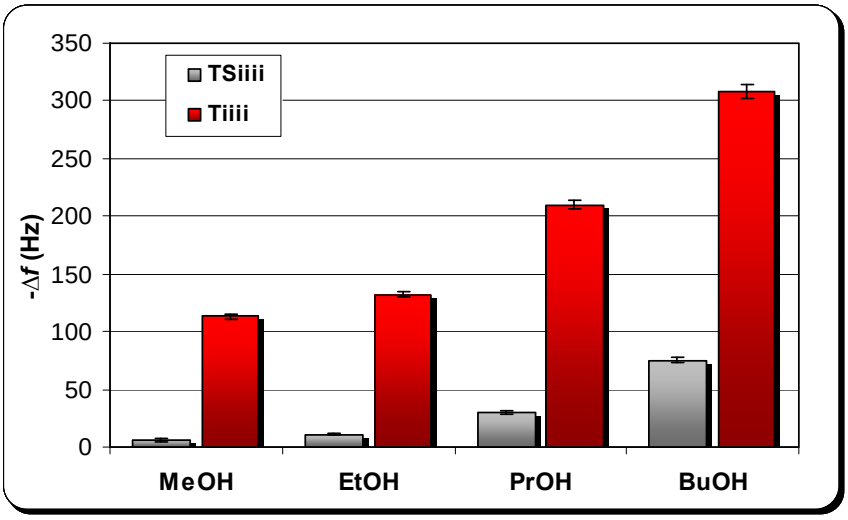

Figure 2.9. Responses of Tiiii[$C_{11}H_{23}$, H, Ph] and TSiiii[$C_{11}H_{23}$, H, Ph] to C_1-C_4 linear alcohols (1500 ppm each).

This substitution strongly reduces the responses across the entire alcohol series, as is shown in Figure 2.9, because sulphur has lower electronic density with respect to the oxygen and consequently less affinity for H-bonding interactions.[26] In addition the cavity of TSiiii is more bulky and less available for guest inclusion because sulphur is larger (atomic radius=1 Å) than oxygen (atomic radius=0.6 Å).
Moreover the dependence of the mass sensor performances on H-bonding interactions is reflected in the different behaviour of the two cavitands responses toward linear alcohols. The general enhancement of the responses in both cavitands, associated with the increasing chain length of the alcohols, is

due to the greater number of dispersion interactions experienced by the analyte, as is shown by the similar behaviour of the TSiiii cavitand.
Upon entering the solid layer the analyte can position itself not only into the cavity but also between the host structures.

2.4 Next generation of cavitand receptors: tetraphosphonate cavitands

The presence of unspecific interactions turned out to be the key element in diluting the complexation properties at the gas-solid interface. Therefore to maintain high selectivity toward alcohols but reduce these dispersive interactions, we conceived a new tetraphosphonate cavitand without chains at the lower rim.

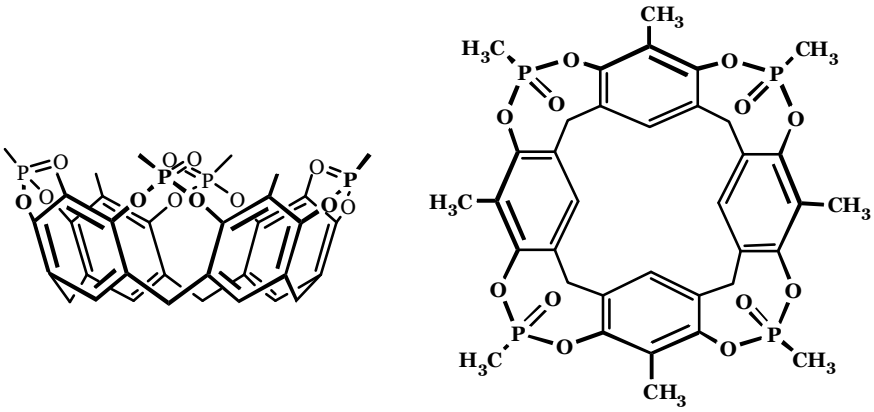

Tiiii[H, CH_3, CH_3]

Scheme 2.10. Tetraphosphonate cavitand Tiiii[H, CH_3, CH_3].

The lack of these long chains decreases the possibility of extra *versus* intracavity positioning of the guest; indeed the structure of Tiiii[H, CH_3, CH_3] cavitand is more compact and when it is deposited as solid layer on the QCM (see Appendix C) presents less unspecific sites.
Moreover this cavitand bears methyl groups on the phosphorous centre and in apical positions. This last substitution makes the cavity deeper and enhances its

π-basic character, promoting CH-π interactions between the alcohol alkyl chain and the resorcinarene skeleton.

Tiiii[H, CH_3, CH_3] cavitand was synthesized and purified following a known procedure (see Experimental part and Scheme 2.11).

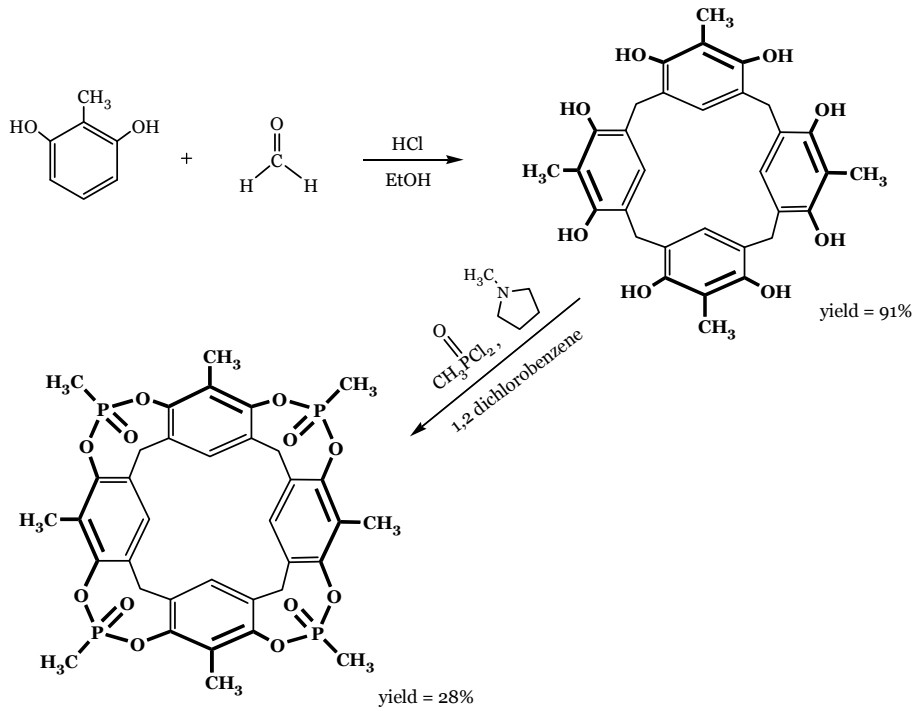

Tiiii[H, CH_3, CH_3]

Scheme 2.11. Synthesis of Tiiii[H, CH_3, CH_3].

In the first step, the resorcin[4]arene synthesis,[27] it is fundamental to use paraformaldehyde and absolute ethanol as solvent because the presence of water in the reaction mixture lead also to the formation of resorcin[n]arene, where n=5, 6 and 7. Recently, Konishi *et al.* demonstrated that resorcin[5]arene and resorcin[6]arene cyclocondensation products can be isolated from the reaction of 2-methylresorcinol with formaldehyde.[28] These higher resorcinarenes are favoured kinetically and can be obtained using shorter reaction times. By using solid paraformaldehyde instead aqueous formaldehyde and leaving the reaction to proceed for long time (48 hours), only the cyclic tetramer is obtained.

The bridging reaction, performed in anhydrous dichlorobenzene in presence of N-methylpyrrolidine, mainly leads to the formation of the Tiiii stereoisomer together with a small amount of Tiiio. In this specific case the low yield of the second step is principally due to the low solubility of the resorcinarene in apolar solvents, the only ones compatible with Tiiii isomer formation.
Before the separation step via column chromatography, a sonication treatment with distilled water is necessary to remove the N-methylpyridinium salt formed. This overture turns out to be pivotal for the increase of the column output. Moreover, for the final sensing purpose the cavity of the Tiiii must be empty, without any guest inside that could interfere with the analyte in the sensing process.

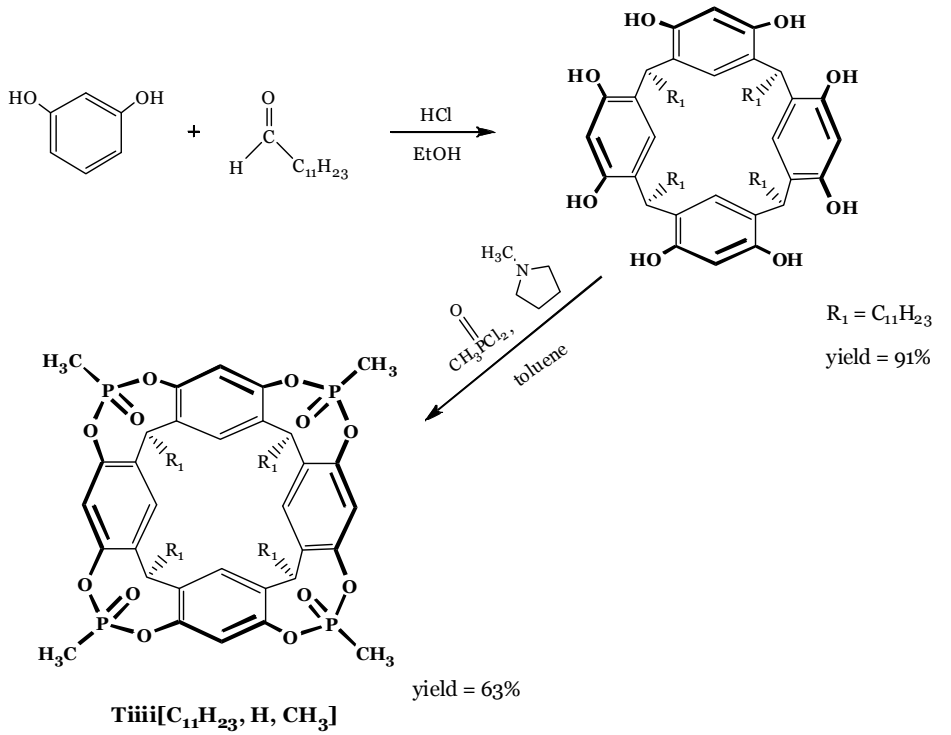

Tiiii[$C_{11}H_{23}$, H, CH_3]

Scheme 2.12. Synthesis of Tiiii[$C_{11}H_{23}$, H, CH_3].

For a meaningful comparison of the sensor responses also the Tiiii[$C_{11}H_{23}$, H, CH_3] cavitand with long chains at the lower rim and the MeCav[H, CH_3] cavitand without chain at the lower rim were synthesized (see Experimental

part, Scheme 2.12 and Scheme 2.13). In this case the bridging reaction is analogous at the previous case except that with long chains at the lower rim the problem of the resorcinarene and cavitand solubility is remove. Therefore this reaction gives the final product in higher yield.

On the other hand, the bridging reaction leading to the MeCav[H, CH_3] is completely different. We used dibromomethane in anhydrous DMA and in basic conditions, following the standard procedure.[2]

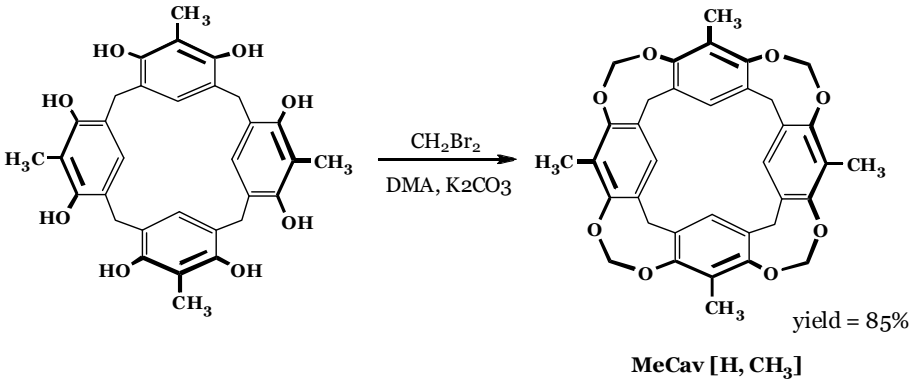

Scheme 2.13. Synthesis of MeCav[H, CH_3].

The methylene bridged cavitand, without P=O at the upper rim, will be used in the QCM measurements and in the solid state studies as reference in comparison with the Tiiii[H, CH_3, CH_3] cavitand.

In the QCM results commented above, we have shown the comparison between the TSiiii and Tiiii cavitands. Since the TSiiii without chains at the lower rim is not soluble in the common solvents, we can not use it neither to grow crystals nor as unspecific interaction indicator at the gas-solid interface. For this reason we have synthesized the MeCav [H, CH_3].

A more appropriate and convenient way to explore the binding preferences of these receptors in terms of gas-solid interactions is the combined use of X-Ray crystallography and mass spectrometry, which provide information about solid state and gas-phase interaction modes, respectively.

2.4.1 Evaluation of Tiiii[H, CH_3, CH_3] properties in the solid state

The goal of crystallization is usually to produce a well-ordered crystal that is lacking in contaminants and large enough to provide a diffraction pattern when hit with X-Rays. Also this concept prompted us to conceive a cavitand with a compact and high symmetric structure, such as Tiiii[H, CH_3, CH_3].
The generality of the cavitand-alcohol interaction mode, based on the synergy between H-bonding to a P=O group and CH-π interactions of the methyl residue with the cavity, is confirmed by the crystal structure of the Tiiii[H, CH_3, CH_3]•MeOH complex (Figure 2.14).

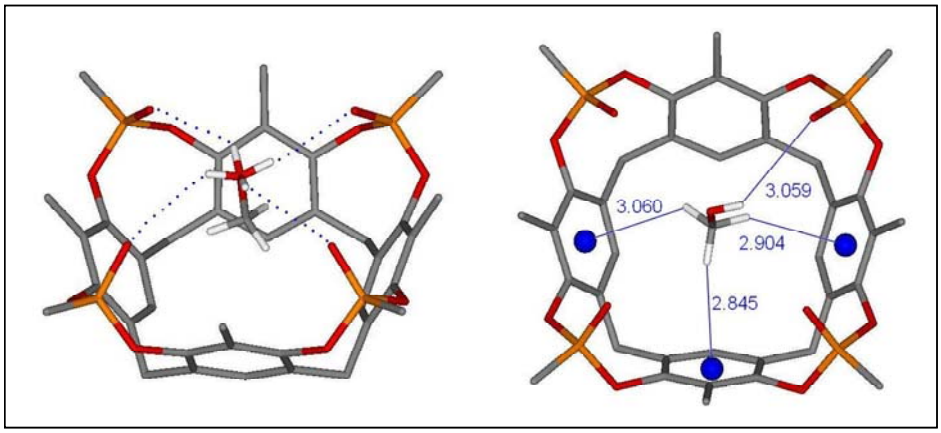

Figure 2.14. Crystal structure of Tiiii[H, CH_3, CH_3]·MeOH complex.

This crystal structure was obtained by evaporation of a CH_3OH/CH_2Cl_2 solution of Tiiii[H, CH_3, CH_3].
In this particular case the complex crystallized in the tetragonal P4/n group, with the methanol C-O bond lying on the four-fold axis, so that the methanol hydrogens are statistically disordered over four equivalent positions. The alcohol interacts with the cavity via three CH-π interactions between the methyl group and the aromatic rings of the cavitand (CH-centroid of aromatic rings from 2.845(7) to 3.060(7) Å) and with weak H-bonds between the hydroxyl group and the phosphonate moieties at the upper rim [MeOH···O=P 3.059(6) Å]. Moreover, due to its statistical disorder around the fourfold axis, the methanol can switch among four different but isoenergetic triplets of CH···π interactions with the host cavity and at the same time it can also switch among four different isoenergetic MeOH···O=P attractive interactions with the host,

leading to an entropic stabilization of the complex. It means that four P=O groups at the upper rim strongly stabilized the host-guest complex.
Further evidence of the importance of both CH-π and H-bonding interactions synergistic presence, is given by the crystal structure of MeCav[H, CH_3] in Figure 2.16. Grown in the same conditions of the previous molecular structure, the crystal shows no guest is present inside the cavity.
The only one difference between this cavitand and the Tiiii[H, CH_3, CH_3] is the absence of four P=O groups ad the upper rim replaced with methylene bridges. We can conclude that CH-π interactions alone are not enough to stabilize the final complex.

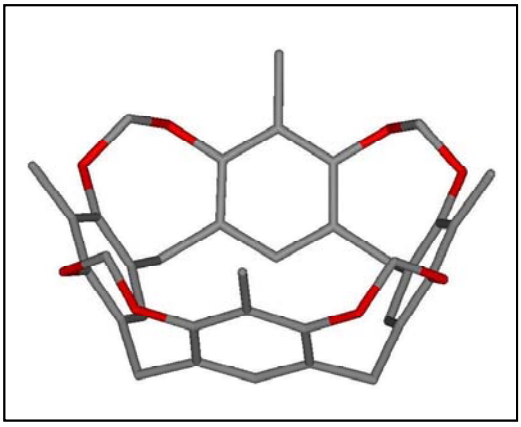

Figure 2.15. Crystal structure of MeCav[H, CH_3].

Additional confirmation of the importance of its two coexisting interactions and of the inclusion mode of the host-guest complexation given by the crystal structure of Tiiii[H, CH_3, CH_3] grown by a solution of trifluoroethanol (Figure 2.16). Indeed, also in this case no guest is included inside the cavity but trifluoroethanol molecules fill the empty spaces in the crystal lattice.

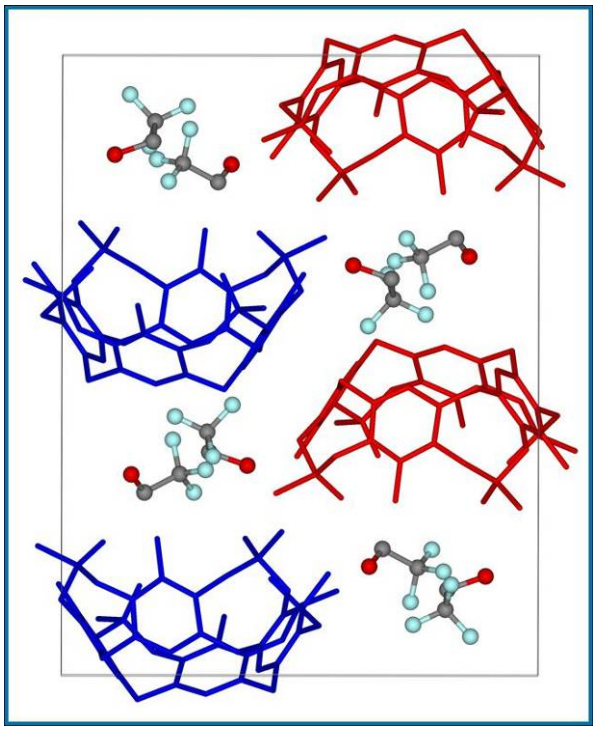

Figure 2.16. Crystal lattice of Tiiii[H, CH_3, CH_3] with CF_3CH_2OH.

It probably means that the trifluoroethanol CF_3 residue is too big to enter inside the cavity or, as it is not able to have CH···π interactions, the only H-bonding is not enough to promote a stable inclusion.

Another important aspect to underline is that the trifluoroethanol is the only pure solvent able to dissolve Tiiii[H, CH_3, CH_3], because in all other cases we need a mixture of an apolar solvent, such as methylene chloride, with a polar one, such as an alcohol.

In order to study the influence of the alcohol chain length on complexation in the solid state, we have grown different crystals of Tiiii[H, CH_3, CH_3] cavitand with different alcohols. Each crystal was obtained by the vapour diffusion of the alcohol-guest in a solution of trifluoroethanol and alcohol-guest, at the same temperature.

In all cases the cavitand-alcohol interaction mode is the same (Figure 2.17, 2.18 and 2.19): the chain fits into the cavity with the methyl residue (CH-π interactions) while the OH moiety forms one H-bonding interaction with the P=O group.

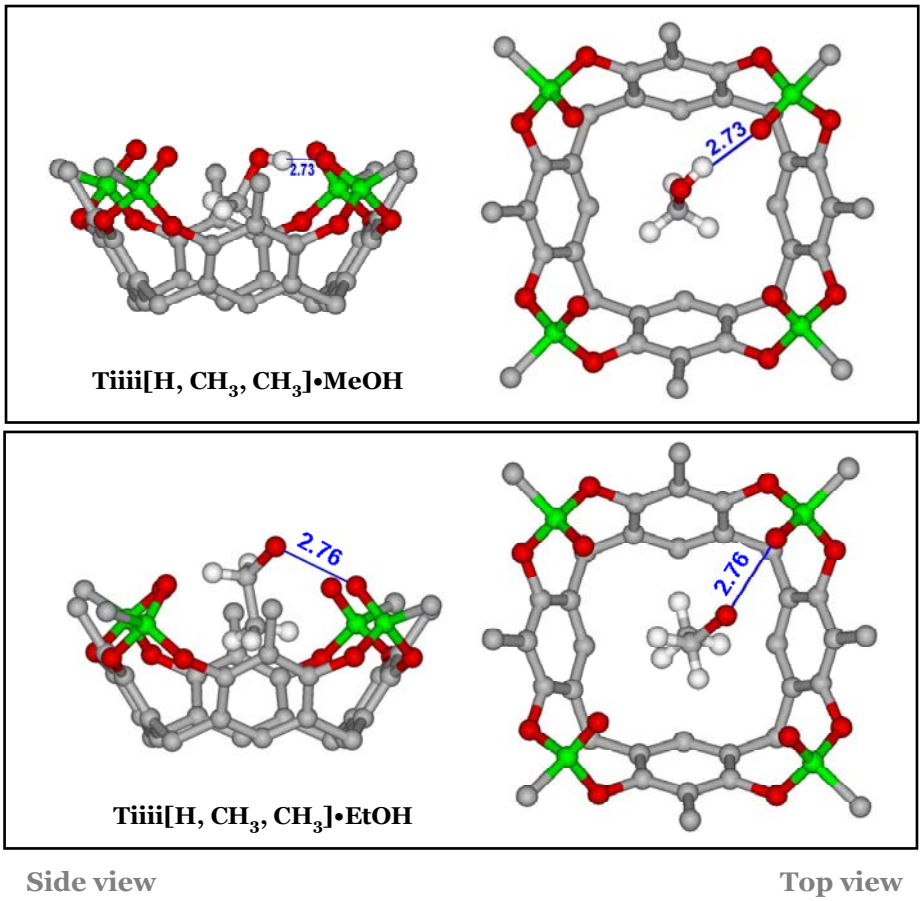

Figure 2.17. Crystal structures of Tiiii[H, CH_3, CH_3] complexed with MeOH and EtOH.

In all cases the alcohol is not positioned in the midpoint of the cavity, as reported in Figure 2.14, but is inclined toward only one orientation assuming a single defined H-bond. These different kind of inclusion is possibly due to a different crystal grown conditions.

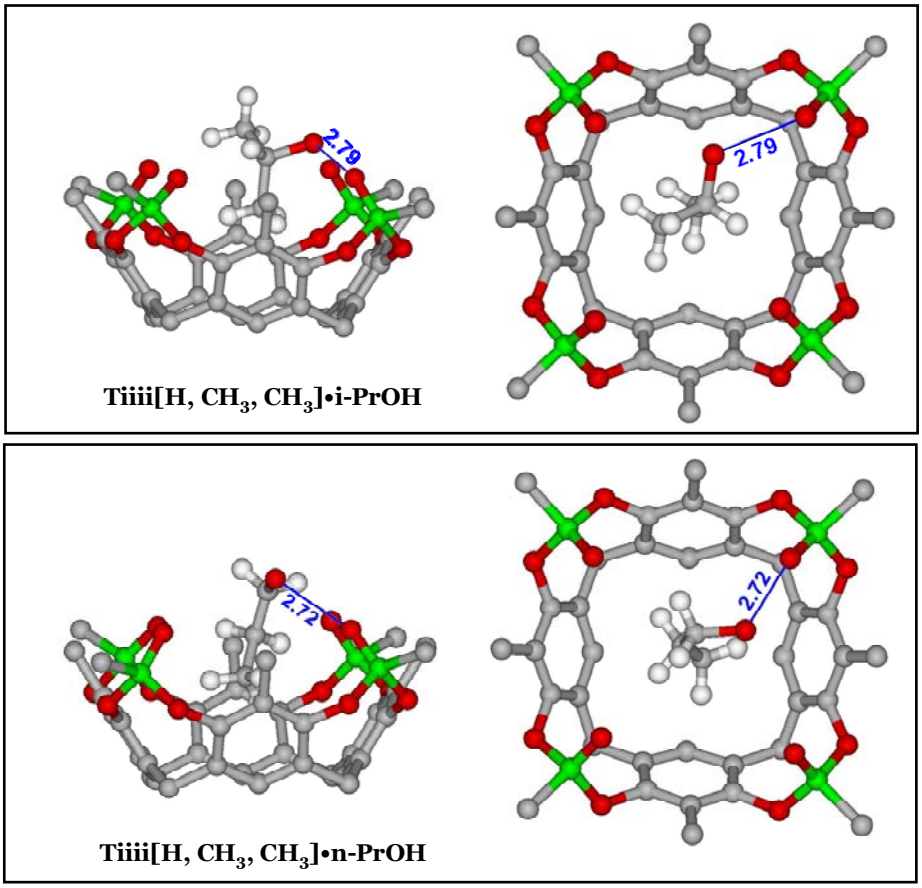

Figure 2.18. Crystal structures of Tiiii[H, CH_3, CH_3] complexed with i-PrOH and n-PrOH.

The H-bonding interactions have the typical length, around 2.7 Å, from MeOH to i-BuOH, independently of the alcohols chain.

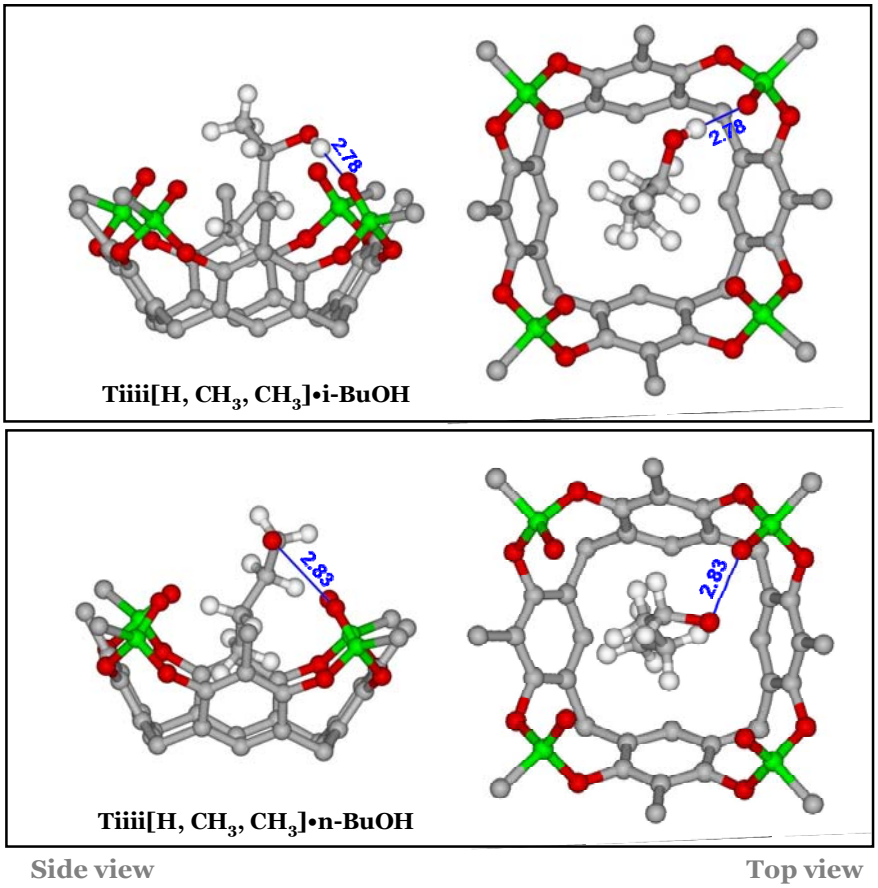

Figure 2.19. Crystal structures of Tiiii[H, CH_3, CH_3] complexed with i-BuOH and n-BuOH.

In the case of n-BuOH however, the H-bond length is longer than the other ones, as if we are near the inclusion limit for both CH-π interactions with the methyl group and H-bonding with the alcoholic moiety.
Indeed with the n-PenOH, as is showed in Figure 2.20, the cavitand has no guest, because in this conditions the alcohol is too long to sit into the cavity and form at the same time H-bonding interactions.

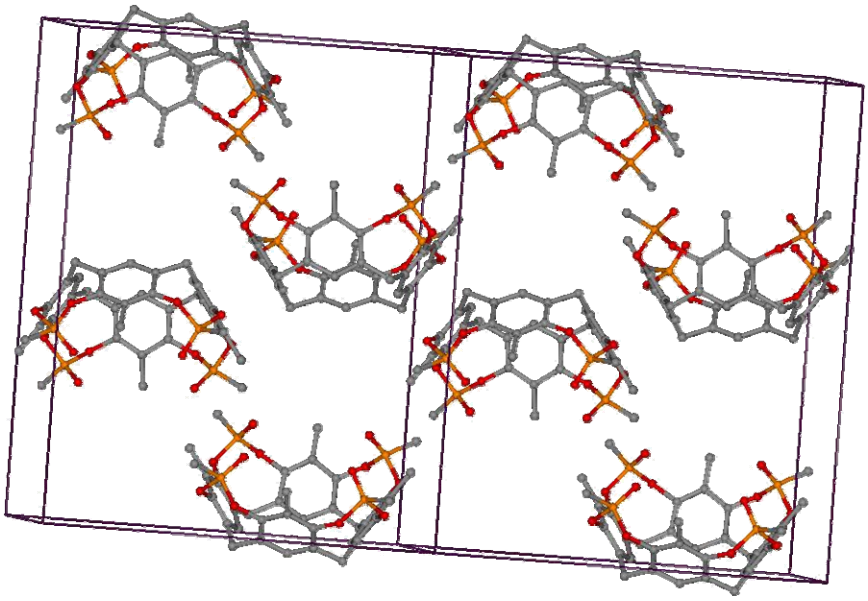

Figure 2.20. Crystal lattice of Tiiii[H, CH_3, CH_3] with n-PeOH.

Pentanol inclusion was attempted several different crystallization experiments. In one case the cavitand did form a complex, but with trifluoroethanol instead of the expected pentanol (Figure 2.21).

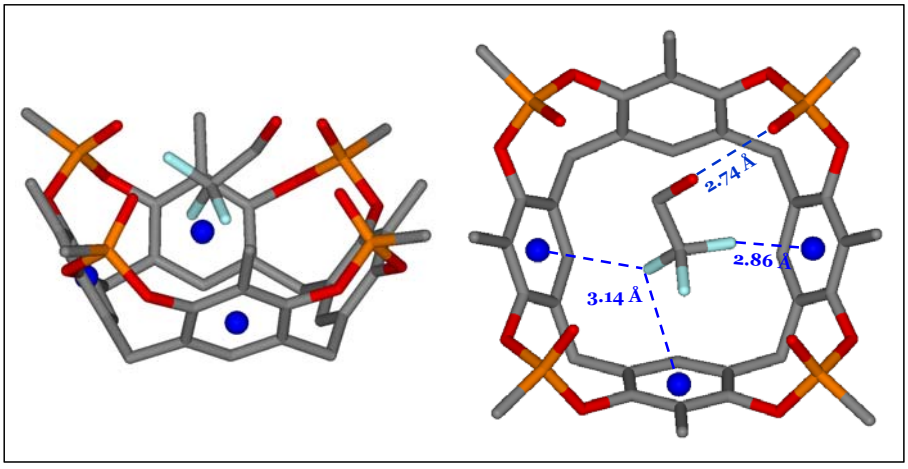

Figure 2.21. Crystal structure of Tiiii[H, CH_3, CH_3] complexed with CF_3CH_2OH.

This unique example indicates that this alcohol, under particular conditions, is able to enter on the cavity with the CF_3 group forming a strong H-bonding between the alcoholic group and one P=O (2.74 Å), and CF-π interactions between the CF_3 moiety and the resorcinarenic skeleton.
Since this event has only occurred once, we can confirm the low affinity of triflouroethanol toward the Tiiii[H, CH_3, CH_3] cavitand.

2.4.2 Solid state competition study with Tiiii[H, CH_3, CH_3]

Starting from these results we have performed several solid state competition experiments, in order to fathom which is the alcohol with the greater affinity for the Tiiii[H, CH_3, CH_3].
Since, attempting to crystallize cavitands without a proven protocol can be very tedious, we used a new method called "crystallization by sitting drop".
Originally it is employed to grow protein crystals because this technique is easy to perform, requires small amount of sample and allows a wide range of conditions. The major advantages of the sitting drop technique are speed and simplicity.
The apparatus is constituted by a special box with numerous wells; the "drop" is placed on a bridge inside the wells and the "reservoir" is outside at the bottom of them.

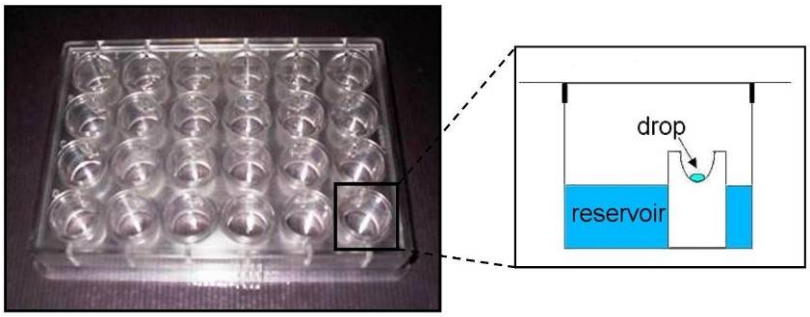

Figure 2.22. Crystallization by sitting drop apparatus.

In our case the drop is composed of 7 μL of cavitand solution 8 mM in trifluoroethanol and 3 μL of reservoir. Instead the reservoir is composed of trifluoroethanol (500 μL) and the two alcohols solution (500 μL) of which we want to study the competition in respect of the cavitand.

The initial precipitant concentration in the drop is less than that in the reservoir, thus the droplet of cavitand solution contains an insufficient concentration of precipitant for crystallization. Over time trifluoroethanol vaporizes from the drop and transfers to the reservoir solution, or *vice versa* the two alcohols vaporized from the reservoir and transfer to the drop solution, it depend upon the vapour tension of alcohols. During this equilibration process the precipitant concentration increases and the sample is also concentrated, increasing its relative supersaturation to a favourable level for crystallization. Since the system is in equilibrium, these optimal conditions are maintained until the crystallization is complete.
Applying this technique we have obtained several crystal structures with different competitive alcohol pairs. For the interpretation of results obtained, it is important to understand the complexation constant ratio concept. This ratio, as shows the equation in Figure 2.23, depends on the occupancy factor and on the molar fraction of the two guests.

$$\frac{K_A}{K_B} = \frac{x_A}{(1-x_A)} \cdot \frac{\%B}{\%A}$$

K_A, K_B: complexation costant of cavitand with alcohols A and B.

$\%A$, $\%B$: molar fraction of alcohols.

x_A: occupancy factor of *host* site by *guest* A.

$$x_A = \frac{\sqrt{I_{hkl}^{(A+B)}} - \sqrt{I_{hkl}^{(B)}}}{\sqrt{I_{hkl}^{(A)}} - \sqrt{I_{hkl}^{(B)}}}$$

I_{hkl}: diffraction intensity of a reflex *hkl*.

Figure 2.23. Equation of complexation constant ratio.

The determination of the occupancy factor of host site by guest A is based on the study of the diffraction intensity. x_A represents the fraction of unit cells in the crystal which contain the guest in question.
All complexation constants, derived from 28 crystal structures determinations, are summarized in Table 2.24.

K_A/K_B		*Guest* A					
		EtOH	n-PrOH	MeOH	i-PrOH	i-BuOH	n-BuOH
Guest B	EtOH		0.24	0.17	0.13	0.09	
	n-PrOH	4.2		1.1	0.37	0.14	0.07
	MeOH	5.9	0.9		0.34	0.16	0.04
	i-PrOH	7	2.7	2.9		0.25	0.14
	i-BuOH	11	7	6.2	4.0		0.49
	n-BuOH		14	25	7	2.0	

Table 2.24. Complexation constant ratio obtained for C_1-C_4 alcohols.

We can observe that in all pairs with EtOH, it is the favorite guest. Instead in regard the general trend, the affinity scale becomes: EtOH>MeOH≥n-PrOH>i-PrOH>i-BuOH>n-BuOH.
This result is consistent with our expectation since is reasonable that the major affinity of cavitand is toward alcohols with short chain. Small bulky guest have more possibility to go inside the cavity and adjust their conformation to obtain the most stable complex. Indeed, as shown in the previous crystal structures, we can highlight that the shorter H-bond length is present in the case of MeOH (2.73 Å), EtOH (2.76 Å) and n-PrOH (2.72 Å).
Interesting is pointed out that in presence of water traces in the environment, the affinity scale changes in favour of H_2O-MeOH double guest which become more stable than the other complexes with only one alcohol-guest.

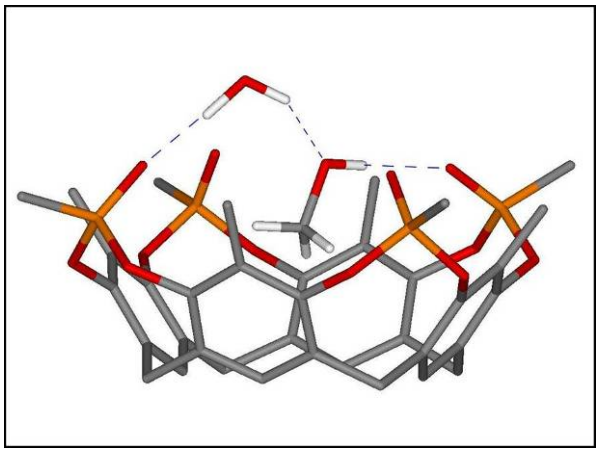

Figure 2.25. Crystal structure of Tiiii[H, CH_3, CH_3]·MeOH·H_2O.

As the X-Ray structure proves in Figure 2.25, water even makes a H-bond bridge between a P=O group and MeOH, stabilizing the overall complex via a zig-zag chain of hydrogen bonds with the two distal P=O groups.

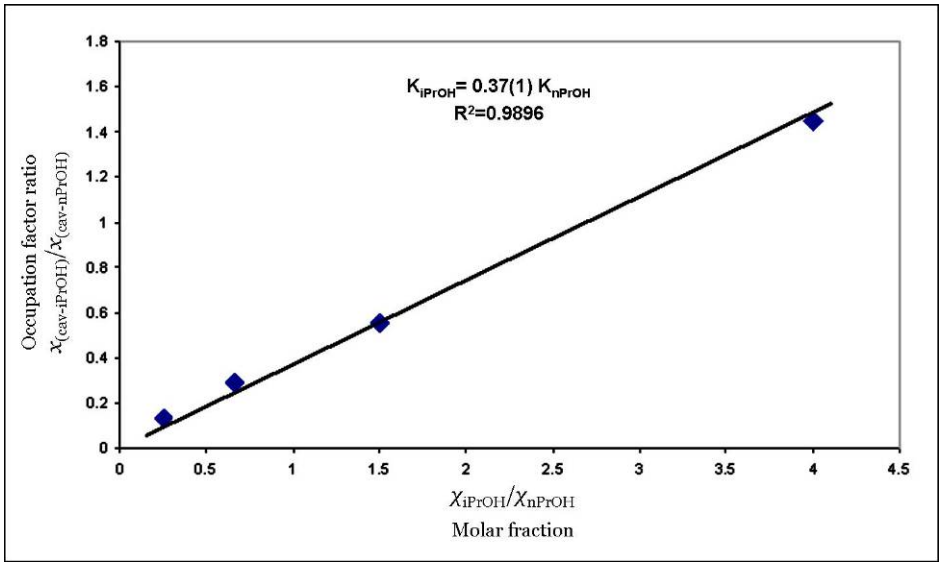

Figure 2.26. Consistency of the relative K values over the entire concentration range.

Finally with this graph, we want to confirm the good consistency of the data gained. In particular, we have plotted the occupancy factor ratio (x_A) obtained

from four crystals grown in different solutions with different concentration of i-PrOH and n-PrOH pair. The linear correlation derived means that the relative complexation constant ratio value is constant across the entire concentration range.

2.4.3 Complexation properties of Tiiii[H, CH_3, CH_3] in the gas phase

An appropriate and convenient way to explore the binding affinity of cavitands, in view to study gas phase interactions is the use of ESI mass spectrometry. ESI-MS offers the opportunity to study host-guest chemistry as a pure bimolecular interaction in the absence of solvents and other interfering species.
Previous studies of complexation properties of tetraphosphonate cavitands toward neutral amine[25] have demonstrated that the stability of the resulting complexes is correlated with number and inward orientation of the P=O groups. The same study showed that the proton affinity of cavitands is higher than that of alcohols. In the context of the present treatment, this mean that one P=O is protonated in the gas phase, since the complex must be charged to be detected by ESI-MS.
Protonation reasonably alters the H-bonding interaction mode between alcohol and cavitand, since can modified the H-bonding acceptor character of one P=O, transforming it in a H-bond donor. Regarding two inward P=O moieties, a donor-acceptor H-bond pattern can be envisioned as sketched in Figure 2.27.[29]

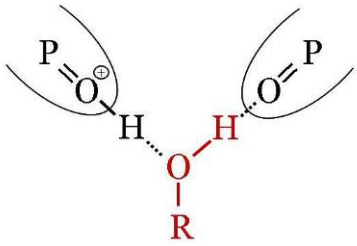

Figure 2.27. Schematic representation of proposed non-covalent interactions between alcohol and two phosphonate moieties.

Despite this difference, we obtained preliminary results concurring with the solid state. Complexation studies of Tiiii[H, CH_3, CH_3] with several alcohols showed the prensence of the $[M+alcohol+H]^+$ complexes. In the case of MeOH, EtOH, n-PrOH and n-BuOH we can see, in each spectrum, that the biggest peak

coincide with the $[M+alcohol+H]^+$ complex. Small peaks of $[M+Na]^+$ or $[M+K]^+$ are evermore present, because of Tiiii great affinity for cations present in the medium. The divergence in respect to the solid state is relative to the formation of the complex also with the n-PenOH. Previously we have assumed that n-PenOH was too long to enter inside the cavity and to form at the same time H-bonding interactions. Nevertheless with ESI-MS we are able to observe this complex.

Therefore the next issue to be addressed is if it is possible compare directly gas phase with solid state. Before to account of this discrepancy we want to show more results that can help us to find the better explanation.

By looking to the trifluoroethanol guest, we find out that in this case no $[M+CF_3CH_2OH+H]^+$ complex is observed, confirming the trifluoroethanol low affinity for Tiiii.

On the other hand, the same complexation experiments with TSiiii[$C_{11}H_{23}$, H, Ph] and MeCav[H, CH_3] cavitands gave further proof of their inability to form complexes with alcohols in general.

The overall view emanating from these experiments confirm the essential role of synergistic H-bonding and CH-π interactions also at the gas phase, while the chain influence on the complexation is underestimated.

To better mimic the solid state, we performed competition experiments with Tiiii[H, CH_3, CH_3] toward the C_1-C_5 series of alcohols. We wanted to establish if with the same cavitand we can obtain an affinity scale consistent with that obtained in the crystal structures study.

All experiments are carried out in an acetonitrile solution of cavitand containing equimolar amounts of the two alcohols (guest A and guest B) of which we want to estimate the affinity. Relative abundance in percentage of each complex considering one pair of alcohols is expressed in the Table 2.28.

Guest A	Guest B	Molar ratio	Intensity ratio	Guest A	Guest B
		X_a / X_b	$[M+H+guestA]^+ / [M+H+guest\ B]^+$	Relative abundance (%)	Relative abundance (%)
MeOH	**EtOH**	0.99	0.18 ± 0.01	15.10 ± 1.37	**84.90** ± 1.37
nPrOH	**EtOH**	0.99	1.33 ± 0.09	**56.96** ± 1.66	43.04 ± 1.66
iPrOH	**EtOH**	1.00	1.72 ± 0.09	**63.23** ± 1.32	36.77 ± 1.32
nBuOH	**EtOH**	0.99	2.52 ± 0.13	**71.53** ± 1.04	28.47 ± 1.04
iBuOH	**EtOH**	1.00	2.91 ± 0.18	**74.37** ± 1.18	25.63 ± 1.18
PenOH	**EtOH**	1.00	4.15 ± 0.33	**80.54** ± 1.28	19.46 ± 1.28

Table 2.28. Relative abundance of Tiiii[H, CH_3, CH_3]·alcohol complexes.

The relative abundance clearly indicated that the general trend is completely different w respect of that in the solid state. More direct are the bar graphs reported in Figure 2.29, which show the intensity ratio and the percentage fraction of the spectra peaks referred to the complexes of cavitand with alcohol.
It is evident that in this case the affinity scale becomes opposite: n-PenOH>i-BuOH>n-BuOH>i-PrOH>n-PrOH>EtOH>MeOH.

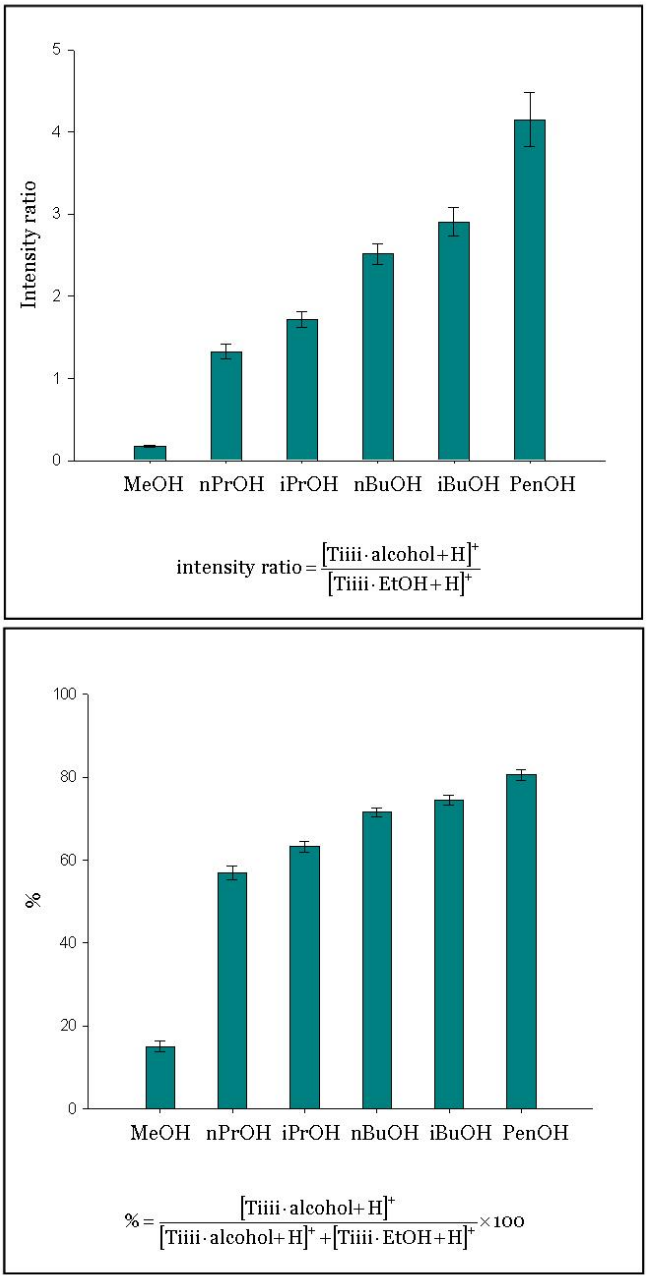

Figure 2.29. Mean intensity ratio and percentage fraction of Tiiii[H, CH_3, CH_3]·alcohol complexes in a competition experiment.

In summary, the stability of the resulting complexes increase with the increasing of the alcohol alkyl chain.
This because the effective parameters dictating complexation in the solid state are not the same in the gas phase. Some non covalent interactions are strengthened in the absence of solvent, while others become less important. Not only the lack of solvent but also the changes in vibrational modes of the host molecules in the gas phase affect the steric factors of the complex formation.
Moreover, compared with short chain alcohols, the longer ones can be considered less solvated because of their hydrophobic alkyl chains. The lower degree of solvation may contribute in the enhancement of complex formation and may increase the ionization efficiency of the complexes promoting the observation of the complexes after the ESI process.[29]

2.4.4 Responses of Tiiii[H, CH_3, CH_3] at the gas-solid interface

The overall set of results obtained so far, shows that the cooperative behaviour of four convergent P=O groups in H-bonding and the synergistic presence of CH-π interactions, drastically enhances and stabilizes the complexation of alcohols in the solid state and in the gas phase.
The progress capability of solid state and gas phase data in predicting the sensor properties of the corresponding cavitands will be tested by coating them on QCM transducers.
In the present work, we extensively study the gas sensing performances of tetraphosphonate cavitands toward several alcohols using QCM devices.
All tested cavitands have been coated on 10 MHz AT-cut QCM using spin coating technique (see Chapter 4), a thorough study of the coated layers morphology is also reported in the Chapter 4.
Moreover all measurements afterward depicted, have been performed following the procedure reported in the Appendix C.
At the beginning of this chapter, we described the reasons because we designed the Tiiii[H, CH_3, CH_3] cavitand was to maintain high selectivity while reducing the dispersive interactions affecting the mass sensing. Therefore we have excised the alkyl chains at the lower rim decreasing the possibility of extra versus intracavity positioning of the guest. On the other hand, a good layer permeability is strongly dependent on the morphology of the deposition: analyte diffusion is highly enhanced in amorphous layer with the respect to microcrystalline ones. In our case, the lack of the chains at the lower rim favours

crystallization, as confirmed by the relative ease that we have obtained the crystal structures in the solid state experiments.
Nevertheless, the Tiiii[H, CH_3, CH_3] cavitand tends to form stable crystals only in presence of an alcohol guest. Therefore spin coating deposition from trifluoroethanol solution leads to a stable amorphous layers (see Chapter 4 for morphological characterization).
Figure 2.31 reports the comparison among Tiiii[$C_{11}H_{23}$, H, CH_3], Tiiii[H, CH_3, CH_3] and TSiiii[$C_{11}H_{23}$, H, CH_3] toward several ppm of EtOH.
In this way, with the two Tiiii cavitands we could evaluate the weight of the long alkyl chain at the lower rim and with the TSiiii cavitand the importance of the H-bonding effect.

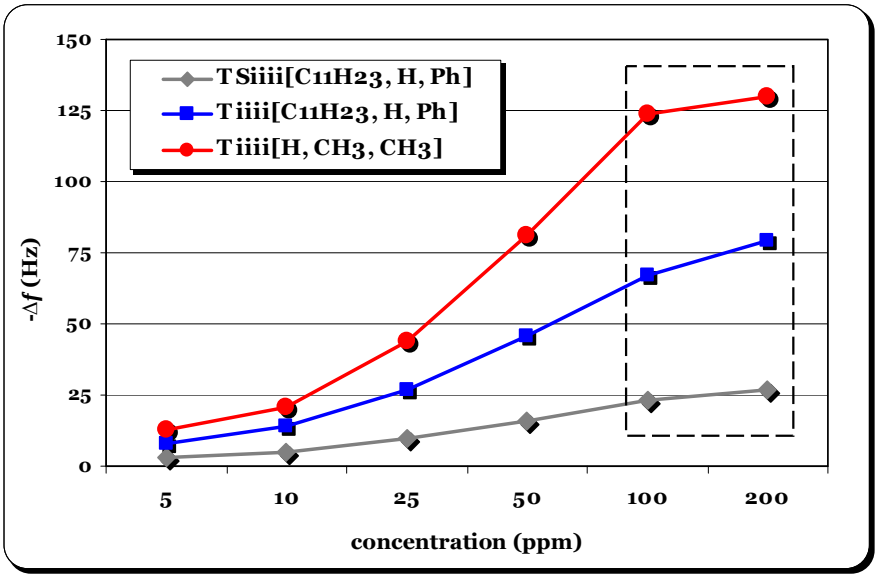

Figure 2.30. Trend of TSiiii[$C_{11}H_{23}$, H, CH_3], Tiiii[$C_{11}H_{23}$, H, CH_3] and Tiiii[H, CH_3, CH_3] to EtOH at several ppm.

The first observation regards the big difference between the responses of the Tiiii and TSiiii, that increases with the increasing of the ethanol concentration. This is consistent with our expectation and with the results already mentioned in the paragraph 2.3, since the TSiiii has limited H-bonding ability and its cavity is smaller, due to the bigger dimension of the sulphur compared to the oxygen.

Moreover also the gap in the responses of the two Tiiii cavitands is considerable and two are the possible reasons of this difference:

- at constant weight deposition (44 μg for 20 KHz), the number of Tiiii[H, CH_3, CH_3] molecules is much higher than that of Tiiii[$C_{11}H_{23}$, H, CH_3], due to the large difference in the MW (784.1 Da *versus* 1345.6 Da).

- the introduction of the methyl group in apical position on the Tiiii[H, CH_3, CH_3] generates a deeper cavity and enhance the π-basic character of the aromatic system. This probably contribute to increase the stability of the host-guest complex and consequently to enhance the responses.

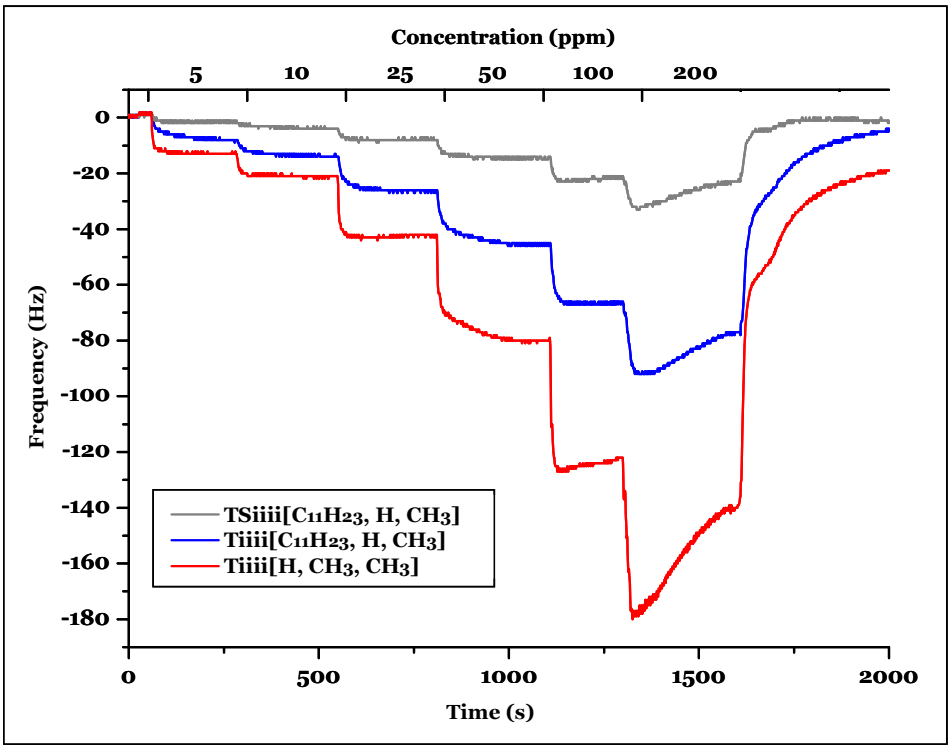

Figure 2.31. Responses traces to several concentration (ppm) of EtOH.

Figure 2.31 shows the response traces obtained exposing the cavitand layers to decreasing concentrations values of ethanol. The traces show a flat characteristic plateau (equilibrium of partition coefficient) up to 50 ppm. Above

this value the cavitand response is higher than the final equilibrium value, indicating extensive physisorption (see Chapter 4). Moreover this effect is much higher with the Tiiii[H, CH_3, CH_3] cavitand without chains at the lower rim.
Similar results were obtained exposing the same cavitand layers to growing concentration of both butanol and pentanol (Figure 2.32).

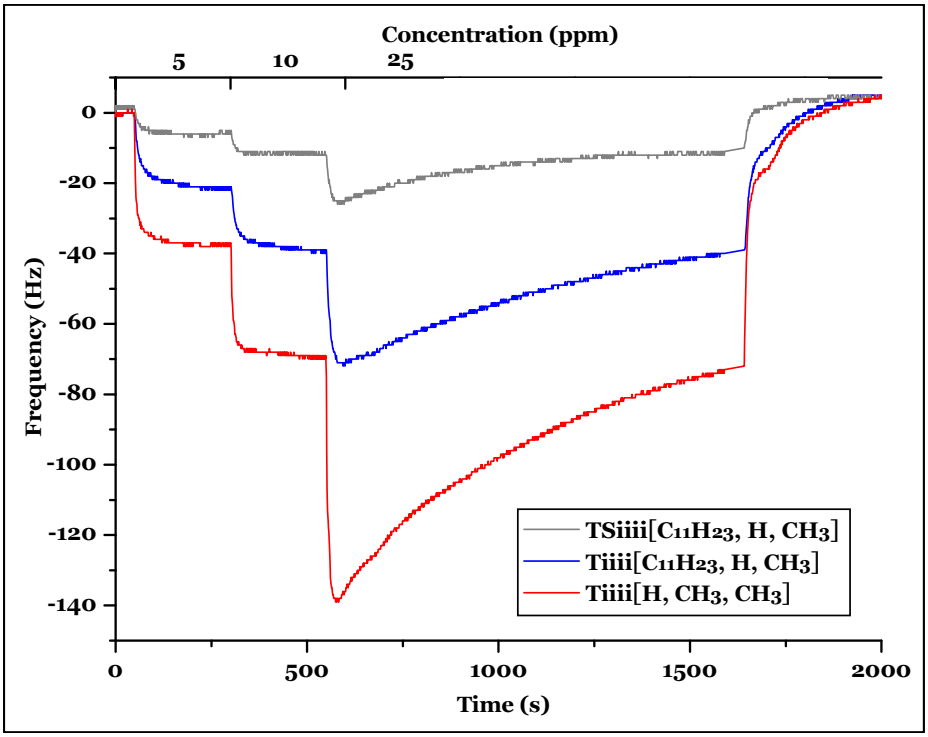

Figure 2.32. Responses traces to several concentration (ppm) of n PeOH.

In either case the saturation of each layer is reached in advance, at 25 ppm.
Why with butanol and pentanol the saturation is already reached at these ppm? A reasonable explanation can be related to the alkyl chain length which probably alter the adsorption of the analytes across the layer. Evidently, the physisorption process is already dominating at 25 ppm, due to higher affinity of long chain alcohols for organic layers.
In the next step, involve the study of the selectivity pattern of these three cavitands toward linear alcohols. We want to see if the trend is consistent with previous results. We performed the same experiment at two different concentrations of each alcohols: 5 and 25 ppm. In the first case, we can exclude

the saturation of the layers and therefore we can evaluate the selectivity toward all alcohols under the same conditions.

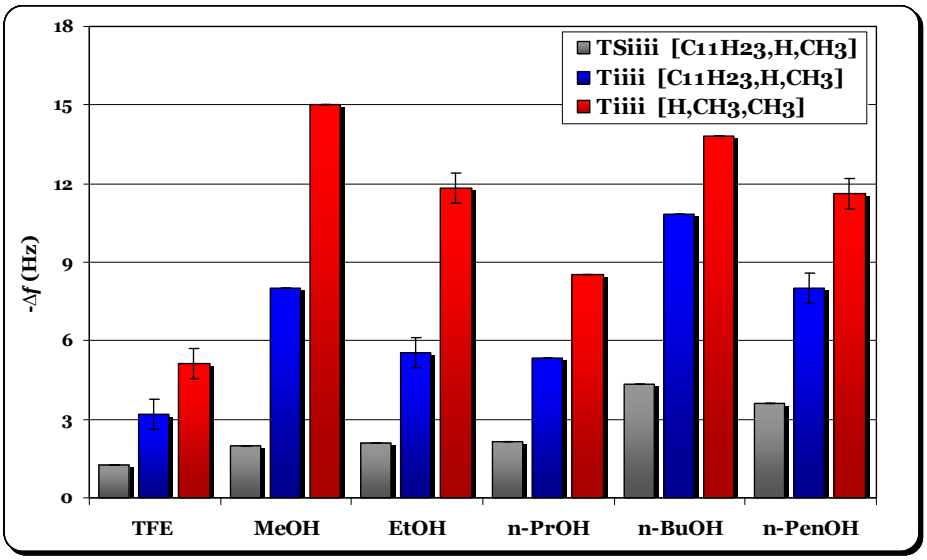

Figure 2.33. Selectivity pattern of TSiiii[$C_{11}H_{23}$, H, CH_3], Tiiii[$C_{11}H_{23}$, H, CH_3] and Tiiii[H, CH_3, CH_3] to TFE and C_1-C_5 linear alcohols at 5 ppm.

Looking Figure 2.33, we can tell that solid state prediction are only partially confirmed. In the case of trifluoroethanol the responses are very low and smaller than the other ones. This result is a further confirmation of the solid state and the gas phase data where trifluoroethanol does not form a stable complex with the tetraphosphonate cavitands.

Moreover also the trend from methanol to propanol follows the solid state behaviour. The affinity scale indeed decrease with the increasing of the chain. The difference appears in the case of n-BuOH and n-PenOH: with butanol the responses became higher than with ethanol, and with pentanol the responses decrease only a partially with respect to butanol. This is due to a significant increase of unspecific interactions, as show the enhancement of the TSiiii responses with these two alcohols, but probably this is not the only one reason.

The contribution of the dispersion interactions experienced by the analytes is small significant when we work at this low concentrations. Indeed the enhancement of the TSiiii responses, observed with the increasing of the alcohol chain length, is little in comparison with the enhancement observed when we

worked at high concentration (1500 ppm) mentioned in the paragraph 2.3 (Figure 2.9).
The comparison between the two Tiiii shows that the cavitand without chains at the lower rim have higher responses than the cavitand with long chains toward all alcohols. Moreover, the difference in the responses between the two Tiiii in the case of MeOH and EtOH (~8 Hz) is bigger than with the longer alkyl chain alcohols (~3 Hz). This means that the dispersive interactions, even if not much decisive at low ppm, increase more the responses of the cavitand with long chains at the lower rim in respect of the cavitand without chains. Therefore the Tiiii[H, CH_3, CH_3] turn out to be slightly more selective for the short alcohols.
Nevertheless in the solid state studies, mentioned above, we have presumed that pentanol were too long to go inside the cavity and form, at the same time, H-bonding with a phosphonate group. The resulting question which arose is: Why pentanol shows responses so high at the gas-solid interface? We would have expected that pentanol had the same behaviour of trifluoroethanol, with responses low and smaller than the other ones.
One explanation can be draw looking the results obtained in the gas phase, where the trend of the affinity scale is completely opposite. At the beginning we have assumed that an appropriate way to explore the binding affinity of cavitands, in view to study gas-solid interactions is the combined use of X-Ray (solid state) and ESI-MS (gas phase) studies.
Moreover we have to remember that in the ESI-MS experiments we have seen the complex of the Tiiii[H, CH_3, CH_3] with n-PenOH. Therefore is not strange if also at the gas-solid interface the cavitand on the layer is able to complex this alcohol. On the other hand, since the energies involved are different, the perfect correlation between these three techniques is certainly possible from the qualitative viewpoint, but probably not always quantitatively.

2.5 Conclusions

The rich chemistry of phosphorous bridged cavitands has been explored, from synthesis and stereochemistry, to complexation properties and sensors applications. In specific, the challenges encountered in tuning cavitands as selective layers for mass sensors toward alcohols have been outlined.
The key factors affecting the sensing performances of phosphorous bridged cavitands toward alcohols are:

- pre-organized cavity: free volume available to the analyte pivotal for effective H-bonding.
- presence of synergistic CH-π and H-bonding interactions (specific interactions).
- network of energetically equivalent H-bonding options available to the analyte.

The combined use of ESI-MS and crystallographic analyses allows to anticipate the molecular recognition properties of cavitands at the gas-solid interface, when the dominant interactions in the two phases coincide.
We have removed the peripheral alkyl chains at the lower rim of the cavitand, minimizing the undesired dispersion interactions between the analyte and the sensing material.
Moreover the Tiiii[H, CH_3, CH_3] coated layer showed a very high sensibility toward all alcohols also a low concentration (5 ppm). On the other hand, it did not show the expected selectivity for short chain alcohols.
Two different approaches can be followed to solve this problem:

- use of an inherently selective transduction mechanism, such as surface plasmon resonance or fluorescence technique.
- modification of the tetraphosphonate cavitands structure by introducing other aspects capable to improve the selectivity toward short chain alcohols, how will be reported in the next chapter.

2.6 Acknowledgements

Special thanks to Prof. Silvano Geremia and Rita De Zorzi of the University of Trieste for the X-Ray crystallographic studies, and to Dr. Elina Kalenius of the University of Joensuu (Finland) for the ESI-MS analyses.

2.7 Experimental section

Resorcinarene [H, CH_3]

To a mixture of 2-methylresorcinol (12.22 g, 0.098 mol) and 95% paraformaldehyde (5.26 g, 1.48 mol) in absolute ethanol (170 mL) concentrated hydrochloric acid (10 mL) was added. The mixture was stirred at 80°C for 48 hours. The resulting precipitate was collected by filtration, washed with water, acetone and methylene chloride several times, to give the desired compound as light pink solid (12.13 g, 91%). **^{1}H NMR** (DMSO-d_6, 300 MHz): δ = 8.58 (s, 8H, ArO*H*), 6.76 (s, 4H, ArH_{down}), 3.58 (s, 8H, Ar_2CH_2), 1.98 (s, 12H, ArCH_3). **ESI-MS**: m/z 543.3 $[M-H]^-$.

Cavitand T_{iiii}[$C_{11}H_{23}$, H, CH_3]

Dichloromethylphosphate (721 µL, 7.96 mmol) and N-methylpirrolidine (213 µL, 2.04 mmol) were added, under nitrogen, to a solution of resorcinarene (2.0 g, 1.81 mmol) in 100 mL of anhydrous toluene. The mixture was stirred at 112°C for 5 hours. After evaporation of the solvent, the crude product was purified by column chromatography (SiO_2, CH_2Cl_2:EtOH, 9:1) to give the desired compound as white solid (1.53 g, 63%).**^{1}H NMR** ($CDCl_3$, 300 MHz): δ = 7.14 (s, 4H, ArH_{down}), 6.81 (s, 4H, ArH_{up}), 4.59 (t, 4H, ^{3}J=7.6 Hz, RC*H*Ar_2), 2.25 (m, 8H, CHCH_2R), 1.85 (d, 12H, ^{2}J=18 Hz, POCH_3), 1.42-1.26 (m, 72H, -CH_2-), 0.86 (t, 12H, ^{3}J=6.9 Hz, -CH_3). **^{31}P NMR** ($CDCl_3$, 162 MHz): δ = 5.83 (s, 4P, *P*OAr). **ESI-MS**: m/z 1345.4 $[M+H]^+$, 1367.3 $[M+Na]^+$.

Cavitand T_{iiii}[H, CH_3, CH_3]

Dichloromethylphosphate (1.46 mL, 16.17 mmol) and N-methylpirrolidine (432 µL, 4.15 mmol) were added, under nitrogen, to a suspension of resorcinarene (2.0 g, 3.67 mmol) in 100 mL of anhydrous dichlorobenzene. The mixture was stirred at 140°C for 24 hours. After evaporation of the solvent, the crude product was purified by column chromatography (SiO_2, CH_2Cl_2:MeOH, 8:2) to give the desired compound as white solid (0.81 g, 28%). **^{1}H NMR** ($CDCl_3$/MeOD, 300 MHz): δ = 6.99 (s, 4H, ArH_{down}), 4.19 (d, 4H, ^{3}J=13 Hz, $Ar_2CH_{2eq.}$), 3.36 (d, 4H, ^{3}J=13 Hz, $Ar_2CH_{2ax.}$), 1.98 (s, 12H, ArCH_3), 1.81 (d, 12H, ^{2}J=18 Hz, POCH_3). **^{31}P NMR** ($CDCl_3$/MeOD, 162 MHz): δ = 22.03 (s, 4P, *P*OCH_3). **ESI-MS**: m/z 785.3 $[M+H]^+$, 823.3 $[M+K]^+$.

2.8 References

[1] D.J. Cram, J.M. Cram, *in Container Molecules and Their Guests* (ED.:J. F. Stoddart), The Royal Society of Chemistry, Cambridge, **1994**, Chapter 5.

[2] D.J. Cram, S. Karbach, H.-E. Kim, C.B. Knobler, E.F. Maverick, J.L. Ericson, R.C. Helgeson, *J. Am. Chem. Soc.* **1988**, *110*, 2229.

[3] a) J.A. Tucker, C.B. Knobler, K.N. Trueblood, D.J. Cram, *J. Am. Chem. Soc.* **1989**, *111*, 3688; b) P. Soncini, S. Bonsignore, E. Dalcanale, F. Ugozzoli, *J. Org. Chem.* **1992**, *57*, 4608; d) T. Haino, D.M. Rudkevich, A. Shivanyuk, K. Rissanen, J. Rebek, Jr., *Chem. Eur. J.* **2000**, *6*, 3797; e) K. Paek, J. Cho, *Tetrahedron Lett.* **2001**, *42*, 1927.

[4] a) M. Vincenti, E. Dalcanale, P. Soncini, G. Guglielmetti, *J. Am. Chem. Soc.* **1990**, *112*, 445; b) M. Vincenti, E. Pelizzetti, E. Dalcanale, P. Soncini, *Pure Appl. Chem.* **1993**, *65*, 1507.

[5] a) A.-M. Caminade, J.-P. Majoral, *Chem. Rev.* **1994**, *94*, 1183. b) L. Van Oostenryck, B. Tinant, J.-P. Declerercq, J.-P. Dutasta, P. Simon, *J. Incl. Phenom.* **1993**, *16*, 383; c) J.-P. Declerercq, P. Delangle, J.-P. Dutasta, L. Van Oostenryck, P. Simon, B. Tinant, *J. Chem. Soc., Perkin Trans. 2* **1996**, 2471.

[6] a) J. Mitjaville, A.-M. Caminade, R. Mathieu, J.-P. Majoral, *J. Am. Chem. Soc.* **1994**, *116*, 5007; b) C.B. Allan, L.O. Spreer, *J. Org. Chem.* **1994**, *59*, 7695; c) A.-M. Caminade, R. Kraemer, J.-P. Majoral, *New J. Chem.* **1997**, *21*, 627.

[7] P. Delangle, J.-P. Dutasta, J.-P. Declerercq, B. Tinant, *Chem. Eur. J.* **1998**, *4*, 100.

[8] a) P. Timmerman, W. Verboom, D.N. Reinhoudt, *Tetrahedron* **1996**, *52*, 2663; b) D.M. Rudkevich, J.Rebek, Jr., *Eur. J. Org. Chem.* **1999**, 1991.

[9] a) A.G.S. Högberg, *J. Am. Chem. Soc.* **1980**, *102*, 6046-6050; b) A.G.S. Högberg, *J. Org. Chem.* **1980**, *45*, 4498; c) L.M. Tunstadt, J.A. Tucker, E. Dalcanale, J. Weiser, J.A. Bryant, J.C. Sherman, R.C. Helgeson, C.B. Knobler, D.J. Cram, *J. Org. Chem.* **1989**, *54*, 1305.

[10] K.D. Stewart, Ph.D. Dissertation, University of California, Los Angeles, **1984**.

[11] a) T. Lippmann, E. Dalcanale, G. Mann, *Tetrahedron Lett.* **1994**, *35*, 1685; b) T. Lippmann, H. Wilde, E. Dalcanale, L. Mavilla, G. Mann, U. Heyer, S. Spera, *J. Org. Chem.* **1995**, *60*, 235.

[12] R. Pinalli , M. Suman, E. Dalcanale, *Eur. J. Org. Chem.* **2004,** *3*, 451.

[13] a) W. Xu, J. P. Rourke, J.J. Vittal, R.J. Puddephatt, *J. Chem. Soc., Chem. Commun.* **1993**, 145; b) W. Xu, J.J. Vittal, R.J. Puddephatt, *J. Am. Chem. Soc.* **1993**, *115*, 6456; c) W. Xu, J. P. Rourke, J.J. Vittal, R.J. Puddephatt, *Inorg. Chem.* **1995**, *34*, 323; d) W. Xu, J.J. Vittal, R.J. Puddephatt, *J. Am. Chem. Soc.* **1995**, *117*, 8362; e) W. Xu, J.J.

Vittal, R.J. Puddephatt, *Inorg. Chem.* **1997**, *36*, 86; f) D.J. Eisler, C.W. Kirby, R.J. Puddephatt, *Inorg. Chem.* **2003**, *42*, 7626; g) D.J. Eisler, R.J. Puddephatt, *Inorg. Chem.* **2005**, *44*, 4666; h) D.J. Eisler, R.J. Puddephatt, *Inorg. Chem.* **2006**, *45*, 7295.

[14] a) E.E. Nifantyev, V.I. Maslennikova, E.V. Panina, A.R. Bekker, L.K. Vasyanina, K.A. Lysenko, M.Y. Antipin, Y.T. Struchkov, *Mendeleev Commun.* **1995**, 131; b) V.I. Maslennikova, E.V. Panina, A.R. Bekker, L.K. Vasyanina, E.E. Nifantyev, *Phosphorus Sulfur Silicon* **1996**, *113*, 219; c) E.E. Nifantyev, V.I. Maslennikova, R.V. Merkulov, *Acc. Chem. Res.* **2005**, 108.

[15] a) P. Delangle, J.-P. Dutasta, *Tetrahedron Lett.* **1995**, *36*, 9325; b) P. Delangle, J.-C. Mulatier, B. Tinant, J.-P. Declercq, J.-P. Dutasta, *Eur. J. Org. Chem.* **2001**, 3695; c) B. Bibal, B. Tinant, J.-P. Declercq, J.-P. Dutasta, *Supramol. Chem.* **2003**, *15*, 25.

[16] P. Jacopozzi, E. Dalcanale, S. Spera, L.A.J. Chrisstoffels, D.N. Reinhoudt, T. Lippmann, G. Mann, *J. Chem. Soc., Perkin Trans. 2* **1998**, 671.

[17] a) B. Bibal, B. Tinant, J.-P. Declercq, J.-P. Dutasta, *Chem. Comm.* **2002**, 432; b) B. Bibal, J.-P. Declercq, J.-P. Dutasta, B. Tinant, A.-G. Valade, *Tetrahedron* **2003**, 5849-5854.

[18] R.M. Yebeutchou, Ph.D. Thesis, University of Parma, **2008**.

[19] L. Pirondini, E. Dalcanale, *Chem. Soc. Rev.* **2007**, *35*, 695.

[20] J. Janata, in Principles of Chemical Sensors, Plenum press, New York, USA, **1989**.

[21] R. Pinalli , F.F. Nachtigall, F. Ugozzoli, E. Dalcanale, *Angew. Chem. Int. Ed. Engl.* **1999,** *38*, 2377.

[22] M. Suman, M. Freddi, C. Massera, F. Ugozzoli, E. Dalcanale, *J. Am. Chem. Soc.* **2003**, *125*, 12068.

[23] R. Paolesse, C. Di Natale, S. Nardis, A. Magagnano, A. D'Amico, R. Pinalli, E. Dalcanale, *Chem. Eur. J.* **2003**, *9*, 5388.

[24] J. Laskin and J.H. Futrell, *Mass Specrom. Rev.* **2005**, *24*, 135.

[25] J.M.J. Nuutinen, A. Irico, M. Vincenti, E. Dalcanale, J.M.H. Pakarien, P. Vainiotalo *J. Am. Chem. Soc.* **2000**, *122*, 10090.

[26] D. Reyntjens-Van Damme, T. Zeegers-Huyskens, *J. Phys. Chem.* **1980**, *84*, 282.

[27] H. Konishi, Y. Iwasaki, O. Morikawa, T. Okano, J. Kiji, *Kinki Chem. Soc.* **1990**, *5*, 869.

[28] H. Konishi, K. Ohata, O Morikawa, K. Kobayashi, *J. Chem. Soc. Chem. Comm* **1995**, 309.

[29] E. Ventola, P. Vainiotalo, M. Suman, E. Dalcanale, *J. Am. Soc. Mass Spectrom.* **2006**, *17*, 213.

Mixed bridged thio-phosphonate cavitands

3

3.1 Introduction

One of the key issue in the development of new, efficient chemical sensors is the quest for selectivity. Selectivity can be defined as the ability of the sensor to respond primarily to only one species in the presence of others analytes.
Biological strategy is to involve *shape recognition*, in other word, stereospecificity. As for biological systems, the concepts of shape recognition and binding site complementarity are central for effective molecular recognition in artificial host-guest systems.
The previous chapter has shown that the use of cavitands as chemically sensitive layers provides alcohols selective QCM sensors if only specific interactions, such as CH-π and H-bonding interactions, are present between the preorganized cavity of the receptor and the analyte. These interactions perturb the selectivity pattern expected on the basis of pure dispersion interactions between the analyte and the cavitand layer by adding their contribution to the sensor responses.

3.2 New mixed bridged thio-phosphonate cavitands

In order to increase the selectivity toward short chain alcohols, we have considered the possibility to modify the structure of the tetraphosphonate cavitands.

The results showed in Chapter 2, have demonstrated that the entropic stabilization of host-guest complexes via energetically equivalent multiple interactions is a viable route to enhance sensitivity in mass sensors, while retaining full reversibility. On the other hand to achieve high selectivity for short chain alcohols we have to improve the structure, conceiving a smaller cavity able to host only some complementary guests.

By comparing the molecular modelling of Tiiii and TSiiii cavitands (Figure 3.1), the idea to replace one or two P=O with P=S groups was conceived. The one and only one structural difference that we can see in the modelling, is the bigger dimension of the sulphur compared to the oxygen. We have already discussed about the different H-bonding ability of these two cavitands, but in this case we want to focus the attention only on the structure.

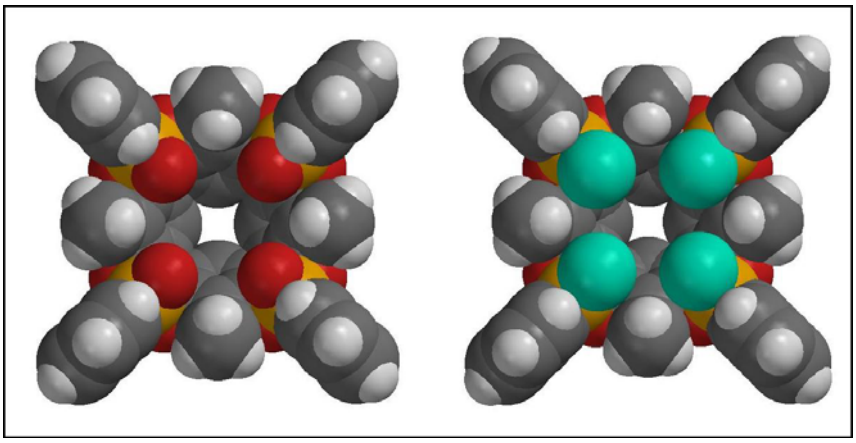

Figure 3.1. Molecular modelling of Tiiii[H, CH_3, Ph] and TSiiii[H, CH_3, Ph].

The presence of one or two P=S groups instead of P=O groups creates a smaller cavity with lower symmetry. This should reduce the access to the cavity for long chain alcohols with a consequent enhancement of the selectivity toward short alcohols, consisting of mainly C_1 and C_2 chains. Obviously this effect occurs at the expense of sensitivity because decreasing the P=O number reduces the

number of energetically equivalent multiple interactions, stabilizing the host-guest complex.

Since the sensitivity of the tetraphosphonate cavitands at the gas-solid interface, is very high, reaching the low ppm regime, the replacement of some P=O with P=S should not create problems in the QCM responses.

Therefore, we have designed the three new tetra thiophosphonate cavitands depicted in Scheme 3.2. The proposed nomenclature shows that: the number and the following capital letter, define number and nature of the bridges, the lower case letters define the in-out stereochemistry, and in the brackets are indicated the substituents at the lower rim are indicated, in the apical positions and on the phosphorous stereocenters respectively. Since in 2POii2PSii[H, CH_3, Ph] the reaction is not selective, it leads to the formation of two different isomers. We use AB or AC prefix to indicate the vicinal or distal position of the P=S groups, respectively.

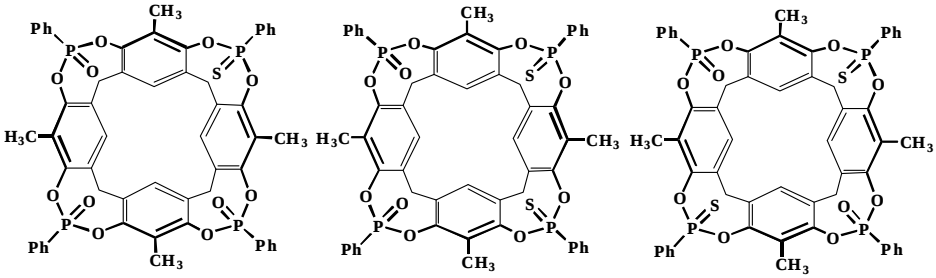

Scheme 3.2. Thio-phosphonate cavitands: 3POiii1PSi[H, CH_3, Ph], AB and AC 2POii2PSii[H, CH_3, Ph].

As in Chapter 2, these cavitands bear a methyl group in apical position and no chains at the lower rim to maximize specific interactions in the solid layer. Therefore, the only two differences are in the partial substitution of the P=O with P=S groups, and in the phenyl group on the phosphonate moiety. The reason of the presence of this phenyl instead of the methyl group, used in all cavitands previously described, is that from now onward, we will follow the new synthetic route already mentioned in paragraph 2.2, completely different with respect to that previously reported (Scheme 2.11). Indeed, the most important advantage of this synthesis, that is the formation of only the stereoisomer Tiiii, is not achievable with the methyl group, probably because the phenyl enables the stabilization of the P^{III} intermediate, depicted below (Scheme 3.3).

We describe this new synthetic approach starting from the synthesis of the corresponding tetraphosphonate Tiiii[H, CH_3, Ph] and tetra thiophosphonate TSiiii[H, CH_3, Ph] cavitands, which will serve as a meaningful comparison in the sensor responses.

As is outlined in Scheme 3.3, this procedure was conducted with dichlorophenylphosphine (P^{III}) instead of dichlorophenylphosphine oxide (P^{V}).

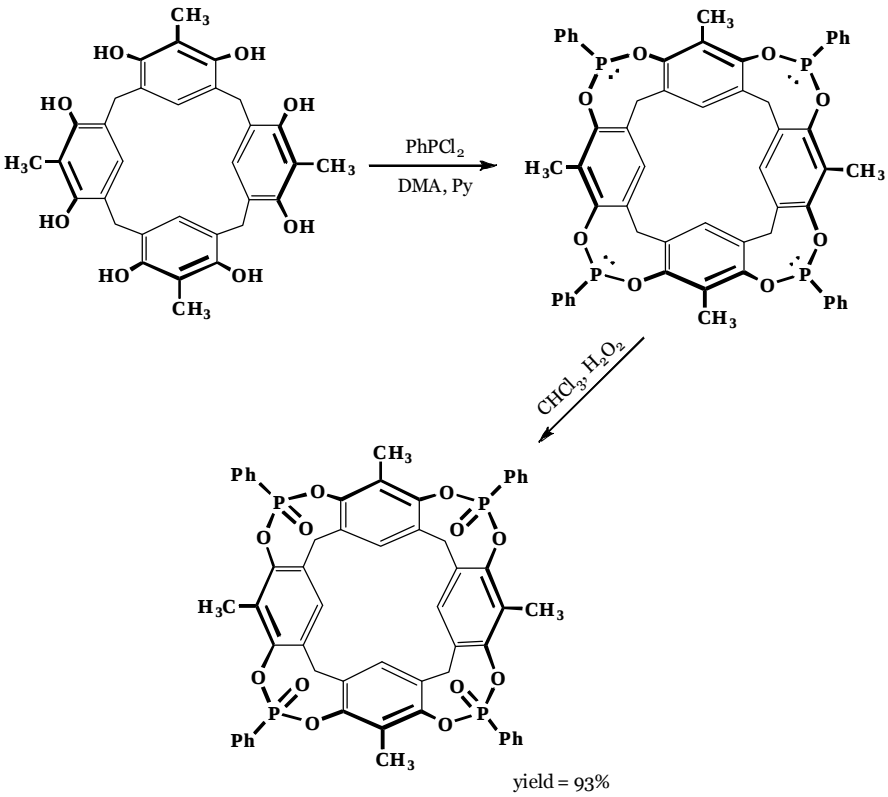

Scheme 3.3. Synthesis of Tiiii[H, CH_3, Ph].

The first important peculiarity of this reaction is that the first step leads to the stereoselective formation of only one non-isolable stereoisomer. Indeed in the presence of anhydrous DMA, as solvent, and distilled pyridine, as base, the only product is the tetraphosphonito cavitand with four lone pair directed inward the cavity.

The second central feature concerns the subsequent *in situ* oxidation with hydrogen peroxide, which proceeds with retention of configuration at the phosphorous centre. In this second step, the addition of the $CHCl_3/H_2O_2$ mixture causes the precipitation of the pure Tiiii[H, CH_3, Ph] cavitand without need of chromatographic purification. This obviously simplifies the procedure and drastically increases the yield (93% instead of 28% of the previous procedure).

The same approach was followed to synthesize the TSiiii[H, CH_3, Ph] cavitand. The only difference is in the second step where the oxidation was made by addition of sulphur (Scheme 3.4). Also in this case we obtained the compound pure by precipitation and in high yield.

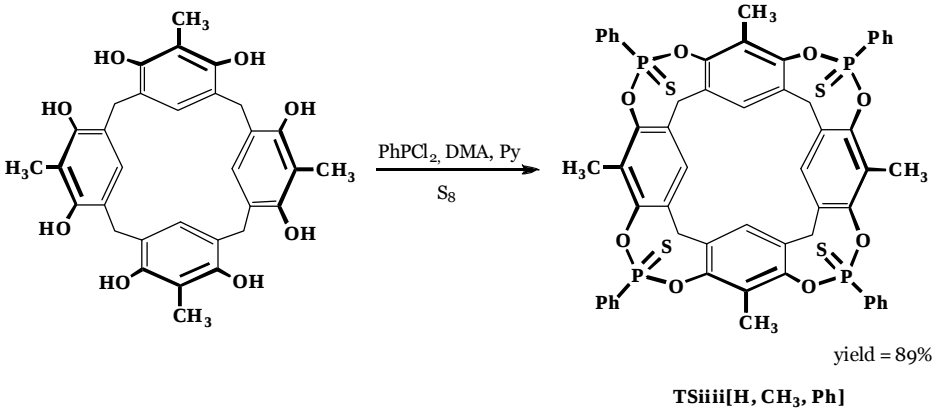

Scheme 3.4. Synthesis of TSiiii[H, CH_3, Ph].

The characterization by the ^{1}H NMR and ^{31}P NMR of Tiiii[H, CH_3, Ph] and TSiiii[H, CH_3, Ph] is a suitable proof of the pure cavitands obtained. We can observe that in the ^{1}H NMR spectra (Figure 3.5), the only difference is in the slight down field shift of the characteristic multiplet (red and blue dashed box) of the ortho aromatic protons of the thio-phosphonate moiety. On the contrary, with the ^{31}P NMR we obtained for each cavitand a diagnostic signal. Indeed the phosphorus chemical shift of the P=O group is in a higher field region (δ=4.82 ppm) than the phosphorus chemical shift of the P=S one (δ=74.55 ppm).

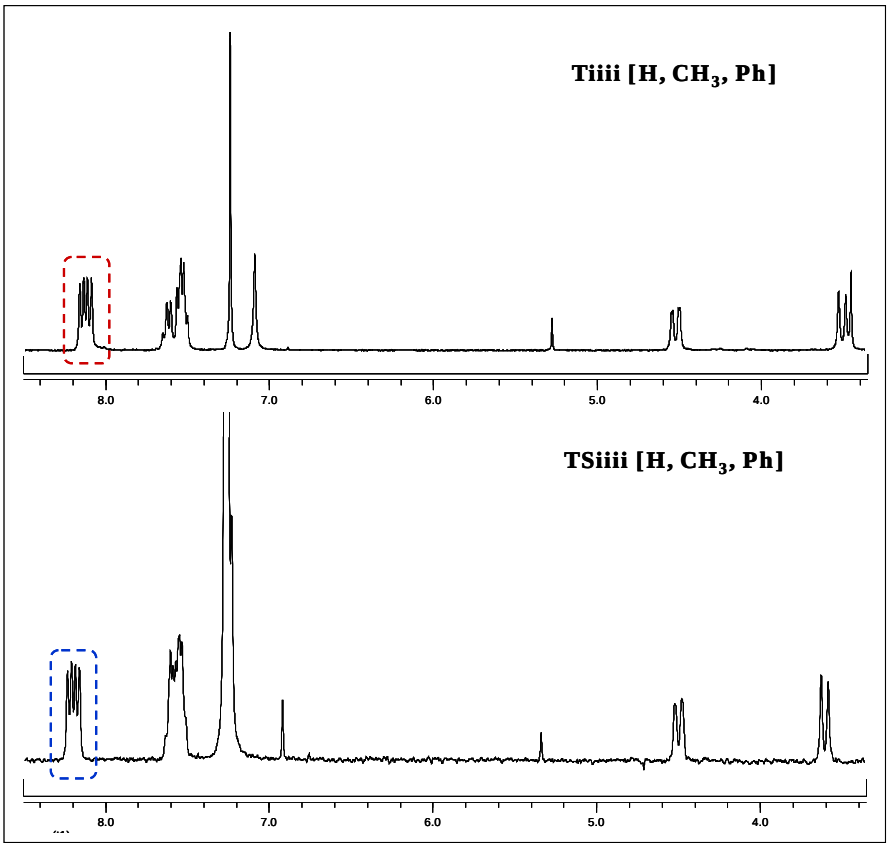

Figure 3.5. ^{1}H NMR of Tiiii[H, CH_3, Ph] and TSiiii[H, CH_3, Ph].

For the synthesis of the partially substituted thio-phosphonate cavitand we just adapted the previous two procedures.

We obtained the 3POiii1PSi[H, CH_3, Ph] by adding, in the second step, one equivalent of sulphur and after 1 hour the mixture $CDCl_3/H_2O_2$, to complete the oxidation.

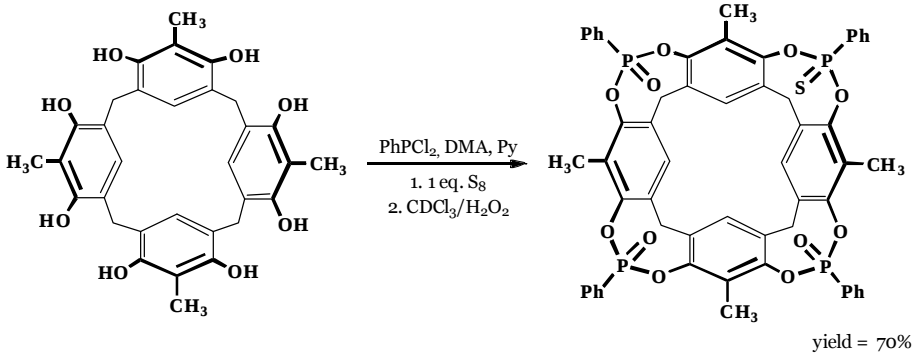

Scheme 3.6. Synthesis of 3POiii1PSi[H, CH_3, Ph].

As predictable, in this case we obtained also the formation of corresponding the tetraphosphonate cavitand corresponding, which was separated via column chromatography. The ^{1}H NMR (Figure 3.7a) confirms the presence of two signals, in 1:3 ratio, regarding the aromatic protons in ortho of the P=S (blue dashed box) and P=O (red dashed box) phenyl group, respectively.

The ^{31}P NMR spectrum is also diagnostic: it shows three different signals belonging respectively to the 3 P=O (red dashed box), in a 2:1 ratio, at high field and to the P=S (blue dashed box) at low field.

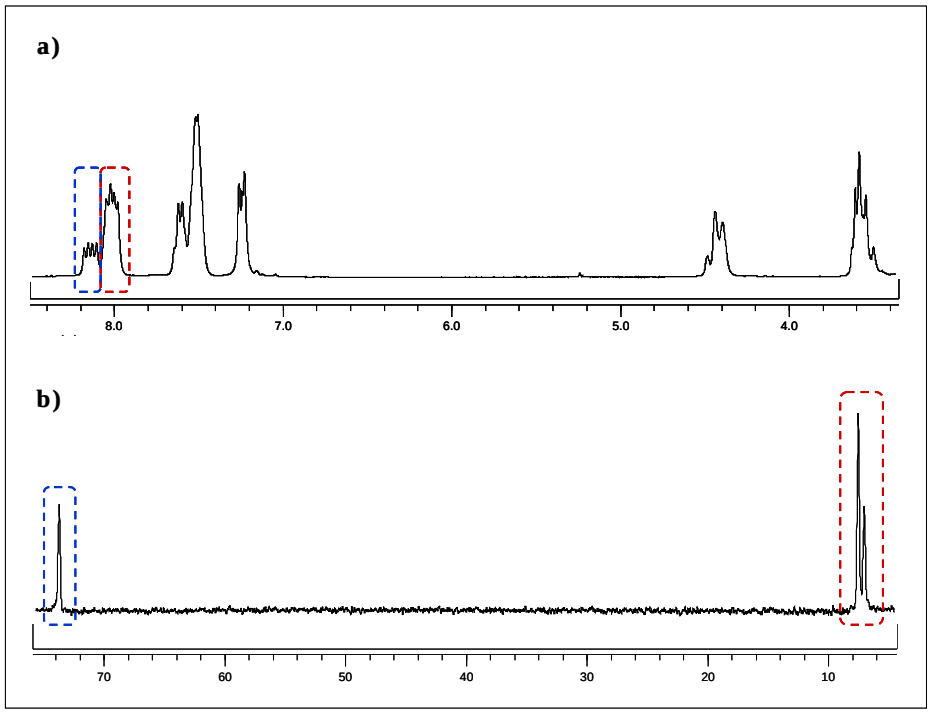

Figure 3.7. ^{1}H NMR (a) and ^{31}P NMR (b) of 3POiii1PSi[H, CH_3, Ph].

Using 2.5 equivalents of sulphur instead of 1 equivalent, we obtained 2POii2PSii[H, CH_3, Ph]. Since the reaction is not selective it leads to the formation of two different isomers which have the P=S groups in vicinal (ABii) or distal (ACii) position.

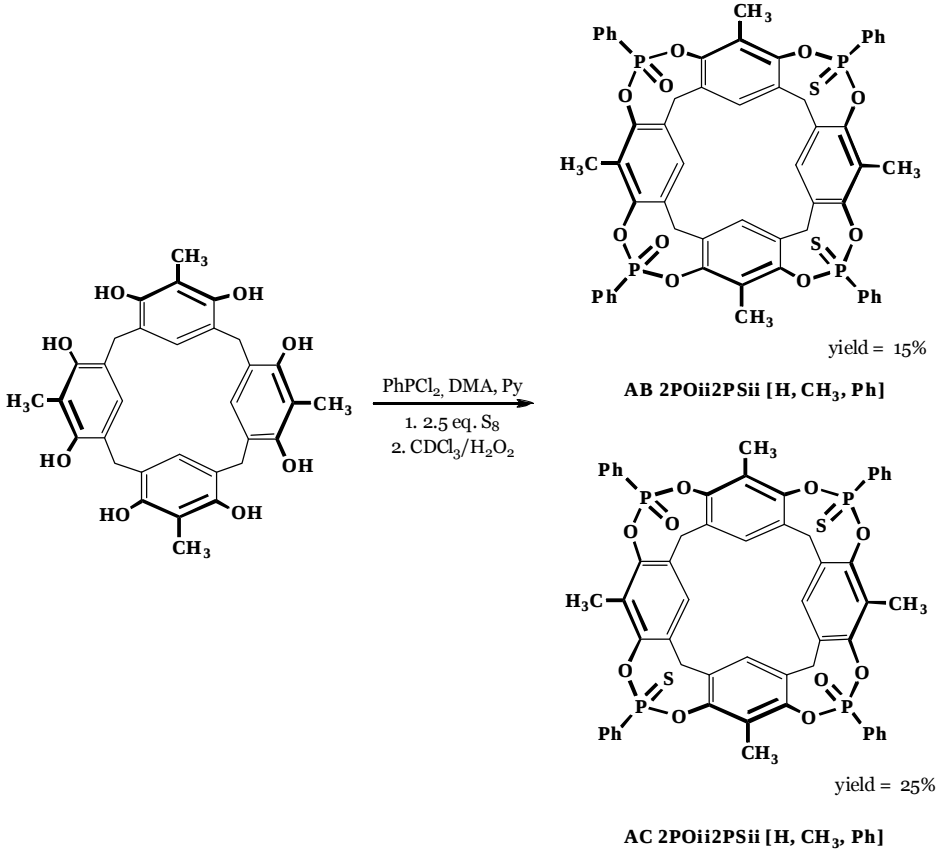

Scheme 3.8. Synthesis of 2POii2PSii[H, CH_3, Ph].

The separation was done by customary chromatographic column because they have a completely different R_f. On the other hand, the identification of the two isomers by ^1H NMR was difficult because the different symmetry of the two structures gives only a slight difference in the signals of the methyl groups in apical position. In the case of ^{31}P NMR, no chemical shift difference is observed for the two stereoisomers. In Figure 3.9, the ^1H NMR and the ^{31}P NMR spectra of the ACii are reported.

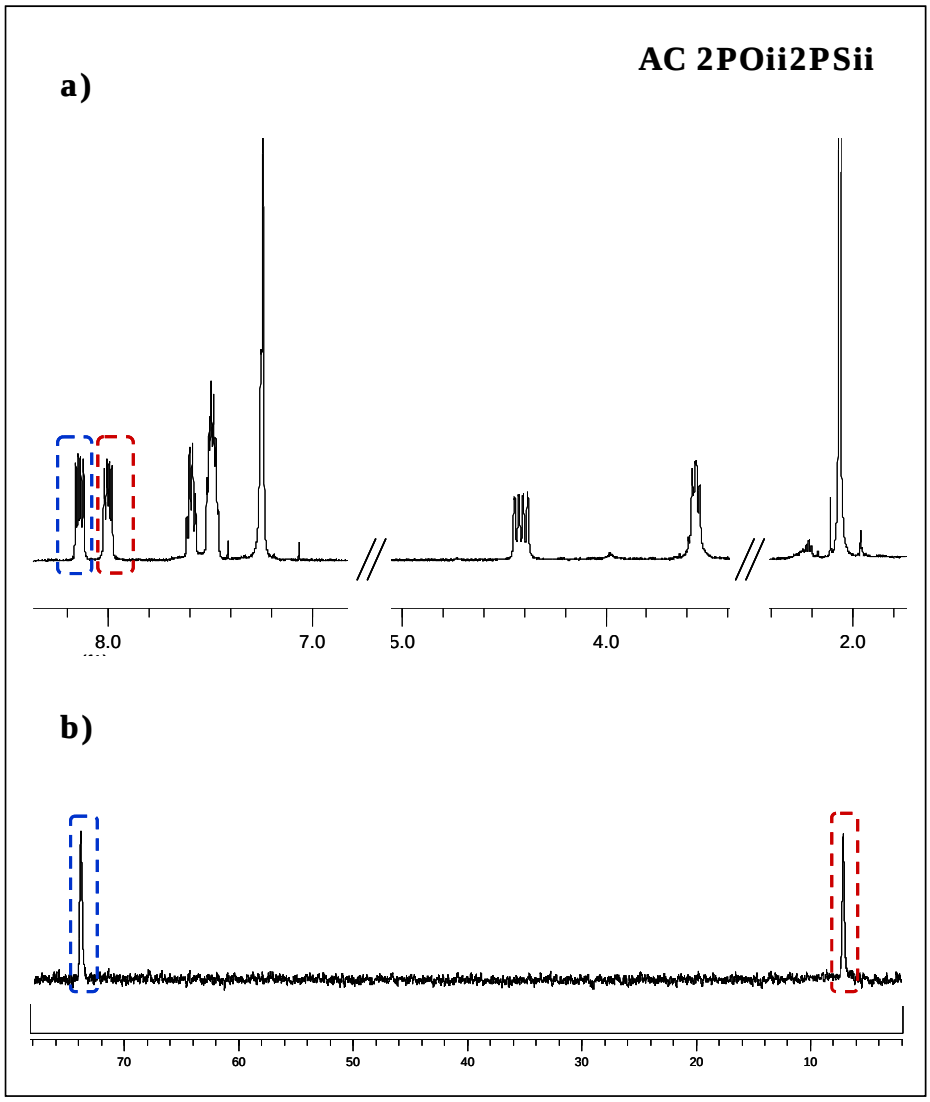

Figure 3.9. ^{1}H NMR (a) and ^{31}P NMR (b) of AC 2POii2PSii[H, CH_3, Ph].

Therefore X-Ray crystallography was employed to asses the correct stereochemistry of the two isomers. The crystal structures (Figure 3.10 and 3.11) show how both the 2POii2PSii[H, CH_3, Ph] isomers are able to complex MeOH according to the generality of the cavitand-alcohol interaction mode, based on the synergy between H-bonding to a P=O group and CH-π interactions of the methyl residue with the cavity.

Both crystals were obtained by evaporation of a CH_3OH/CH_2Cl_2 solution of the AB and AC 2POii2PSii[H, CH_3, Ph] cavitands.

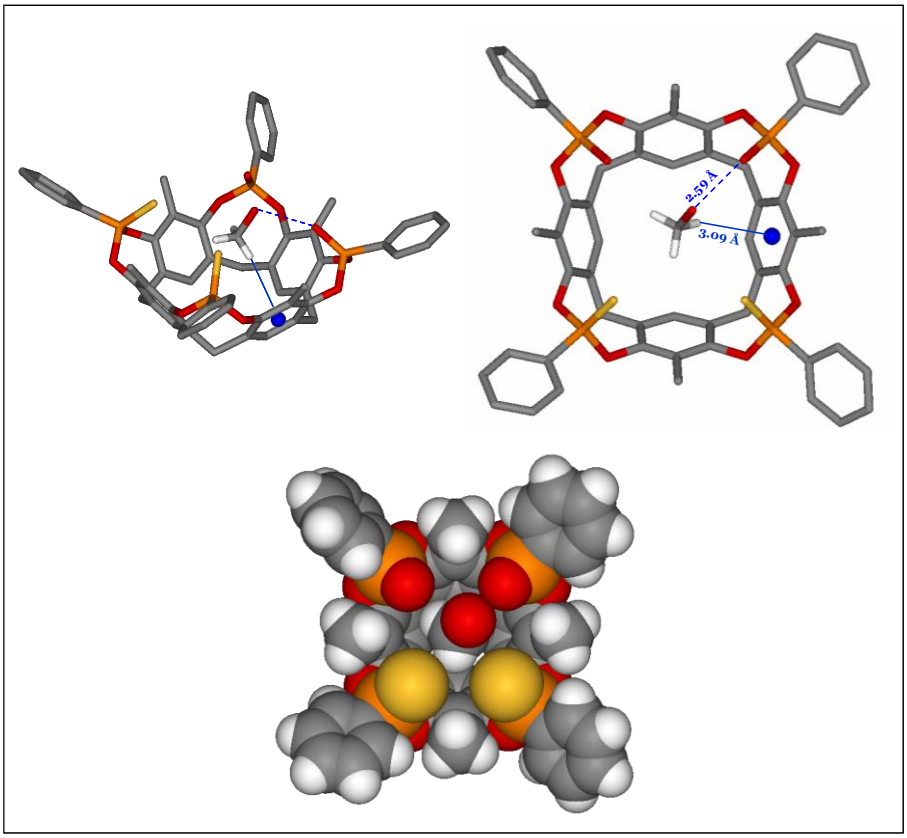

Figure 3.10. Crystal structure of the AB 2POii2PSii[H, CH_3, Ph]•MeOH complex. (Colour code: P, orange; O, red; S, yellow; C, grey; H, white; weak intermolecular interactions and centroids, blue). The hydrogen atoms not involved in the interactions are omitted for clarity.

In the AB isomer, one methanol solvent is located inside the cavity. The host-guest attraction is principally due to:

- a CH···π interaction between one hydrogen atom of the methylic group and one phenyl ring of the resorcinarene skeleton [H···centroid 3.097(5) Å, C-H···centroid 157.12(6)°];
- a strong H-bond involving the hydroxyl group of the alcohol and one phosphonate moiety at the upper rim [MeO···O=P 2.586(9) Å].

In contrast to the behaviour displayed by the cavitands containing only P=O groups, the guest molecule is not disordered over two energetically and geometrically equivalent positions. In this case the stabilization comes from the synergistic enthalpic effect of the hydrogen bond and the CH···π interaction, and not from an entropic contribution. This difference could be ascribed to the presence of the two bulky sulfur atoms in the cavity. In the lattice, the cavitands form sets of parallel channels along the direction *a* of the unit cell. Dichloromethane molecules fill the free spaces among these channels.

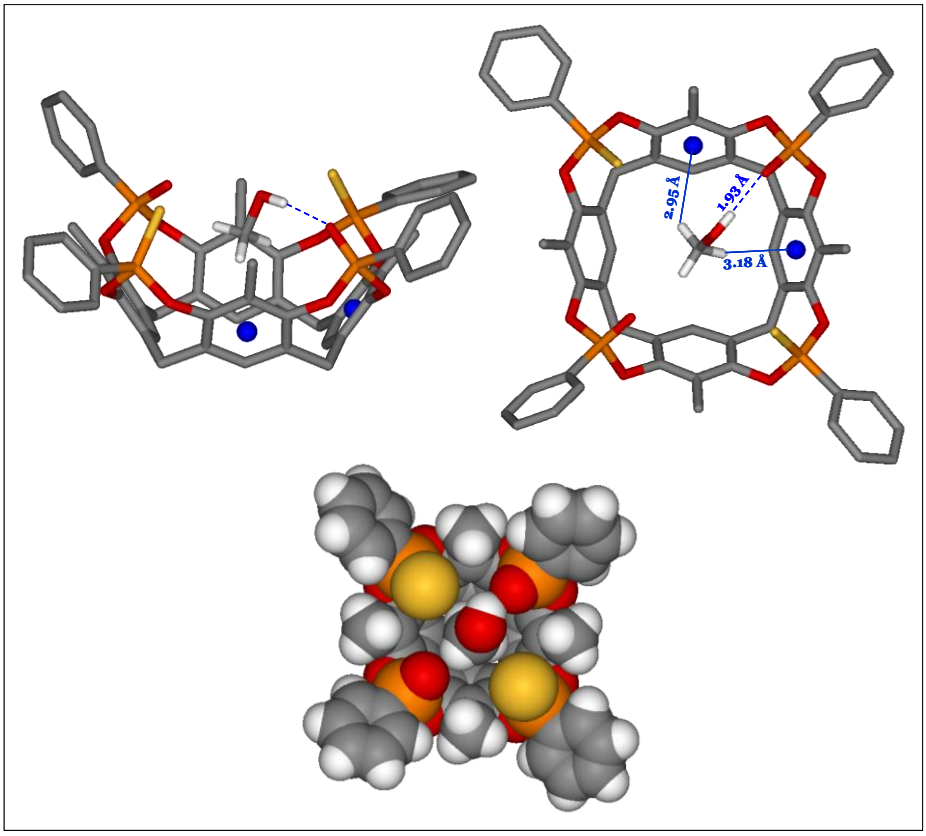

Figure 3.11. Crystal structure of the AC 2POii2PSii[H, CH_3, Ph]•MeOH complex. (Colour code: P, orange; O, red; S, yellow; C, grey; H, white; weak intermolecular interactions and centroids, blue). The hydrogen atoms not involved in the interactions are omitted for clarity.

The AC isomer crystallizes as two independent molecules with slightly different geometrical parameters. Their behaviour towards the alcohol is, however, very similar. Each cavity hosts one methanol molecule, while other alcohol, water and dichloromethane molecules fill the empty spaces in the crystal lattice, forming networks of hydrogen bonds. Also in this case the main interactions responsible for the complex formation are CH-π interactions involving the hydrogen atoms of the methyl group and the π-basic cavity [H···centroid 3.382(2) Å, C-H···centroid 133.48(3)°; H···centroid 2.964(5) Å, C-H···centroid 172.27(3)°] and one H-bond between the OH group and the P=O moiety [O-H···O=P 1.898(3) Å, 171.84(3)°] (the values reported refer to one of the two independent cavitand molecules). As already found for the AB isomer, also in this case the complex formation is favoured by an enthalpic gain and no entropic stabilization occurs.

In both cases, the crystal structures confirm the inability of the P=S moieties to form H-bond with alcohols.

Recalling the results obtained in the gas phase with Tiiii[H, CH_3, CH_3], we wanted to verify if, with these new molecules, the affinity scale toward alcohols series is changed.

Preliminary ESI-MS experiments show that the most interesting case is 2POii2PSii[H, CH_3, Ph]. Indeed the ESI-MS data indicate a remarkable difference in the complexing behaviour of the ABii and ACii isomers (Figure 3.12).

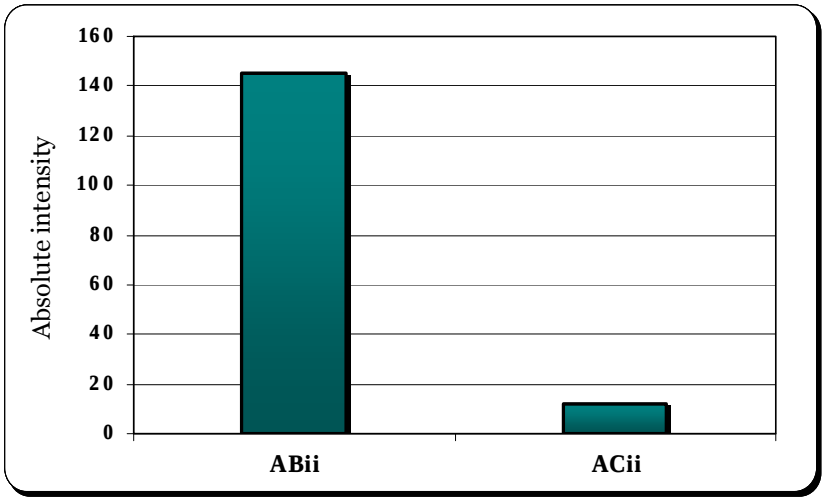

Figure 3.12. Absolute intensity of 2POii2PSii ethanol complexes.

The ACii isomer does not form a complex with EtOH, while the ABii one is very effective. The position of the P=O groups seems to affect the efficiency of ethanol complex formation. These findings confirm the importance of the number and position of the P=O groups with respect to the P=S groups for the stability of the complex and suggest that among the three thiophosphonated cavitand, the AB 2POii2PSii[H, CH_3, Ph] isomer appears to have a prerequisite for a good selectivity in terms of short chain alcohols recognition.
To study the effect of the guests in the complex formation, we performed gas-phase tests with the ABii cavitand toward a series of C_1-C_6 alcohols.
Samples for measurement contained a solution of cavitand in acetonitrile with 1% of trifluoroacetic acid and 1% of the alcohol guest.

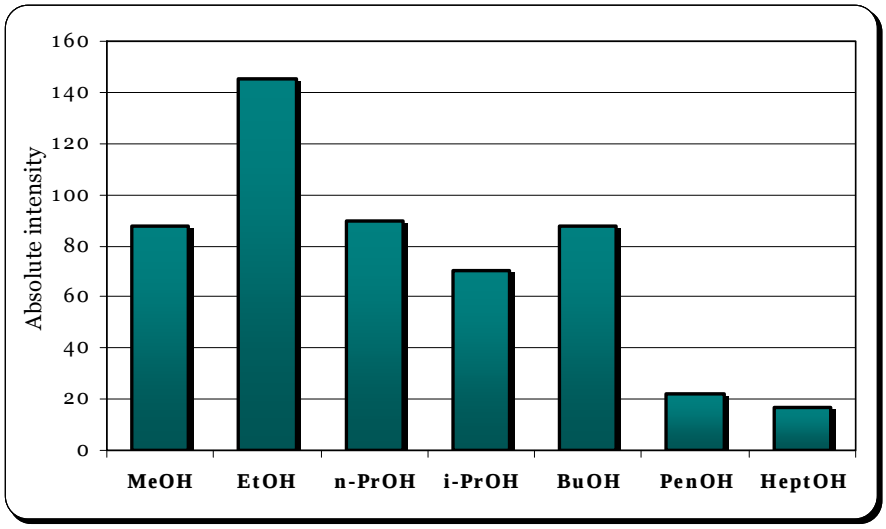

Figure 3.13. Absolute intensity of AB 2POii2PSii[H, CH_3, Ph]·alcohol complexes.

As expected, the available space in the cavity of AB 2POii2PSii[H, CH_3, Ph] is reduced and less symmetric with respect to Tiiii[H, CH_3, Ph], and the sterically more demanding pentanol and heptanol are not favoured over the corresponding short chain alcohols.
We can conclude that in this case the modification of the cavitand structure led to the desired selectivity, despite the unfavourable aspects mentioned in the paragraph 2.4.4. Probably in this case, the optimization of the cavity structure is able to mitigate the problems concerning for example the solvation and the ionization efficiency previously observed in the gas phase.

At this point, we tested the predictive value of the gas phase analysis in the real world of sensor measurements.

With this aim we proceeded with a comparison among the QCM responses of MeCav[H, CH_3], 2POii2PSii[H, CH_3, Ph], 3POiii1PSi[H, CH_3, Ph] and Tiiii[H, CH_3, Ph] toward the entire series of C_1-C_5 alcohols (Figure 3.14).

In these measurements we used the MeCav[H, CH_3] cavitand as meaningful unspecific interactions indicator, instead of the TSiiii with long chains at the lower rim, tested in the experiments reported above, because we wanted to compare cavitands without chains a the lower rim.

We could not use the corresponding TSiiii[H, CH_3, Ph] without chains at the lower rim because this cavitand is not soluble in the common solvent employed for the spin coating deposition (see Chapter 4 for other type of depositions). For this reason we used the methylene bridged cavitand, which as we have already reported (paragraph 2.4) is unable to form host-guest complexes, both in solid state and in gas phase.

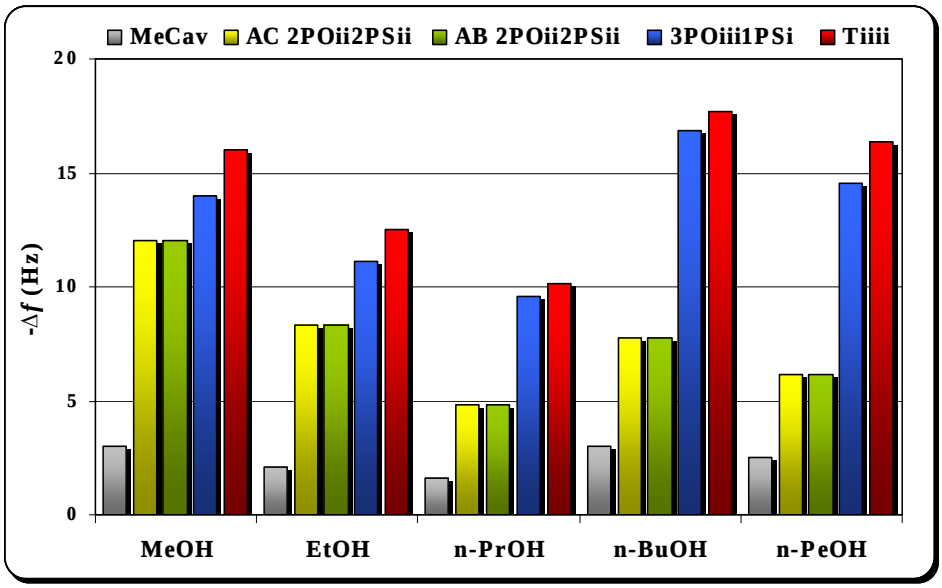

Figure 3.14. Selectivity pattern of MeCav[H, CH_3], 2POii2PSii[H, CH_3, Ph], 3POiii1PSi[H, CH_3, Ph] and Tiiii[H, CH_3, Ph] to C_1-C_5 linear alcohols at 5 ppm.

The comparison among tetraphosphonate and thiophosphonate cavitands, shows how 3POiii1PSi shows responses quite similar to Tiiii, only a little smaller. Therefore the introduction of a single P=S group does not change significantly the selectivity.
On the other hand, the expected trend is shown by 2POii2PSii, the responses of which decrease with the increasing of the alcohol chain. The large increase in the n-BuOH response experienced by 3POiii1PSi and Tiiii is much less pronounced for the ACii and ABii cavitand layers.
In this case, the relative position of the two P=O groups (ACii *vs* ABii) is not determinant, contrary to the ESI-MS results.
If we compare directly Tiiii and ACii we can appreciate more the large gap in the responses to butanol and pentanol (Figure 3.15).

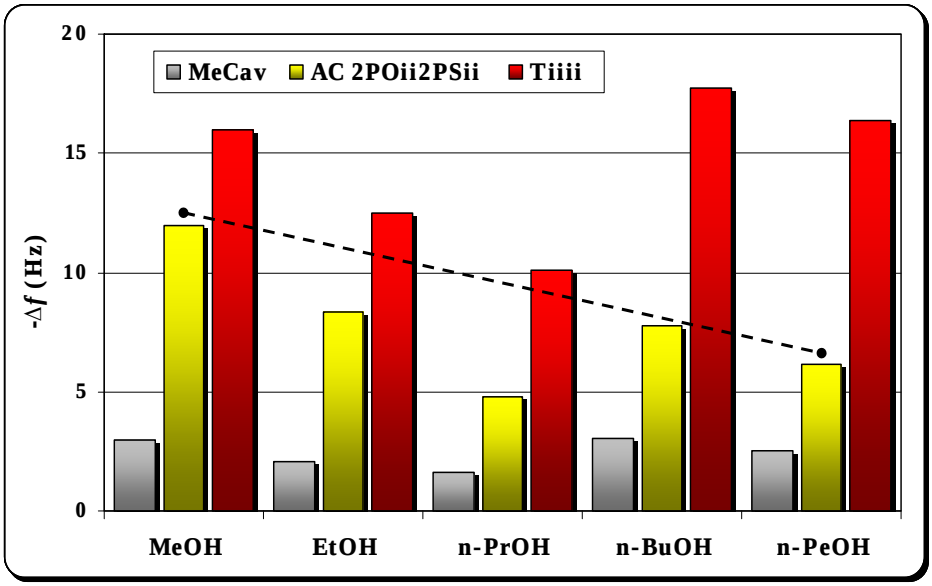

Figure 3.15. Selectivity pattern of MeCav[H, CH_3], 2POii2PSii[H, CH_3, Ph], and Tiiii[H, CH_3, Ph] to C_1-C_5 linear alcohols at 5 ppm.

Indeed, the dashed line highlights how the response of butanol and particularly of pentanol are smaller than the ethanol one. We can conclude that with 2POii2PSii we have reached the selectivity limit compatible with QCM transduction. With this cavitand we are able to have both sensitivity and selectivity in the gas sensing of alcohols with short chain.
Further improvements in selectivity can only be obtained by changing the transduction mode, for example using fluorescence spectroscopy with cavitands equipped with fluorescent probes.[*]

[*] P. Betti, Ph.D. Thesis, University of Parma, **2008**.

3.3 Conclusions

Rational design can be used to create synthetic receptors with a good deal of predictability and selectivity. The key factors affecting the sensing performances of these new type of phosphorous bridged cavitands toward alcohols, are the same already seen in the tetraphosphonate cavitands.
However, with the 2POii2PSii cavitands there is an acceptable agreement in the trend selectivity between the ESI-MS and the gas-solid interface results.
The present work has demonstrated that it is possible to enhance the sensors selectivity by changing the shape of the receptor cavity. The presence of two bulky P=S bridges, unable to H-bond to the analytes, makes the resulting cavitands by far, more specific in recognizing MeOH and EtOH with the respect to the parent Tiiii compound. By comparing the crystal structures of the Tiiii alcohol complexes of Chapter 2 with those of Figure 3.10 and 3.11, it appears that MeOH in particular should be favoured by the reduction in size of the cavity. This is observed experimentally in the sensor responses (see Figure 3.14). For the longer chain alcohols the simultaneous presence of H-bonding and CH-π interactions requires a conformational arrangement which is disfavoured in the ABii and ACii cavitands.

3.4 Acknowledgments

Special thanks to Dr. Chiara Massera of the University of Parma for the X-Ray crystallographic studies, and to Dr. Elina Kalenius of the University of Joensuu (Finland) for the ESI-MS analyses.

3.5. Experimental section

Cavitand T_{iiii}[H, CH_3, Ph]

Dichlorophenylphosphine (1.02 mL, 7.49 mmol) and pyridine (1.22 mL, 1.51 mmol) were added, under nitrogen, to a solution of resorcinarene (1.0 g, 1.84 mmol) in 40 mL of anhydrous DMA. After 1 hour a mixture of $H_2O_2/CHCl_3$ was added dropwise and the reaction was vigorously stirred for 1 hour. The $CHCl_3$ was removed *in vacuo* and the resulting precipitate was filtered and washed with water (3 x 30 mL). The solid was treated with 200 mL of water, sonicated, filtered and dried *in vacuo* to yield the desired compound as white solid (1.79 g, 93%). **^{1}H NMR** ($CDCl_3$/MeOD, 300 MHz): δ = 8.16-8.09 (m, 8H, POArH_o), 7.63-7.52 (m, 12H, POArH_m + POArH_p), 7.09 (s, 4H, ArH_{down}), 4.52 (d, 4H, ^{3}J=13 Hz, $Ar_2CH_{2eq.}$), 3.51 (d, 4H, ^{3}J=13 Hz, $Ar_2CH_{2ax.}$), 2.28 (s, 12H, ArCH_3). ^{31}P NMR ($CDCl_3$, 162 MHz) δ = 4.82 (s, 4P, *P*OPh). **ESI-MS**: m/z 1033.3 $[M+H]^+$, 1055.2 $[M+Na]^+$.

Cavitand TS_{iiii}[H, CH_3, Ph]

Dichlorophenylphosphine (1.02 mL, 7.49 mmol) and pyridine (1.22 mL, 1.51 mmol) were added, under nitrogen, to a solution of resorcinarene (1.0 g, 1.84 mmol) in 40 mL of anhydrous DMA. After 1 hour S_8 (0.98 g, 1.28 mmol) was added and the reaction was stirred for another 1 hour at 50°C. The resulting precipitate was filtered and washed with water (3 x 30 mL). The solid was treated with 200 mL of water, sonicated, filtered and dried *in vacuo* to yield the desired compound as white solid (1.49 g, 89%). **^{1}H NMR** ($CDCl_3$, 300 MHz): δ = 8.22-8.16 (m, 8H, PSArH_o), 7.59-7.52 (m, 12H, PSArH_m + PSArH_p), 6.89 (s, 4H, ArH_{down}), 4.45 (d, 4H, ^{3}J=13 Hz, $Ar_2CH_{2eq.}$), 3.54 (d, 4H, ^{3}J=13 Hz, $Ar_2CH_{2ax.}$), 2.09 (s, 12H, ArCH_3). **^{31}P NMR** ($CDCl_3$, 162 MHz): δ = 74.55 (s, 4P, *P*SPh). **ESI-MS**: m/z 1097.3 $[M+H]^+$, 1119.3 $[M+Na]^+$, 1135.3 $[M+K]^+$.

Cavitand $3PO_{iii}1PS_i$[H, CH_3, Ph]

Dichlorophenylphosphine (1.02 mL, 7.49 mmol) and pyridine (1.22 mL, 1.51 mmol) were added, under nitrogen, to a solution of resorcinarene (1.0 g, 1.84 mmol) in 40 mL of anhydrous DMF. After 1 hour S_8 (58 mg, 0.23 mmol) was added and the reaction was stirred for another 1 hour at 50°C. Then a mixture of $H_2O_2/CHCl_3$ was added dropwise and the reaction was vigorously stirred for 1 hour. The $CHCl_3$ was removed under vacuum and the resulting precipitate was

filtered and washed with water (3 x 30 mL). The solid was treated with 200 mL of water, sonicated, filtered and dried *in vacuo*. The crude product was purified by column chromatography (SiO_2, CH_2Cl_2:MeOH, 95:5) to give the desired compound as white solid (1.35 g, 70%). **^{1}H NMR** ($CDCl_3$/MeOD, 300 MHz): δ = 8.17-8.11 (m, 2H, PSArH_o), 8.05-7.98 (m, 6H, POArH_o), 7.62-7.50 (m, 12H, POArH_m + POArH_p + PSArH_m + PSArH_p), 7.26-7.23 (m, 4H, ArH_{down}), 4.48-4.39 (m, 4H, $Ar_2CH_{2eq.}$), 3.61-3.55 (m, 4H, $Ar_2CH_{2ax.}$), 2.07 (s, 12H, ArCH_3). **^{31}P NMR** ($CDCl_3$/MeOD, 162 MHz): δ = 73.70 (s, 1P, *P*SPh), 7.53 (s, 2P, *P*OPh), 7.04 (s, 1P, *P*OPh). **ESI-MS**: m/z 1049.6 $[M+H]^+$, 1071.5 $[M+Na]^+$.

Cavitand 2PO$_{ii}$2PS$_{ii}$[H, CH$_3$, Ph]

Dichlorophenylphosphine (1.02 mL, 7.49 mmol) and pyridine (1.22 mL, 1.51 mmol) were added, under nitrogen, to a solution of resorcinarene (1.0 g, 1.84 mmol) in 40 mL of anhydrous DMF. After 1 hour S_8 (147 mg, 0.574 mmol) was added and the reaction was stirred for another 1 hour at 50°C. Then a mixture of H_2O_2/$CHCl_3$ was added dropwise and the reaction was vigorously stirred for 1 hour. The $CHCl_3$ was removed *in vacuo* and the resulting precipitate was filtered and washed with water (3 x 30 mL). The solid was treated with 200 mL of water, sonicated, filtered and dried *in vacuo*. The crude product was purified by column chromatography (SiO_2, CH_2Cl_2:MeOH, 95:5) to give two desired isomers as white solids (ABii 263 mg, 15% and ACii 439 mg, 25%). **(ABii) ^{1}H NMR** ($CDCl_3$, 300 MHz): δ = 8.17-8.11 (m, 2H, PSArH_o), 8.05-7.98 (m, 6H, POArH_o), 7.62-7.50 (m, 12H, POArH_m + POArH_p + PSArH_m + PSArH_p), 7.26-7.23 (m, 4H, ArH_{down}), 4.48-4.39 (m, 4H, $Ar_2CH_{2eq.}$), 3.61-3.55 (m, 4H, $Ar_2CH_{2ax.}$), 2.07 (s, 12H, ArCH_3). **^{31}P NMR** ($CDCl_3$/MeOD, 162 MHz): δ = 73.70 (s, 1P, PSPh), 7.53 (s, 2P, POPh), 7.04 (s, 1P, POPh). **(ACii) ^{1}H NMR** ($CDCl_3$, 300 MHz): δ = 8.22-8.06 (m, 8H, POArH_o + PSArH_o), 7.63-7.53 (m, 12H, POArH_m + POArH_p + PSArH_m + PSArH_p), 7.26-7.23 (m, 4H, ArH_{down}), 4.48-4.39 (m, 4H, $Ar_2CH_{2eq.}$), 3.61-3.55 (m, 4H, $Ar_2CH_{2ax.}$), 2.07 (s, 12H, ArCH_3). **^{31}P NMR** ($CDCl_3$/MeOD, 162 MHz) δ = 73.84 (s, 2P, PSPh), 7.00 (s, 2P, POPh). **ESI-MS**: m/z 1065.4 $[M+H]^+$, 1087.3 $[M+Na]^+$, 1103.3 $[M+K]^+$.

New techniques of cavitand layers deposition and their influence on the QCM sensing performances*

4

4.1 Introduction

In the previous Chapters we have described our efforts to improve the performances of supramolecular mass sensors by changing the chemical nature of the coated receptor. However, also the physical properties of the produced films are very important because the gas sensing capabilities of the samples are strongly related to them.

Ideally Self Assembled Monolayers (SAM) of cavitands would guarantee the best arrangement of receptors with the minimal number of unspecific sites. Nevertheless, a single monolayer of cavitands on a QCM does not bind enough analytes to reach the "transducer threshold" (lower limit of the dynamic range).[1] Indeed the number of the cavitand receptors in the monolayer is not sufficient to lead to a noteworthy variation of the mass necessary to have a detected variation on the quartz frequency.

Moreover, application of the Sauerbrey equation in its linear range requires the presence of a uniform and homogeneous layer across the entire active region of the resonator, but this assumption is reasonable only for non-polar polymers

* This work has been carried out in collaboration with the group of Prof. G. Della Mea at the INFN of Legnaro (Pd).

and has to be tested for any new kind of receptor. In this respect the control of sensitive layer morphology and permeability becomes essential.
In order to achieve the best layer properties of our cavitand receptors, in this work we have performed new different physical deposition techniques: the vacuum evaporation (VE) and Glow-discharge-induced sublimation (GDS).
In the next paragraphs, we will show in detail the spin-coating, VE and GDS deposition procedures in the cavitand films production. Moreover chemical and morphological characteristics of the samples have been investigated and related to their sensing capabilities.

4.2 Spin-coating technique

Spin coating is one of the simplest and cheapest way of depositing organic layers on surfaces. A typical process involves the deposition of a small amount of a solution onto the center of a substrate and then the spinning of the substrate at high speed (typically around 2000 rpm). Centripetal acceleration causes the solution to spread to, and eventually off, the edge of the substrate leaving, upon evaporation of the solvent, a thin film of compound on the surface. Final film thickness and other properties depend on the nature of the solution (viscosity, drying rate, percent solids, surface tension, etc.) and on the parameters chosen for the spin process.
The optimization of the operative conditions for the spin-coating deposition of cavitand layers onto gold surface has led to the following parameters:

- rotation speed: 2000 rpm;
- spinning time: 20 s;
- solvents: methylene chloride (with 1%-5% of trifluoroethanol in the case of low solubility of the cavitand);
- a 2% in weight solution of cavitand.

Each microbalance is coated with the same amount of cavitand which is verified by measuring the frequency shift of $\Delta f=20\pm0.5$ kHz on the final coated QCM.
With the Sauerbrey equation we can correlate this frequency change with the corresponding mass change:

$$\Delta f = -\frac{2 f_0^2}{A \cdot \rho_q \cdot \nu_q} \cdot \Delta m$$

where Δf is the frequency change (Hz), f_o^2 the resonant frequency (10 MHz), A the piezoelectrically active crystal area (0.496 mm^2), ρ_q the density of quartz (2.648 g/cm^3), ν_q the transverse wave velocity in quartz ($3.336 \cdot 10^5$ cm/s) and Δm the mass change (g).
Therefore, a change in the quartz frequency of 20 KHz is equal to a mass change of 44 μg of cavitand.

4.2.1 Morphological studies

The surface morphology of the organic samples was investigated in air by no contact mode atomic force microscope (AFM) model C-21 produced by Danish Micro Engineering, mounting a DualScope Probe Scanner 95-50. The observations were performed by using a Si_3N_4 pyramidal tip having a curvature radius lower than 50 nm.
For each sample, several images from different positions were recorded and acquired with scan sizes ranging from 1 x 1 μm^2 to 50 x 50 μm^2 in order to check the uniformity of the samples. All the images were acquired using the AC mode, at a very slow speed (typically under 1 μm/s) and, analysed and processed using the standard software supplied with the control electronics. The thickness of the films was measured by scratching (with a doctor blade) a small area of the samples and then acquiring an AFM image of the borderline between the exposed substrate and the pristine film.
AFM images of a Tiiii spin-coated sample are reported in Figure 4.1: the topography of the sample shows a particular surface morphology, consisting of globular islands and craters (emphasized in the higher magnification 5 x 5 μm^2), the latter due to the fast evaporation of the solvent.

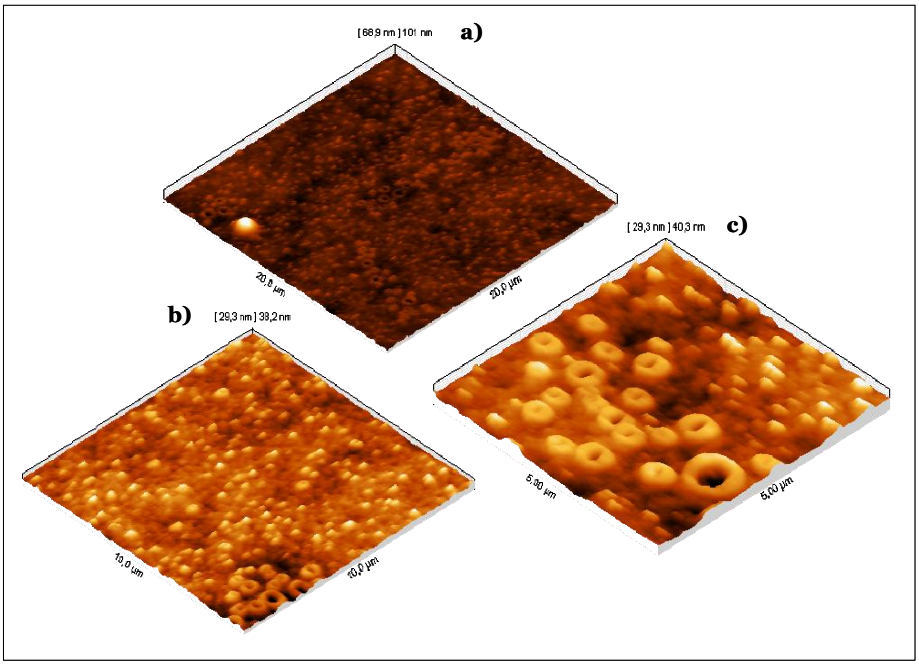

Figure 4.1. AFM images of a Tiiii[H, CH_3, Ph] deposited by spin coating: a) 20 x 20 µm², b) 10 x 10 µm² and c) 5 x 5 µm².

The average roughness, calculated on a 10 x 10 µm² area, the thickness and the density of the sample are reported in Table 4.2.

	Tiiii[H, CH_3, Ph]
Thickness (nm)	490
Roughness (nm)	5.2

Table 4.2. Thickness and roughness of the Tiiii spin-coated film.

The sample does not exhibit a distinctive values of thickness and roughness because these features are variable, and dependent on the deposition operative conditions and on the nature of the coated compound.

4.3 VE deposition technique

Till now, the standard method to obtain cavitand solid films has been the spin-coating, because of its easiness and low costs. Nevertheless, this technique is affected by several drawbacks such as poor reproducibility, inaccurate thickness uniformity and solvent retention. Moreover, with the spin-coating we can deposit layers only starting from a solution of the desired compound, thus we are unable to deposit films starting from insoluble powders.
For these reasons, we performed the production of thin cavitand films by vacuum evaporation (VE) technique. VE deposition, performed in high vacuum conditions, has been demonstrated as fundamental for obtaining highly controlled and uniform coating films through strictly controlled and highly reproducible procedures.[2] The VE technique enables to produce thin solid films starting from the compound powder and thus without using any solvent. This means that we can deposit of insoluble cavitands, and obtain layers with higher purities than via the common chemical techniques.
The experimental equipment used for the evaporation of the cavitands is comprised of a stainless steel vacuum chamber evacuated by a turbomolecular pump to a base pressure of 1×10^{-4} Pa. The chamber is equipped with copper crucibles that are wrapped with a heating wire. In the case of the production of thin cavitand films, a crucible was filled with the cavitand powder and heated up to 500 °C. The substrates were placed on a fixed sample holder placed 11 cm above the crucible and the substrates were maintained at room temperature during the deposition process.
The deposition rate and film thickness were measured by a quartz crystal microbalance thickness sensor (Sycon) put in the centre of the sample holder. A movable shutter was put between the crucible and the sample holder: before and after the deposition, when the crucibles were either heated up to the deposition temperature or cooled down to the room temperature, the shutter was placed between crucibles and substrates in order to prevent the uncontrolled deposition of organic molecules onto the substrates. When the deposition temperature of the crucible was achieved, the shutter was removed and the deposition started.
The films were deposited on two different substrates: P-doped (1 0 0) silicon wafers lapped on both faces (Bayville Chemical Co.) for characterization analyses (ESI-MS, ^{1}H NMR and AFM), and QCM for sensing measurements.

In specific, this paragraph reports the employment of VE technique for the deposition of Tiiii[H, CH_3, Ph] and TSiiii[H, CH_3, Ph] films. The synthesis and characterization of these compounds have already reported in Chapter 3 but, since the TSiiii[H, CH_3, Ph] cavitand is insoluble in most solvents, it was not possible the spin coating deposition and consequently the sensing tests.
Now, with this new technique we are able to produce a TSiiii film and test its sensing behaviour.
Regarding the deposition of the two cavitand layers, we adopted the same parameters in order to compare the final samples. In both cases, the total mass deposited on the QCM is equal to 20 KHz (~10 KHz for each transducer side), the same value used for all coated QCMs previously reported (Chapter 2 and 3).
The distances between the crucible (containing the cavitand powder) and the substrate was fixed at 10 cm, the base pressure at the beginning of the process was kept at 2 x 10^{-4} Pa for all the depositions and the crucible temperature was maintained at 440°C.
The most important growth parameters to be controlled are the film thickness and the deposition rates, which strictly affects the final roughness and porosity of the samples.[3] The deposition rate is evaluated as number of molecules deposited in the unit of surface and time (molecules·cm^{-2}·s^{-1}), by normalizing the values of the thickness sensor to the molecular weight of each compound. Each curve can be fit by the following function:[4]

$$\log D = A - \frac{B}{T}$$

where D is the deposition rate, T the absolute temperature and, A and B are constants determined from the curves fitting. For Tiiii A=17.9 and B=8378 K and for TSiiii A=24.6 and B=12817 K.
As reports in Figure 4.3, at 440°C the deposition rate of TSiiii (D=5.7·10^6 molecules·cm^{-2}·s^{-1}) is approximately three times Tiiii one (D=2.0·10^6 molecules·cm^{-2}·s^{-1}). One explanation of this diversity can be draw regarding the different polarity of the two compounds. Since the Tiiii is more polar than the TSiiii, the interactions created between the molecules in the layer are stronger; this requires more energy in the Tiiii sublimation with respect to the TSiiii, and therefore the TSiiii deposition rate is higher.

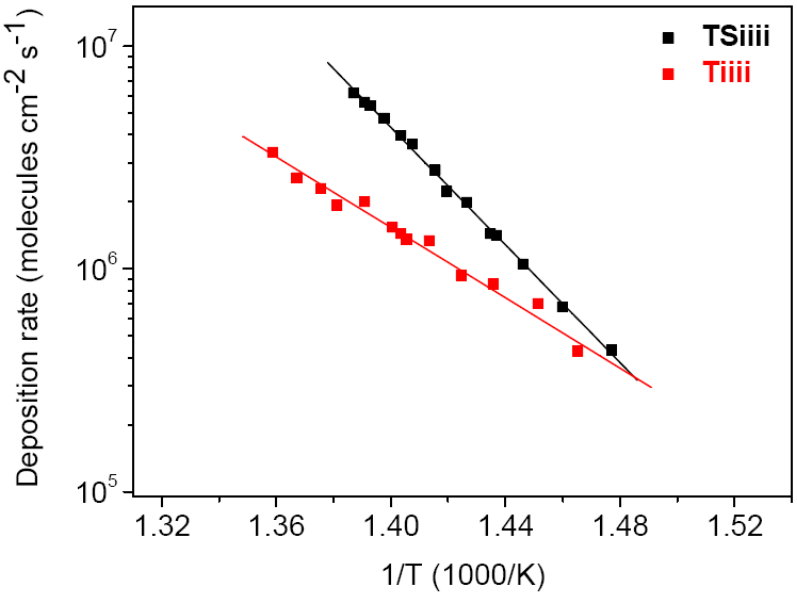

Figure 4.3. Deposition rates of Tiiii[H, CH_3, Ph] and TSiiii[H, CH_3, Ph] *vs* temperature.

The VE technique assures highly controlled deposition processes. Indeed the deposition rates are accurately adjustable through the crucible temperature, as illustrated in Figure 4.3, and the *in situ* sample growth is easily controlled with the QCM quartz both in terms of deposition rates and final thickness.

Moreover, this technique allows to monitor the vacuum chamber pressure over the whole heating phase. Both Tiiii and TSiiii powders show an abrupt pressure increase in the 100-250 °C temperature range, due to the release of volatile impurities adsorbed during the purification phase, such as the recristallization water. For this reason, in both cases the crucible containing the cavitand powder has been pre-heated at 300 °C for 30 minutes, maintaining the shutter closed in order to purify the compound without contamination of the substrate and thus of the final samples.

An accurate characterization of the properties of the deposited films was carried out, focusing the attention especially on the purity and the integrity of the cavitand films (ESI-MS and ^{1}H NMR characterization), on the surface roughness and on the porosity of the samples (AFM analysis).

The comparison of the ^{1}H NMR and ESI-MS spectra between the VE films and the starting powders, demonstrates that both TSiiii and Tiiii coatings show the

same characteristic peaks. Therefore both films are characterized by highly pure and undamaged molecules. This important result confirms that the two cavitands have high thermal stability in vacuum, and it is possible to use the VE technique to produce reproducible and homogeneous cavitand films.

4.3.1 Morphological studies

The surface morphology of the cavitand samples was investigated using the same apparatus and procedure previously reported.
A quartz microbalance was used for monitoring the *in situ* quantity of deposited cavitand. Usually, quartz microbalances are used to measure the *in situ* thickness increasing of the samples during the deposition process: these measurements require knowledge of the film density, which depends on the nature of the material and crystal structure or molecular arrangement in the film. In this work we used the reverse approach: by comparing the *in situ* quartz microbalances monitoring with the results of *ex situ* AFM measurements, the densities of TSiiii and Tiiii vacuum evaporated films were established.
Since this work represents the first attempt to produce cavitand coatings by VE technique, the densities of these VE films were unknown; for this reason the in situ QCM was set up introducing a fictitious density of 1 g/cm^3, and the fictitious thickness of the resulting coating on each face of QCM sensor is measured to be 463 nm for both Tiiii and TSiiii samples. On the other hand, we have measured the real thickness of the films obtained by AFM, deriving that are equal to 355 nm and 340 nm for the Tiiii and TSiiii, respectively. Now, as the theoretical and real quantity of deposited material have to be the same, it is possible to draw the density of the solid coating by solving the following simple equation:

$$\mathrm{M} = \mathrm{T}^{*} \cdot \mathrm{D}^{*} \cdot \mathrm{A} = \mathrm{T} \cdot \mathrm{D} \cdot \mathrm{A} \quad \text{therefore} \quad D = (D^{*} \cdot T^{*})/T$$

where M is the mass of the coating, T* the thickness of the coating measured by the *in situ* QCM (set up with a fictitious density value D*), D* the fictitious density value (1 g/cm^3), A the QCM surface area, T the real thickness of the coating measured by AFM (Figure 4.4) and D the real density of the coating.

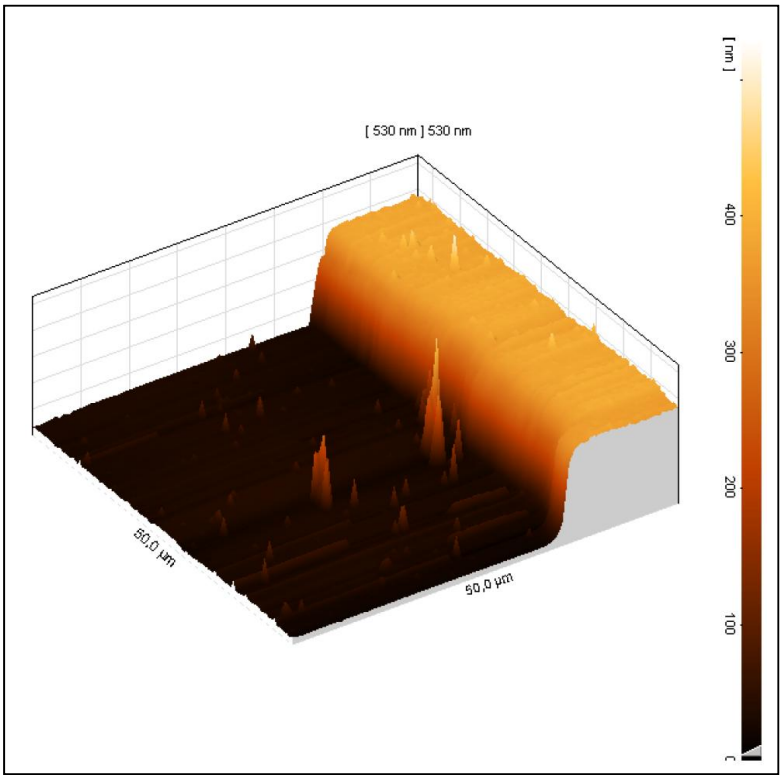

Figure 4.4. AFM image of the scratched layer used for the thickness measurement in the case of Tiiii[H, CH_3, Ph] VE film.

The derived density values are showed in Table 4.5.

	Tiiii[H, CH_3, Ph]	**TSiiii[H, CH_3, Ph]**
Measured thickness (nm)	355	340
Density (g/cm^3)	1.30	1.36

Table 4.5. Thickness and density of the Tiiii and TSiiii EV films.

The similar values of the two cavitands coating densities, represent an interesting result taking into account that the density of the samples, which is in inverse relation to the porosity, greatly influences the interaction between the analyte and cavitand layers.

AFM images of vacuum evaporated Tiiii and TSiiii coatings are reported in Figure 4.6.

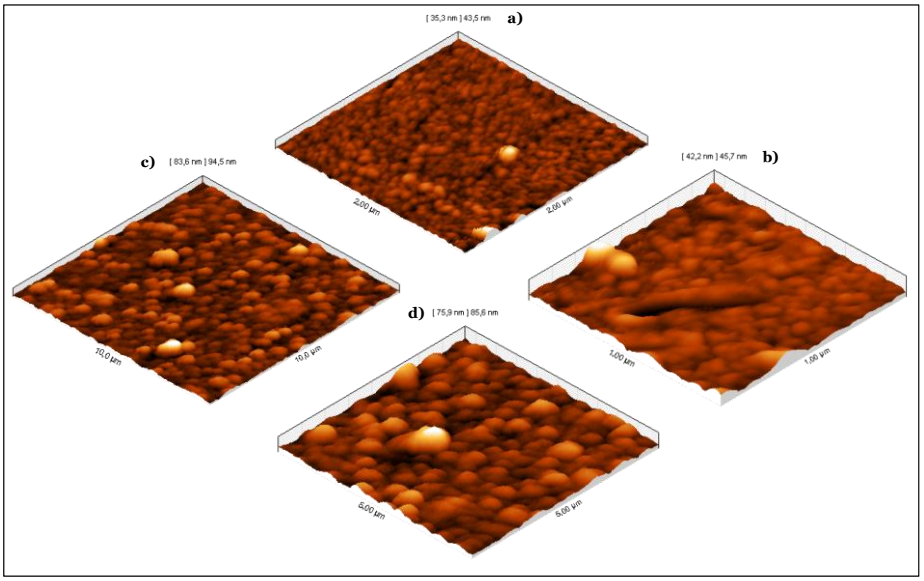

Figure 4.6. AFM images of VE films: a) 2 x 2 μm² and b) 1 x 1 μm² scan of Tiiii[H, CH_3, Ph] surface and, c) 10 x 10 μm² and d) 5 x 5 μm² scan of TSiiii[H, CH_3, Ph] surfaces.

Instead the average roughness, calculated on a 10 x 10 μm² area, and the thickness of the samples are reported in Table 4.7.

	Tiiii[H, CH_3, Ph]	**TSiiii[H, CH_3, Ph]**
Roughness (nm)	4.4	10.7
Islands lateral dimension (nm)	60	420
Islands height (nm)	5	15

Table 4.7. Average roughness, lateral dimensions and heights of the surface islands of the Tiiii and TSiiii VE films, measured by AFM.

The TSiiii sample exhibits a higher roughness with respect to the Tiiii ones; in particular it is possible to note that the average square roughness (Rq) of TSiiii (Rq=10.7 nm) is approximately three times the Tiiii (Rq=4.40 nm) one.

As regards the topography, both the Tiiii and TSiiii VE samples show surface morphologies consisting of globular islands. The substantial difference between the two cavitand samples consists in the islands dimensions, as investigated by AFM profilometric analysis and as reported in Table 4.7. The TSiiii films show surface islands characterized by an average height of 15 nm and lateral dimensions of 420 nm, while the Tiiii coatings are characterized by a greater number of small globular islands characterized by average height and lateral dimension respectively of 5 nm and 60 nm. Nevertheless, it is possible to distinguish on the Tiiii surfaces the presence of some big islands characterized by heights and lateral dimensions similar to those of TSiiii ones.
Some considerations on the growth mode of the deposited films can be drawn from these results. The lower roughness, the smaller lateral dimensions and heights of the morphological features of Tiiii cavitand than TSiiii one, suggest different growth modes in the deposition processes of the two different compounds. In particular, the growth of different structures is can due to concomitant effects relative to the deposition rate. The slower the rate of the film deposition, the longer is the time available for molecules on the surface to adjust to their thermodynamic equilibrium positions, before to be trapped by the arrival of subsequent molecules. Therefore, the bigger deposition rate of TSiiii compound (Figure 4.3) causes the production of films characterized by rougher surface morphologies than Tiiii ones, in which the deposition rate is lower.

4.3.2 Comparison between Tiiii and TSiiii in the sensing performances

Sensing measurements have been performed by exposing cavitand-coated QCMs to several concentrations of EtOH and monitoring the shift of the QCM fundamental resonance frequency, induced by the mass changes, as a function of time.
Figure 4.8 reports the comparison between Tiiii[H, CH_3, Ph] and TSiiii[H, CH_3, Ph] toward 25 ppm of EtOH. We have to remember, as already mentioned in the Chapter 3, that the only one difference between these two cavitands is the presence of 4P=S groups, in the TSiiii, instead of 4P=O groups, in the Tiiii. In this way, we could evaluate only the importance of the H-bonding effect on the sensors measurement.

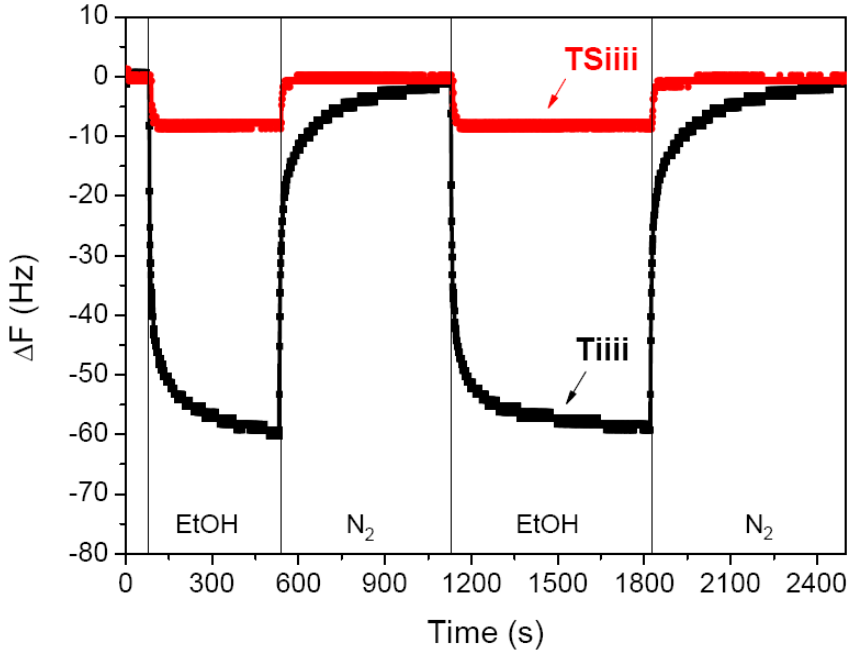

Figure 4.8. Responses traces of Tiiii[H, CH_3, Ph] and TSiiii[H, CH_3, Ph] to 25 ppm of EtOH.

The big gap between the two coatings is consistent with our expectation and with the results already obtained in Chapter 2, since sulphur has lower electronic density with respect to the oxygen and consequently less affinity for H-bonding interactions. In addition the cavity of TSiiii is more bulky and less prone to guest inclusion because sulphur is larger than oxygen.

In order to quantify the response speed of the samples toward EtOH, the parameters t_{50} and t_{90} have been measured; they are defined as the time taken for the signal intensity to reach the 50% and the 90% its final plateau value, respectively. Similarly, for the evaluation of the recovery speed the parameters t_{50} and t_{10}, defined respectively as the time taken for the signal intensity to decrease to the 50% and the 10% its plateau value during the ethanol desorption, have been estimated. The two couples of response (t_{50} and t_{90}) and recovery (t_{50} and t_{10}) times for both Tiiii and TSiiii samples are reported in Table 4.9.

Samples	Response times (s)		Recovery times (s)	
	t_{50}	t_{90}	t_{50}	t_{10}
Tiiii[H, CH_3, Ph]	4	78	5	152
TSiiii[H, CH_3, Ph]	5	12	5	15

Table 4.9. Response and recovery times of Tiiii and TSiiii films upon exposure to 25 ppm EtOH.

As can be seen, both the samples are characterized by fast responses. Nevertheless, as regards the Tiiii sample, it can be noted that while the t_{50} response and recovery times are extremely fast, both the t_{90} during the response and the t_{10} during the recovery are slower than the TSiiii ones.
These data can be explained on the basis of the different interaction processes occurring between the analyte and the different cavitand molecules. Usually this interaction is the result of two different processes:[5]

- the fast sorption in which analyte molecules are adsorbed/desorbed to/from the aspecific sites;
- the slow diffusion of the gas molecules into/out from the buried layers of the film;
- a third process typical for effective supramolecular receptors, must be considered in our case: specific chemisorption due to cavity inclusion.

From the point of view of the analyte molecules, in fact, the "surface" of such a thin films may not only be confined to the upper edge of the film and it may occur thorought the film rather like the surface of a sponge.
Moving from these results, we have performed the study of the sorption mechanisms involved in the thin film responses. For these analyses, the decay of the Elovich kinetics model was applied.[6]
According to T. H. Richardson et al.,[7] the surface coverage Θ, when the solid film are exposed to the analyte (exposure phase), and the release by the absorbed analyte ($1-\Theta$), when the analyte molecules are removed from the films

(recovery phase), as a functions of the time are given by the following symmetrical formula:

$$\Theta(t) = \frac{1}{\beta}\ln(t) + K \quad \text{and} \quad 1 - \Theta(t) = \frac{1}{\beta_1}\ln(t) + K_1$$

where the first one is the Elovich model during analyte adsorption, the second one is the Elovich model during analyte desorption and β, β_1, K and K_1 are constants.

Elovich kinetics model founds itself on the principle that the adsorption probability of an analyte molecule during the analyte exposure decreases exponentially as a function of the number of analyte molecules already adsorbed to the solid surface. Analogously the desorption probability of the molecules during the recovery phase decreases exponentially as a function of the number of analyte molecules already desorbed. Therefore, as the change of the resonant frequency (Δf) is related only to the interaction between the QCM cavitand coating and the analyte molecules, Θ should be proportional to Δf. Consequently, by plotting Δf as a function of *ln(t)* a linear relationship should be obtained.

In this work, the study of the Elovich kinetics model has been focused on the desorption phase of EtOH molecules from the Tiiii and TSiiii VE coatings. In particular, the plots of Δf *vs ln(t)* of the Tiiii and TSiiii samples recovery phases, exposed respectively to 5 and 100 ppm of EtOH are reported in Figure 4.10.

The amount of EtOH to which TSiiii is exposed is 20 times larger in order to obtain Δf values comparable to those produced by the Tiiii layer upon exposure to 5 ppm.

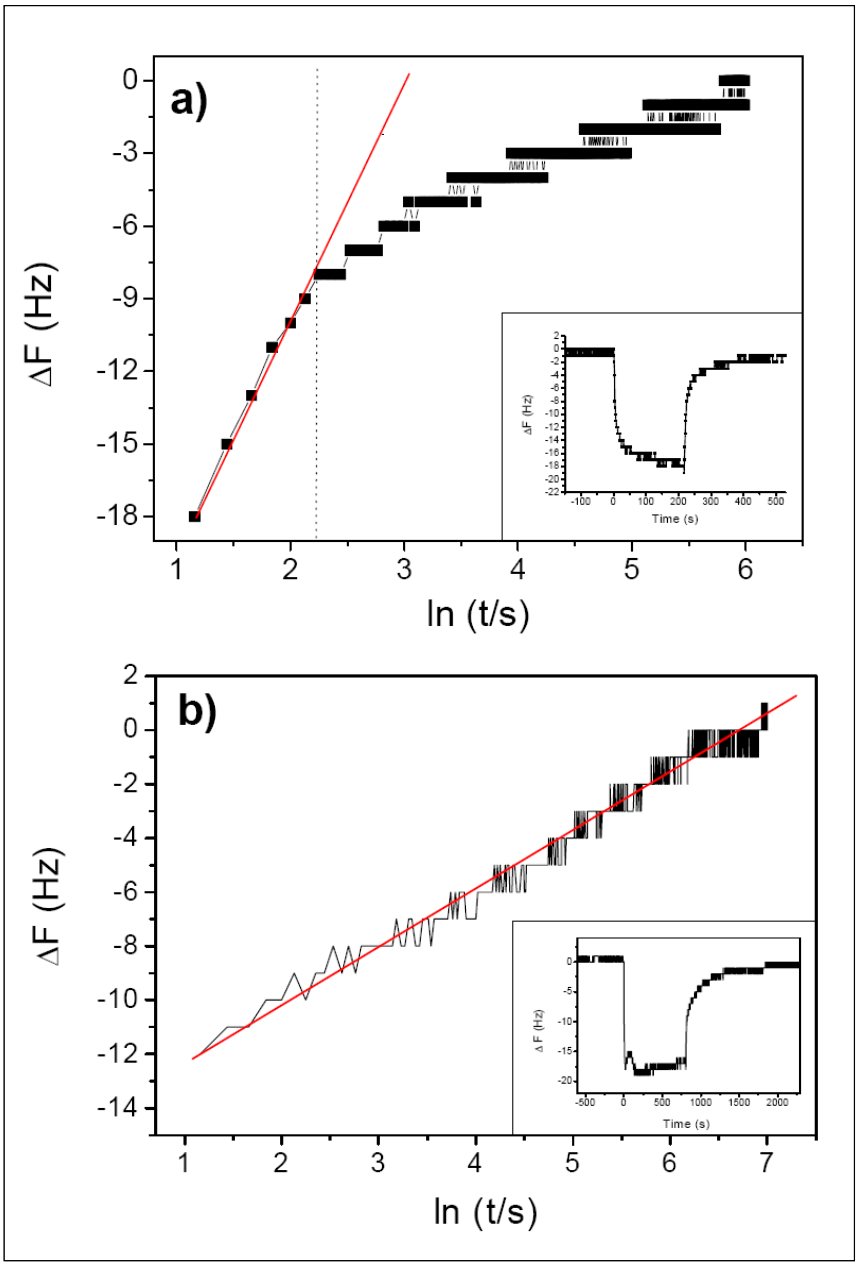

Figure 4.10. Elovich recovery kinetics for Tiiii VE coating exposed to 5 ppm of EtOH (a) and for TSiiii coating exposed to 100 ppm of EtOH (b).

At a glance observation, we can highlight how the trends of Tiiii and TSiiii coated QCM are characterized by different behaviours. In particular, the Tiiii trace is linear approximately over the first 10 s, deviating from the linearity at higher time values. This behaviour indicates a chemidesorption process.[8] The linear region represents an unspecific desorption process in which EtOH molecules are removed from the unspecific sites of the Tiiii coating, while the divergence from the linearity is due to the chemidesorption of the anayte molecules from the specific sites of the domains. Since this process is much slower than the unspecific desorption, is represented by the slowly changing data on the right side of the Elovich plot, which indicates that the unspecific desorption is practically complete while the chemidesorption process is still ongoing. On the contrary, the TSiiii shows a completely linear behaviour, pointing out that in this case the interaction between the EtOH and TSiiii molecules is exclusively unspecific giving rise to physisorption and physidesorption processes.

This result is in perfect agreement with our expectations and with all results obtained in previous chapters.

At this point, we want to investigate the effect of the analyte concentration increase on the coated QCMs frequency change.

Figure 4.11 reports the trend of the frequency values of Tiiii[H, CH_3, Ph] and TSiiii[H, CH_3, Ph] at increasing EtOH concentration.

The comparison between the two calibration curves confirms that the responses of the Tiiii sample are much more intense than TSiiii ones at all tested concentrations. Moreover, the ratio between the frequency changes of Tiiii and TSiiii coatings increases with the increasing of the ethanol concentration (from 5 up to 7 times over whole the 5-200 ppm range).

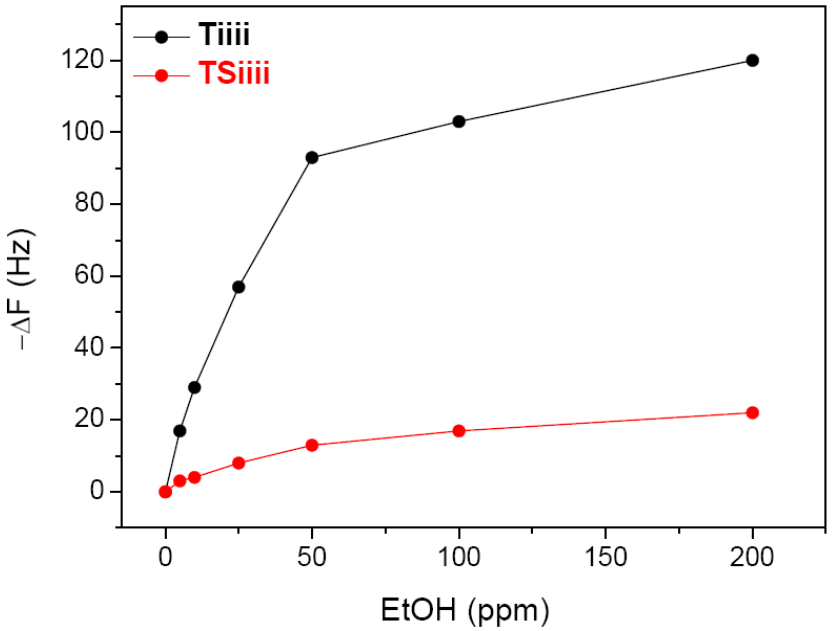

Figure 4.11. Trend of Tiiii[H, CH_3, Ph] and TSiiii[H, CH_3, Ph] to EtOH at several ppm.

Analyzing the Tiiii behaviour, it is worth to note that at EtOH concentrations higher than 50 ppm the sensibility (the slope of the curve) decreases, indicating a progressive saturation of the sites available for the analyte molecules.
The Tiiii curve of Figure 4.11 is the result of the chemisorption of two different adsorption modes:[9]

- the specific host-guest interactions dominate a low EtOH concentrations;
- the unspecific layer interactions contribute at high EtOH ppm, where the available cavitand sites are satured (see Figure 4.12).

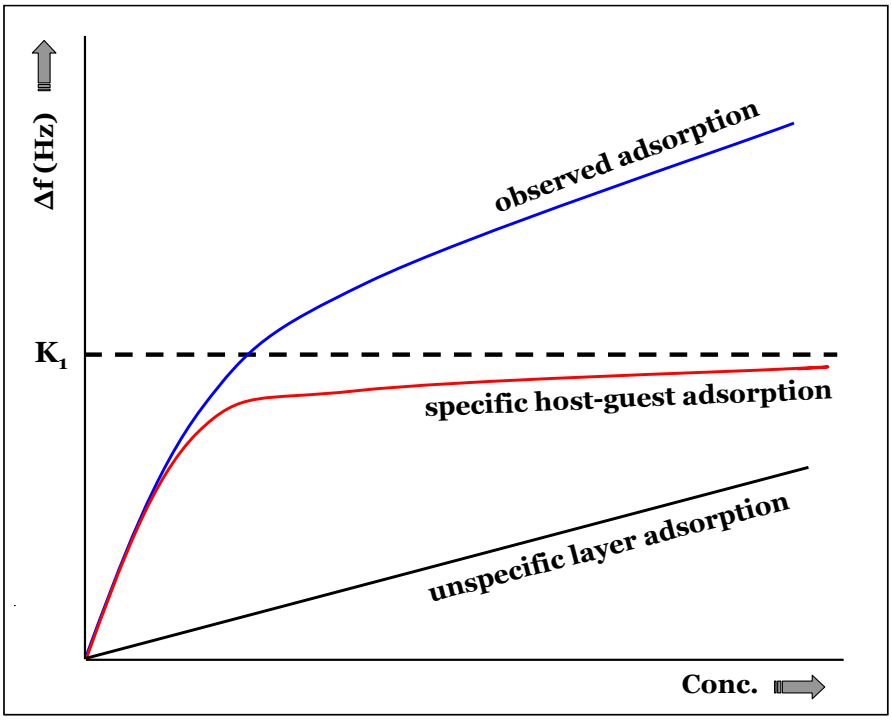

Figure 4.12. Sensor responses versus analyte concentrations according to the Göpel model.

In order to investigate the possible adsorption processes involved in the response of the cavitand toward EtOH, several isotherm models which describe the adsorption/desorption of the analyte molecules onto a solid surface can be applied, including the BET,[10] Toth[11] and Freundlich[12] models. To describe the gas adsorption, the most used model is the Langmuir adsorption isotherm,[13] which provide a preliminary insight into the active process. The Langmuir adsorption isotherm is usually expressed by:

$$\frac{n_{ads}}{N_s} = \frac{\lambda \cdot c}{1 + \lambda \cdot c}$$

where n_{ads} is the number of adsorbed gas molecules (which is proportional to the change in Δf frequency), N_s is the number of adsorption sites, λ is a constant

related to the analyte adsorption capability and c is the analyte concentration. The rearrangement of this equation leads to:

$$\frac{c}{n_{ads}} = \frac{c}{N_s} + \frac{1}{N_s \cdot \lambda}$$

This expression is known as the linear form of Langmuir adsorption isotherm. The theory indicates that a plot of c/Δf versus c should be linear if the basic assumptions are respected. These assumptions are:

- the activation energy for adsorption is the same for all the binding sites in the thin films;
- there is no adsorption of analyte molecules striking sites where an adsorbed analyte molecule already resides (thus, there is limiting adsorption at the surface to a single monolayer);
- there is no lateral motion of analyte molecules over the surface.

In Figure 4.13 the Langmuir adsorption plots and the linear fitting lines for vacuum evaporated Tiiii and TSiiii films are reported.

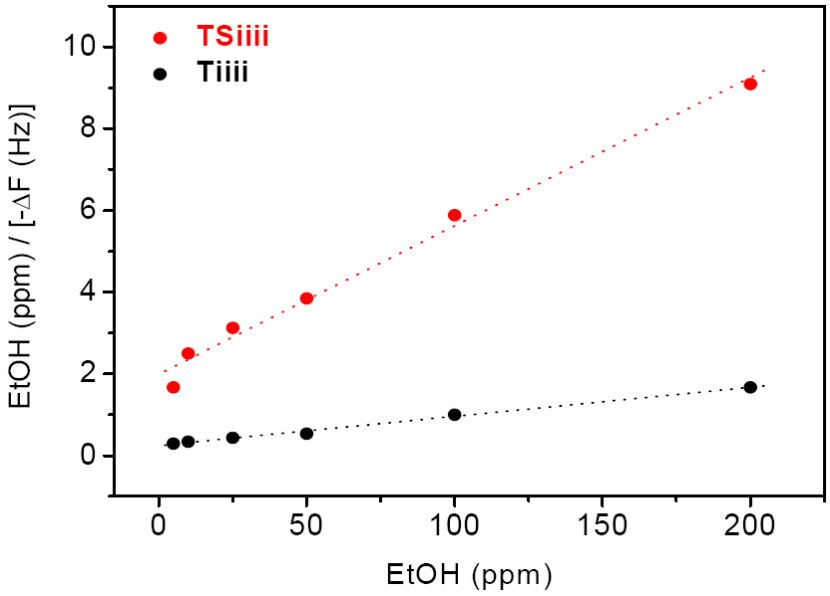

Figure 4.13. Langmuir adsorption plot for Tiiii[H, CH_3, Ph] and TSiiii[H, CH_3, Ph] to EtOH at several ppm.

As can be observed, Tiiii sample shows the best linear correlation. Indeed, the regression coefficients of interpolating straight lines for Tiiii and TSiiii samples are 0.998 and 0.995, respectively. As expected, these data indicate that Tiiii films exhibit a higher amount of active sites on which the analyte molecule can be trapped and detected.
In summary, with the VE technique we have improved the deposition method obtaining homogeneous and reproducible coating. Nevertheless the morphological features of the resulting coated layers are not much different of the spin-coated layers. To solve this issue we have decided to performed also another type of physical deposition: the GDS technique.

4.4 GDS deposition technique

Recently, a glow-discharge-based deposition technique has been developed for the realization of organic coatings.[14] Glow discharge-induced sublimation (GDS) is a method recently added to the more widely used spin coating and vacuum evaporation methods, mentioned above. The GDS method is based on a plasma-induced sublimation process, promoted by a weakly ionized gas discharge produced in radio frequency magnetron sputtering equipment. Low-energy (E < 500 eV) ions impinge on the solid organic precursors, leading to the sublimation of the organic molecules and to their condensation onto the substrate. The extension of the GDS method to cavitands suitable for sensors applications, requires a deeper knowledge of the deposition process of the precursor monomers. In particular, the discharge-induced damage, the morphology, and the aggregation state of the different molecules must be investigated to work out the deposition parameters which allow to achievement of a homogeneous and reproducible films. Moreover, the comprehension of the physical process governing the interaction between a low-energy glow discharge and organic molecules is still relatively unaccomplished, and systematic studies are needed to understand it in detail.
In this work the study of the GDS deposition on QCM transducer of Tiiii[H, CH_3, Ph] cavitand is reported. In that context the properties of the deposited films were investigated, as for the VE technique, by mass spectrometry to evaluate the damage and by AFM to analyze the morphology aspects.
The films were deposited on two different substrates: P-doped (1 0 0) silicon wafers lapped on both faces (Bayville Chemical Co.) for characterization

analyses (ESI-MS and AFM), and QCM for sensing measurements. The substrates were mounted on a routable sample holder placed 6 cm above the source. The thickness of the organic layer and the deposition rate were measured in real time by a quartz crystal microbalance. The experimental equipment used for the glow-discharge deposition of thin organic films consisted of a stainless steel vacuum chamber evacuated by a turbomolecular pump to a base pressure of 10^{-4} Pa. The device used to sustain the glow discharge was a 1-in. cylindrical magnetron sputtering source connected to a radio frequency power generator (600 W, 13.56 MHz) through a matching box. The organic powders were placed on the surface of an aluminum target, and placed on the sputtering source. The glow discharge feed gas used in all the depositions was argon. The pressure inside the chamber was measured through a capacitance gauge. Also in this case, the total mass deposited on the QCM is equal to 20 KHz (~10 KHz for each transducer side), the same value used for all coated QCMs previously reported. An accurate characterization of the properties of the deposited films was carried out, focusing the attention especially on the purity and the integrity of the cavitand films (ESI-MS characterization), on the surface roughness and on the porosity of the samples (AFM analysis).
The comparison of the ESI-MS spectra between the GDS films and the starting powders, demonstrates that in all cases the Tiiii coatings show several peaks diagnostic of the damage of the coated layer. This result contends that this cavitand is not fully stable under these conditions. The GDS deposition conditions probably break the P=O bridges, giving partially bridged cavitands and phosphines. Nevertheless, the layers obtained have been characterized by AFM and tested as sensor layers.

4.4.1 Morphological studies

The surface morphology of the cavitand samples was investigated using the same apparatus and procedure previously reported. Also in this case, as for the VE coatings characterization, since this work represents the first attempt to produce cavitand layers by GDS technique, the densities of samples were unknown; for this reason, initially we set up a fictitious density (1 g/cm^3) and a fictitious thickness (102.7 nm) on the *in situ* QCM. After the deposition we have measured the real thickness of the resulting coating and with the suitable equation (see paragraph 4.3.1) we have drawn the real density of the cavitand

coating. The average roughness, the thickness and the density of the samples are reported in Table 4.14.

	Tiiii[H, CH_3, Ph]
Thickness (nm)	1000
Roughness (nm)	31.2
Density (g/cm³)	0.10

Table 4.14. Thickness, roughness and density of the Tiiii GDS films.

As regards the topography, AFM images of GDS evaporated Tiiii coating are reported in Figure 4.15.

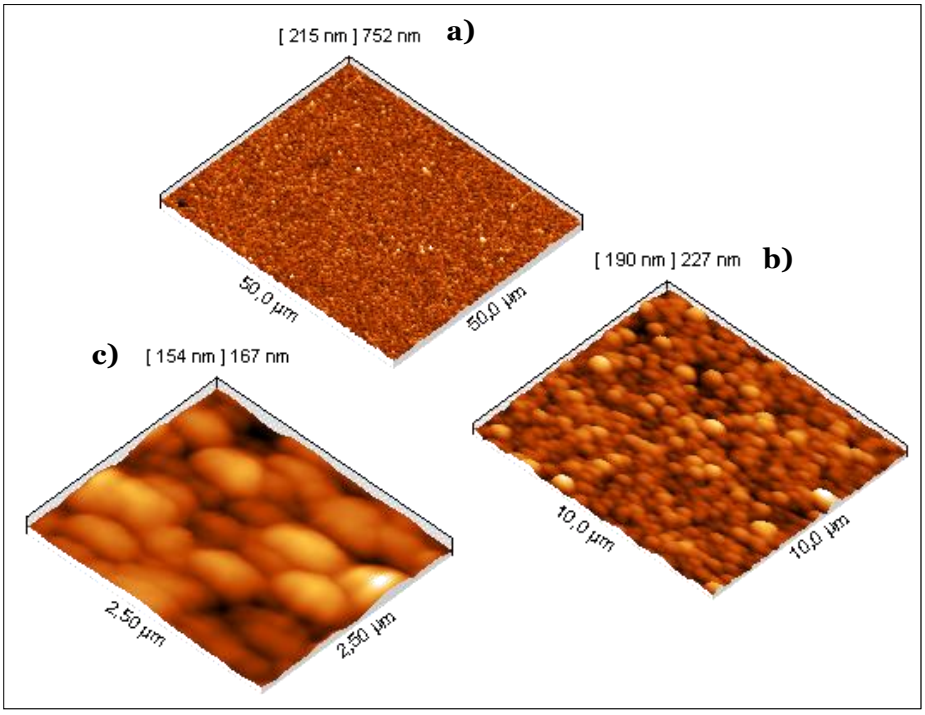

Figure 4.15. AFM images of GDS films: a) 50 x 50 µm², b) 10 x 10 µm² and b) 2.5 x 2.5 µm² scan of Tiiii[H, CH_3, Ph] surface.

Tiiii GDS samples show surface morphologies consisting of globular islands as in the case of VE surface coatings. The substantial difference between the two different coated samples consists in the thickness and in the roughness. Indeed the thickness in this case is very high, three times the VE coating layer thickness. Moreover the GDS coating exhibits a higher roughness with respect to the VE one; in particular it is possible to note (looking also the Table 4.14) that the average square roughness (Rq) of GDS sample (Rq=31.2 nm) is approximately eight times the VE sample (Rq=4.4 nm) one.
The very low value of the GDS cavitands coating density, in comparison than the spin-coating and VE one, represents an interesting result taking into account that the density of the samples, which is in inverse relation to the porosity, greatly influences the interaction between the analyte and cavitand layer.
These results based on the morphology lead to guess that the sensing responses of the GDS coating should be better than the spin-coating and VE one. The only one problem concerning the damage of the cavitand molecules within the layer. In the next paragraph we will compared the sensing performances of the Tiiii[H, CH_3, Ph] cavitand, coated by spin-coating, VE and GDS techniques.

4.5 Comparison between the performances of spin-coated, VE and GDS deposited QCMs at the gas solid-interface

The overall set of results obtained so far, shows that the cooperative behaviour of four convergent P=O groups in H-bonding and the synergistic presence of CH-π interactions, drastically enhances and stabilizes the complexation of alcohols in the gas phase. Indeed in the Chapter 2, we concluded that the Tiiii[H, CH_3, CH_3] coated layer shows a very high sensibility toward all alcohols also a low concentration (5 ppm). At the gas-solid interface not only the chemical but also the physical properties of the layer can play an important role in the sensing processes.
In this chapter we have described new deposition methods, VE and GDS techniques, which should be able to improve the performances of supramolecular mass sensors by changing the physical properties of the produced films.
The physical properties of the coated layers are very important because the gas sensing capabilities of the samples are strongly related to them. We have already

seen how surface roughness and porosity can influence the sensing capability of the VE coated films.

Now, we want to analyze the responses of the Tiiii[H, CH_3, Ph] cavitand deposited on the QCM transducers by spin coating, VE and GDS technique.

Among the comparison of this three different deposited QCMs, we can evaluate if the improvement in the deposition processes has a positive feedback in the sensing responses.

The response traces obtained exposing the three different Tiiii[H, CH_3, Ph] coating layers to 5 ppm of ethanol are depicted in Figure 4.16.

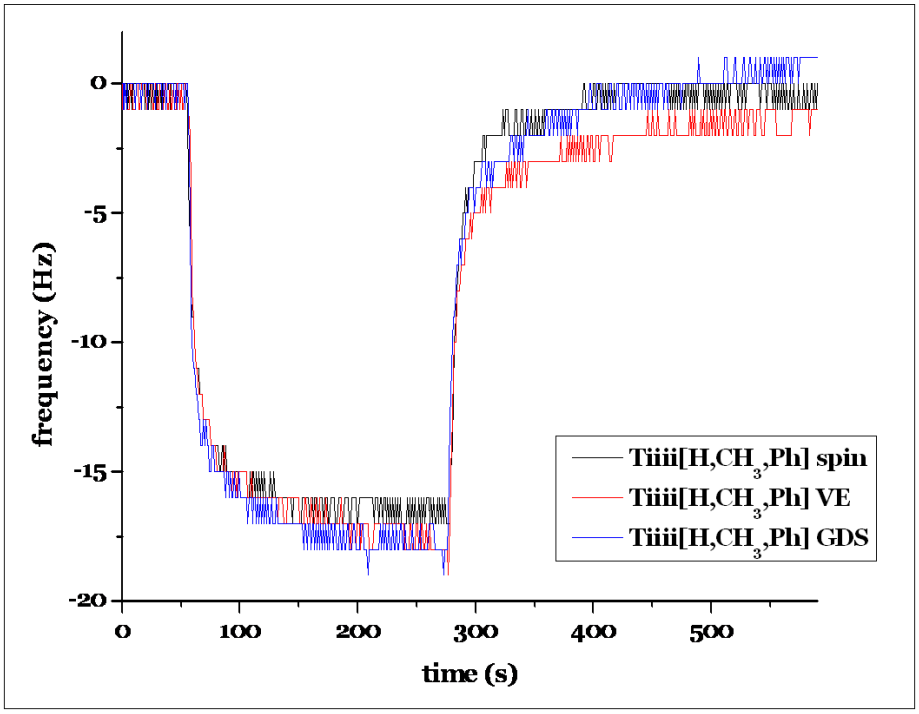

Figure 4.16. Responses traces to several concentration (ppm) of EtOH.

We can immediately observe that the three responses of sensors having differently deposited Tiiii[H, CH_3, Ph] layers are equivalent. Not only the magnitude of the responses are the same but both response and recovery times, too. This could mean that in this case the morphological improvement does not affect the gas-solid interaction processes. Before to draw any conclusions is better to deeply analyze the morphological data of the three layers, summarized in Table 4.17.

	Thickness (nm)	Roughness (nm)	Density (g/cm^3)
Tiiii[H, CH_3, Ph] spin	490	5.2	0.96
Tiiii[H, CH_3, Ph] VE	355	4.4	1.32
Tiiii[H, CH_3, Ph] GDS	1000	31.2	0.10

Table 4.17. Thickness , roughness and density of the Tiiii VE and spin-coated films.

Comparing the spin and VE layers, the substantial difference that we can observe is in the thickness of the coatings. In the case of VE film the thickness is slightly smaller than the spin-coated one. Instead the roughness and the density values are quite similar. This is the reason because the sensors responses have the same behaviour. Different is the case of the GDS layer, which shows very high values of thickness (approximately two times the spin-coated value) and roughness (approximately six times the spin-coated value). On the other hand, the density value is surprisingly low, therefore the porosity of the film is very high. These results relating to the Tiiii[H, CH_3, Ph] cavitand coated by GDS technique should have caused a consistent improvement in the sensing responses. But the GDS layer, toward ethanol, has the same behaviour of the spin-coating layer (Figure 4.16). The reason is not in the morphology but in the integrity of the film. Probably, in the GDS coated layer, the damage of the cavitand molecules is so high to suppress any advantage from the best morphological aspects. Finally, preliminary results obtained with the GDS technique prove the capabilities of this new deposition method. On the other hand, we have to change the operative conditions in order to avoid the damage of the cavitand layer.

4.6 Conclusions

Thin films of tetraphosphonate and tetrathio-phosphonate cavitands have been produced for the first time by high Vacuum Evaporation (VE) and Glow discharge-induced sublimation (GDS) techniques.
With the VE technique we have improved the deposition method (on QCM transducers) obtaining homogeneous, high pure and reproducible coatings. Moreover, since in this technique the deposition starts from the compound powders, we have obtained, for the first time, films of TSiiii[H, CH_3, Ph] cavitand, less soluble in any solvents. Consequently, we have compared the sensing performances of TSiiii and Tiiii cavitands toward ethanol, and deeply analyzed the sorption processes involved in the sensing at the gas-solid interface. The results obtained show how the morphological features of the VE coated layers are not much different from that of the spin-coated ones.
To solve this issue we have decided to try the new GDS technique. The morphologies analyses of the layers prove the capability, to form permeable layers, of this new deposition method. Preliminary tests at the gas-solid interface show that the sensing performances of the GDS layers are camparable to the spin-coating and VE one, even if they have a much high layer thickness. This reduced response is attributed to the damage of the cavitand molecules that occurs during the deposition. We are now performing the operative conditions in order to avoid this damage.

4.7 Acknowledgements

Special thanks to Dr. Gianluigi Maggioni, Dr. Michele Tonezzer and Dr. Riccardo Milan of the INFN of Legnaro (Pd) for the layer depositions and the AFM morphological analyses.

4.8 References

[1] J.Janata, M. Josowicz, *Anal. Chem.* **1998**, *70*, 179.

[2] M. Tonezzer, G. Maggioni, A. Quaranta, S. Carturan, G. Della Mea, *Sens. Actuators B* **2007**, *122*, 613.

[3] a) G. Maggioni, A. Quaranta, E. Negro, S. Carturan, G. Della Mea, *Chem. Mater.* **2004**, *16*, 2394; b) G. Maggioni, A. Quaranta, S. Carturan, A. Patelli, M. Tonezzer, R. Ceccato, G. Della Mea, *Chem. Mater.* **2005,** *17*, 1895.

[4] R.G. Pethe, C.M. Carlin, H.H. Patterson, W.N. Unertl, *J. Mater. Res.* **1993**, *8*, 3218.

[5] Nakagawa K, Sadaoka Y, Supriyatno H, Kubo A, Tsutsumi C, Tabuchi K, *Sens. Actuators B* **2001**, *76*, 42.

[6] S. Yu. Elovich and G.M. Zhabrova Zhur, *Fiz. Khim.* **1939**, *13*, 1761.

[7] C.M. Dooling, O. Worsfold, T.H. Richardson, R. Tregonning, M.O. Vysotsky, C.A. Hunter, K. Kato, K. Shinbo and F. Kaneko, *J. Mater. Chem.* **2001**, *11*, 392.

[8] D.P. Arnold, D. Manno, G. Micocci, A. Serra, A. Tepore, L. Valli, *Langmuir* **1997**, *13*, 5951-5956.

[9] K. Bodenhöfer, A. Hierlemann, M. Juza, V. Schurig, W Göpel, *Anal. Chem.* **1997**, *69*, 4017.

[10] S. Braunauer, P. H. Bennet, *J. Am. Chem. Soc.* **1937**, *10*, 2682.

[11] J. Toth, *Acta Chimica, Acad. Sci. Hung* **1971**, *69*, 311.

[12] H. Freundlich, *Kapillarchemie*, vol. 1, Akademische Verlagsgellaschaft mbH, Leipzig, **1909**.

[13] a) I. Langmuir, *J. Am. Chem. Soc.* **1918**, *40*, 1361; b) O. Worsfold, C.M. Dooling, T.H. Richardson, M.O. Vysotsky, R. Tregonning, C.A. Hunter, C. Malins, *J. Mater. Chem.* **2001**, *11*, 399.

[14] a) G. Maggioni, S. Carturan, V. Rigato, U. Pieri, *Nucl. Instr. Methods B* **2000,** *166-167*, 737; b) G. Maggioni, S. Carturan, A. Quaranta, A. Patelli, G. Della Mea, *Chem. Mater.* **2002,** *14*, 4790.

Rational design of water clusters with phosphonate cavitands

5

5.1 Introduction

As the most abundant and cheapest compound on earth, water plays an important role in most biological systems and, chemical and physical processes. Supramolecular association of water molecules in diverse environments has been a subject of considerable current interest. This is because the key to test and calibrate theoretical studies in order to understand the properties of bulk water is the precise structural data of hydrogen-bonded small water clusters in different environments. The advantage of clusters is the possibility to simply vary the size and to investigate the development of properties of the condensed phase in a step by step manner. Bulk water exhibits a fascinating array of properties, some of which are considered anomalous, and this is due to tremendous fluctuations in H-bonding interactions and rearrangement dynamics among the water molecules in a group. Although much progress has been made, some of the water properties still can not be accurately described. Up to now, several water clusters have been obtained in diverse hosts.[1,2,3,4,5,6] The presence of water molecules in solid-state structures can play an important role in stabilizing supramolecular structures. For example, synergistic hydrogen bonding between water and organic molecules has helped to stabilize vase-like conformations of hosts for organic molecules[7] and to induce the formation of

intricate hexameric nanoscale capsules stitched together with the aid of eight water molecules.[8] Conversely, such supramolecular scaffolds can also stabilize unusual morphologies of water that may not be at the global energy minimum expected from theoretical calculations.[9] Nevertheless, the predictability and rational design of water morphologies still remain a challenge. From a detailed structural perspective, the key questions to be addressed are what effect do water molecules have on their neighbours and on their surroundings, and how do water–water interactions compete with water-solute (or, in the solid state, hydrate-host) interactions?
Herein we report the phosphonate cavitands as scaffolds that surprisingly form complexes with discrete monomer, dimer and tetramer of water. To our knowledge, this is the first example of water clusters confined in cavitand structures.

5.2 Crystal structures of Tiiii[H, CH_3, CH_3] with water

We have already discussed in Chapter 2, the great capability of Tiiii[H, CH_3, CH_3] cavitand to crystallize. The reason of this tendency has to be found in the rigid, compact and high symmetric structure of this tetraphosphonate cavitand.
The presence of four phosphonate (P=O) groups at the upper rim, with great affinity for H-bonding interactions, prompted us to study the complexation properties of this cavitand toward water.

5.2.1 Crystal structure of Tiiii[H, CH_3, CH_3]·4H_2O

Here we reports the Tiiii[H, CH_3, CH_3]·4H_2O complex crystal structure (Figure 5.1), which was obtained adding water to a suspension of the tetraphosphonate cavitand in acetonitrile (which immediately caused the complete solubilization of the suspended cavitand) followed by slow evaporation.

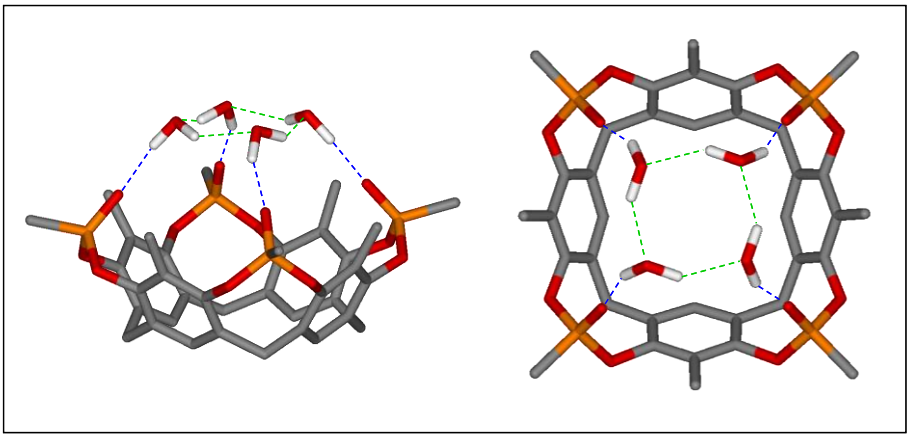

Figure 5.1. Side and top view of Tiiii[H, CH_3, CH_3]·4H_2O. (Colour code: P, orange; O, red; C, grey; H, white; weak intermolecular interactions, blue and green). The hydrogen atoms not involved in the interactions are omitted for clarity.

The complex crystallizes in the tetragonal group P4/n: only one fourth of the molecule is independent and the rest is generated by symmetry via the fourfold axis passing through the center of the cavitand. This leads to a highly symmetric structure in which every water molecule acts as a hydrogen bond donor to a P=O group [O-H···O(P) 1.850(5), 159.35(9)°, blue dotted line in Figure 5.1] and at the same time as a hydrogen bond donor and acceptor with two adjacent water molecules, respectively [O-H···O 2.050(5) Å, 138.88(9)°, green dotted lines in Figure 5.1]. In this way the four water molecules are linked each other to form a tetramer cluster.

Among the water clusters, the cyclic water tetramer is of particular interest. According to a simple two-structure model for liquid water, cubic-shaped water octamers can dissociate into two cyclic water tetramers, which appear to be the principal species present in liquid water. For this reason, tetrameric clusters of water molecules were widely investigated both theoretically and experimentally.[4,9b,10] Both theoretical calculations and vibration rotation tunnelling spectroscopy of the water tetramer in the gas phase, indicated a quasi planar cyclic structure, in which each water molecule forms two hydrogen bonds; one as a donor and the other as acceptor. In the tetramer all the H_2O molecules are equivalent to each other and the directions of their dipoles (being approximately along the bisector of the intermolecular H-O-H angle) alternate above and below the plane of the cluster (Figure 5.2). Assuming an S_4 symmetry

(are possible C_4 and C_s symmetry, too) for the tetramer, the average O-H····O bond length was estimated to be 2.83 Å.

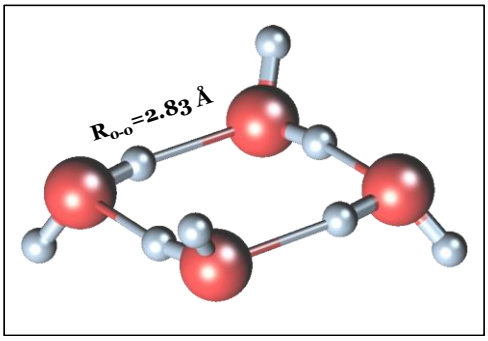

Figure 5.2. Optimal configuration of water tetramer at the gas phase.

In the complex presented herein, the water cluster has C_4 symmetry with quasi planar ring structure where each water monomer acting as both single H-bond donor and acceptor, and all four hydrogens, bonded to the P=O groups, are oriented in the same direction below the ring. Moreover, the four H-bonds distances of the cluster are the same (2.86 Å) and consistent with the theoretical result (Figure 5.2).

Interestingly, this water cluster is also responsible for a three-dimensional pattern of the crystal lattice, where each water molecule is involved in four H-bonds (see Figure 5.3). There is only another case of a discrete water cluster, described by F. Oberdorfer *et al.*,[9c] where the water molecules are virtually tetrahedrally coordinated in a three-dimensional network through hydrogen bonds.

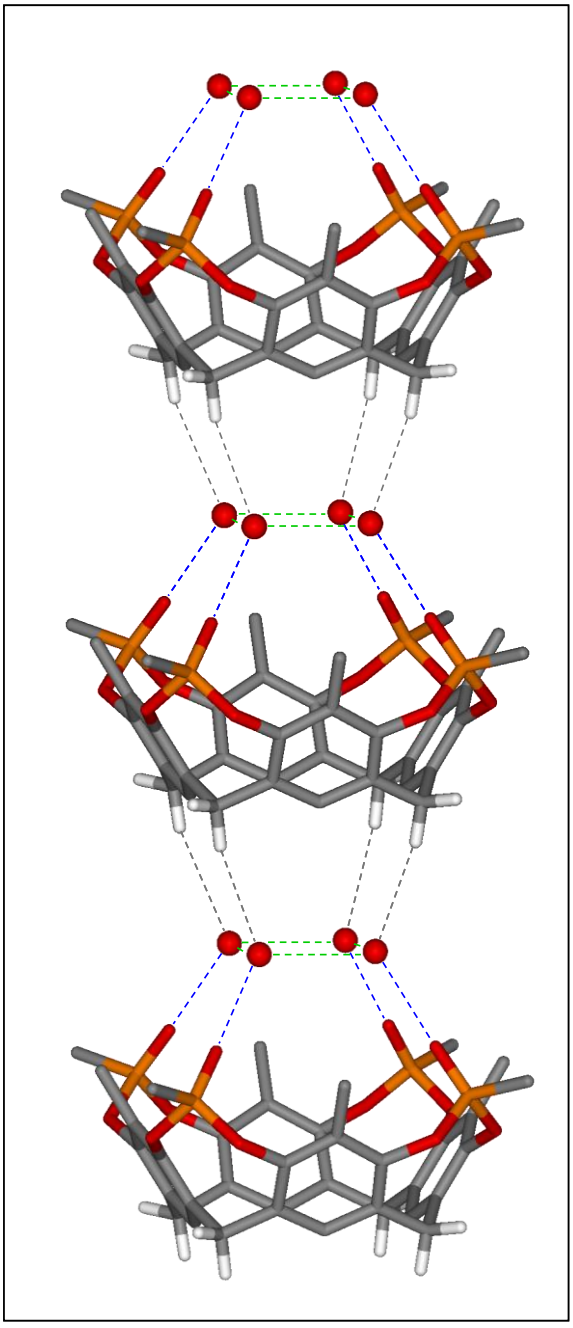

Figure 5.3. One of the two sets of parallel channels formed by Tiiii[H, CH_3, CH_3]·4H2O along the *c* direction of the unit cell. Only relevant hydrogen atoms have been reported in the drawing. Water molecules are represented as red balls.

In detail, the cavitands form two sets of parallel channels (with opposite orientation of the cavitands in each set) along the *c* axis of the unit cell. The interactions which keep the cavitands piled one above the other are four equivalent hydrogen bonds involving the water molecules and the hydrogen atoms of the methylenic groups at the lower rim [C-H···O, 2.669(4) Å, 160.56(9)°].

5.2.2 Crystal structure of Tiiii[H, CH_3, CH_3]·2H_2O

Here we reports the Tiiii[H, CH_3, CH_3]·2H_2O·2TFE crystal structure, which is obtained by slow diffusion of water into a CH_2Cl_2/trifluoroethanol (TFE) solution of the cavitand. The crystal structure depicts (Figure 5.4) how only two water molecules are involved in a zig-zag chain of hydrogen bonds with two distal P=O groups, instead of binding each of them as in the previous case.

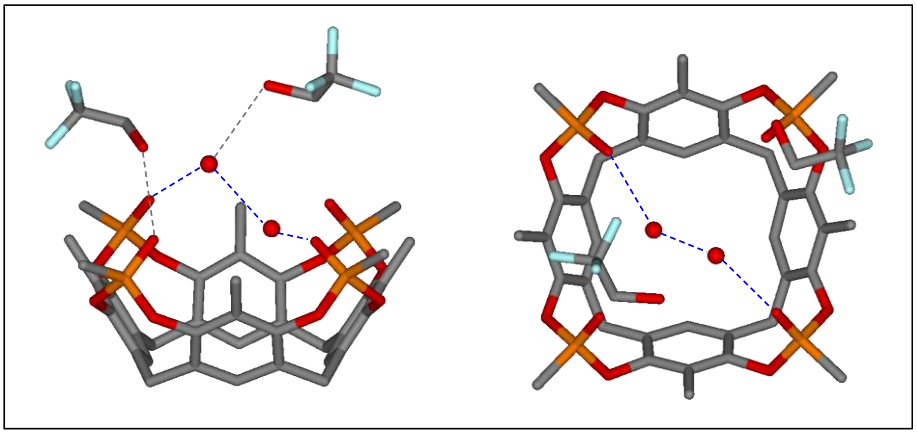

Figure 5.4. Side and top view of Tiiii[H, CH_3, CH_3]·2H_2O·2TFE. (Colour code: P, orange; O, red; C, grey; H, white; weak intermolecular interactions, blue). Hydrogen atoms are omitted for clarity.

In detail, a cluster of two water molecules, bonded to each other by a strong hydrogen bond, [O···O 2.62(1) Å] is also interacting with the two distal P=O groups of the cavitand, giving rise to a zig-zag chain of hydrogen bonds [O···O=P 2.73(1) Å and 2.80(1) Å]. Of the two TFE molecules, one is linked to the cavitand through a hydrogen bond with a P=O group [O···O=P 2.82(1) Å], whereas the second TFE lies in the second coordination sphere connected through a weaker hydrogen bond to one of the two water molecules [O···O 3.03(1) Å].

This means that the crystallization conditions, that is the presence of an alcohol molecule capable of forming hydrogen bonds, influence the water cluster formation pattern. Both one of the P=O groups and one water molecule are in fact involved in interactions with the TFE, which prevents the formation of a larger water cluster like the one described in the previous example.
Indeed in this case we are able to isolate a water dimer instead a tetramer.
The water dimer is the most simple water-water system and its geometry, predicted by several calculations of molecular orbital theory[11] was perfectly confirmed by experimental studies.[12]

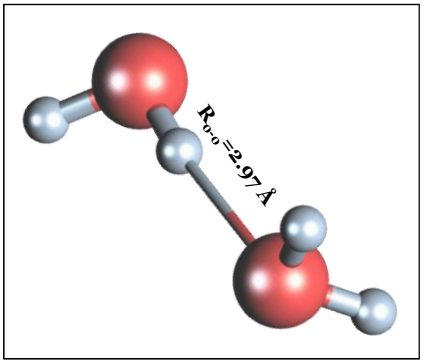

Figure 5.5. Optimal configuration of water dimer in the gas-phase.

We want highlight that the O···O distance in the water dimer, depicted as a guest of the Tiiii cavitand in Figure 5.4, is 2.62 Å. For comparison, the corresponding values in regular ice, in liquid water and in the gas phase (Figure 5.5) are 2.74, 2.85 and 2.97 Å, respectively.[13] In our case the smaller length of the H-bond, between the two water molecules, is due to the stabilization and constrain generated by the cavity in the host-guest final complex.

5.3 Crystal structures of 2POii2PSii[H, CH_3, Ph] with water

In Chapter 3 we have demonstrated that it is possible to enhance the sensors selectivity by changing the shape of the receptor cavity. Indeed, the introduction of two bulky P=S bridges, unable to H-bond to the analytes, makes the resulting cavitands by far more specific in recognizing of small alcohols with the respect to the parent Tiiii compound. In this work we wanted to exploit the difference

between the Tiiii and 2POii2PSii cavitands to create a specific and predictable water-cavitand complexes.

5.3.1 Crystal structure of AB 2PO2iiPSii[H, CH_3, Ph]·H_2O

Here we report the structure of the AB 2PO2iiPSii[H, CH_3, Ph]·H_2O complex, the crystals of which were obtained by slow diffusion of water in a CH_2Cl_2/TFE solution of the cavitand.

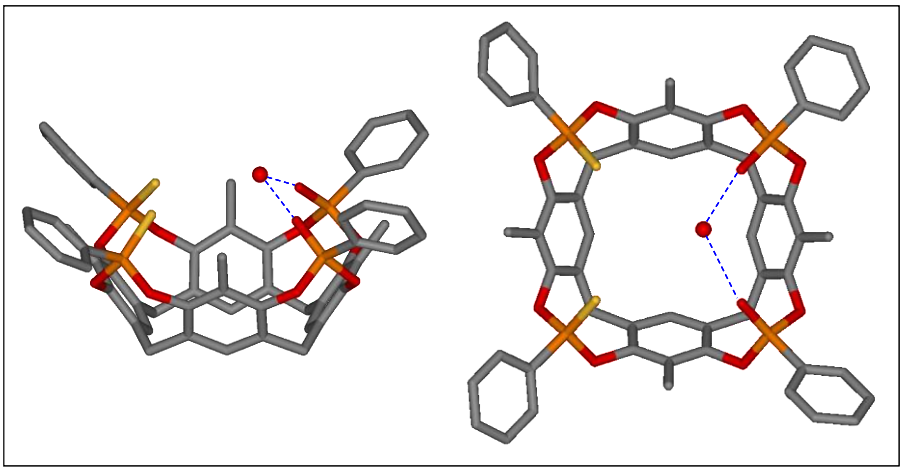

Figure 5.6. Side and top view of AB 2PO2iiPSii[H, CH_3, Ph]·H_2O. (Colour code: P, orange; O, red; C, grey; H, white; weak intermolecular interactions, blue). Hydrogen atoms are omitted for clarity.

Only one water molecule interacts with the cavitand forming two geometrically different hydrogen bonds with the to adjacent P=O groups [O-H···O(P) 2.480(9) and 2.847(9) Å] (see Figure 5.6).
In the lattice, the cavitands form channels along the *a* directions of the unit cell, stabilized by the presence of weak interactions involving the hydrogen atoms of the lower rim, the water molecules and the oxygen atoms of the P=O groups (Figure 5.7).

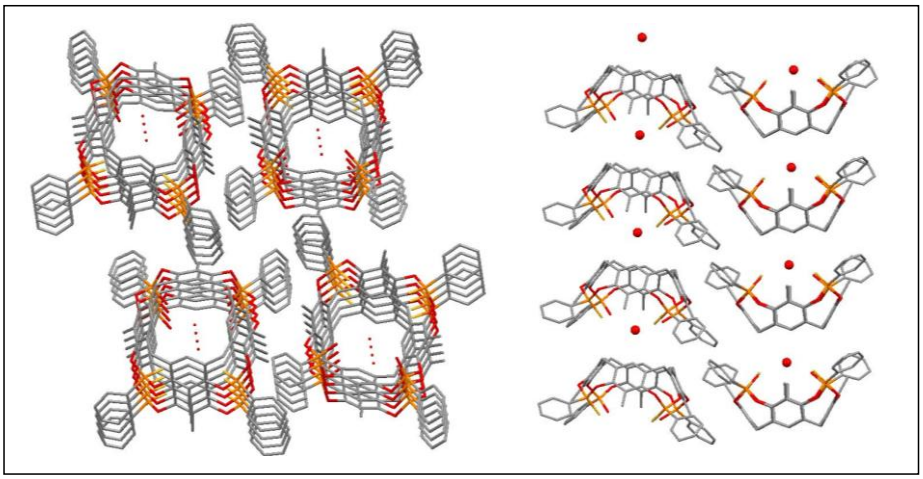

Figure 5.7. Top and side view of AB 2PO2iiPSii[H, CH_3, Ph]·H_2O lattice. (Colour code: P, orange; O, red; C, grey; H, white; weak intermolecular interactions, blue). Hydrogen atoms are omitted for clarity.

In contrast to the two structures previously reported no water cluster is formed. This result is expected by looking the structure of the cavitand. Indeed, the presence of two P=S moieties unable of H-bonding, and of only two P=O moieties in vicinal position give rise preferably a coordination of only one water molecule.

5.4 Conclusions

Cavitand hosts show the ability to organize H-bonds and "to freeze" water in definite clusters. We have presented for the first time, discrete water tetramer, dimer and monomer, confined in cavitand structures. Moreover, we have shown the cooperative contribution of the crystallization environment and of the receptor cavity shape to the final topology of the cluster formed.
Because it is possible for water clusters in solution and in solid state to be discrete, the precise structural data and cooperative association of the water cluster and the host may be helpful in improving our understanding of the contribution of water cluster to the stability and function of the biological assemblies, as well as anomalous properties of water.

5.5 Acknowledgments

Special thanks to Dr. Chiara Massera of the University of Parma for all X-Ray crystallographic analyses.

5.6 References

[1] H_2O dimer: S. Manikumaei, V. Shivaiah, S.K. Das, *Inorg. Chem.* **2002**, *41*, 6953.

[2] H_2O trimers: (a) L.R. Macgillivary, J.L. Atwood, *J. Am. Chem. Soc.* **1997**, *199*, 2592; b) F.N. Keutsch, J.D. Cruzan, R.J. Saykally, *Chem. Rev.* **2003**, *103*, 2533.

[3] H_2O tetramers: a) S. Supriya, S. Manikumari, P. Raghavaiah, S. K. Das, *New J. Chem.* **2003**, *27*, 218; b) S. Supriya, S.K. Das, *New J. Chem.* **2003**, *27*, 1568; c) L.-S. Long, Y.-S. Wu, R.-B. Huang, L.-S. Zheng, *Inorg. Chem.* **2004**, *43*, 3798; d) J. Tao, Z.-J. Ma, R.-B. Huang, L.-S. Zheng, *Inorg. Chem.* **2004**, *43*, 6133.

[4] H_2O hexamers: a) J. N. Moorthy, R. Natarajan, P. Venugopalan, *Angew. Chem. Int. Ed. Engl.* **2002**, *41*, 3417; b) S.K. Ghost, P.K. Bharadwaj, *Inorg. Chem.* **2004**, *43*, 5180; d) B.-H. Ye, B.-B. Ding, Y.-Q. Weng, X.-M. Chen, *Inorg. Chem.* **2004**, *43*, 6866; e) Y.-C. Liao, Y.-C. Jiang, S.-L. Wang, *J. Am. Chem. Soc.* **2005**, *127*, 12794.

[5] H_2O octamers: a) J.L. Atwood, L.J. Barbour, T.J. Ness, C.L. Raston, P.L. Raston, *J. Am. Chem. Soc.* **2001**, *123*, 7192; b) R.J. Doedens, E. Yohannes, M.I. Kahn, *Chem. Commun.* **2002**, 62; c) B.-Q. Ma, H.-L. Sun, S. Gao, *Chem. Commun.* **2005**, 2336; d) T.K. Prasad, M.V. Rajasekharan, *Cryst. Growth. Des.* **2006**, *6*(2), 488.

[6] H_2O decamers: a) L.J. Barbour, G.W. Orr, J.L. Atwood, *Nature* **1998**, *393*, 671; b) L.J.Barbour, G.W. Orr, J.L. Atwood, *Chem. Commun.* **2000**, 859; c) A. Michaelides, S. Skoulika, E.G. Bakalbassis, J. Mrozinski, *Cryst. Growth. Des.* **2003**, *3*, 487; d) R. D. Bergougant, A. Y. Robin, K. M. Fromm, *Cryst. Growth. Des.* **2005**, *5*, 1691.

[7] F. Hof, L. Trembleau, E.C. Ullrich, J. Rebek, *Angew. Chem. Int. Ed. Engl.* **2003**, *42*, 3150.

[8] M. Yamanaka, A. Shivanyuk, J. Rebek, *J. Am. Chem. Soc.* **2004**, *126*, 2939.

[9] a) S. Pal, N.B. Sankaran, A. Samanta, *Angew. Chem. Int. Ed. Engl.* **2003**, *42*, 1741; b) M. Zuhayra, W. U. Kampen, E. Henze, Z. Soti, L. Zsolnai, G. Huttner, F. Oberdorfer, *J. Am. Chem. Soc.* **2006**, *128*, 424; c) S.O. Kang, D. Powell, V.W. Day, K. Bowman-James, *Cryst. Growth. Des.* **2007**, *7* (4), 606; d) M. H. Mir, J.J. Vittal, *Angew. Chem. Int. Ed. Engl.* **2007**, *46*, 5925.

[10] a) S.S. Xantheas, T.H. Dunning, *J. Chem. Phys.* **1993**, *99*, 8774; b) J.D. Cruzan, L.B. Braly, K. Liu, M.G. Brown, J.G. Loeser, R.J. Saykally, *Science* **1996**, *271*, 59.

[11] a) T. Ziegler, *Chem. Rev.* **1994**, *100*, 7523; b) S.S. Xantheas, *J. Chem. Phys.* **1994**, *100*, 7523; c) S.S. Xantheas, *J. Chem. Phys.* **1991**, *91*, 651; d) R. Knochenmus, S. Leutwyler, *J. Chem. Phys.* **1991**, *96*, 5233.

[12] K. Liu, M.G. Brown, R.J. Saykally, *J. Phys. Chem.* **1997**, *101*, 8995.

[13] R. Ludwig, *Angew. Chem. Int. Ed. Engl.* **2001**, *40*, 1808.

Large and stable synthetic ion channels from lipophilic guanosine*,†

6

6.1 Introduction

The formation of duplex DNA from its single stranded constituents is a result of a panoply of intermolecular forces, including aromatic π-stacking, van der Waals forces, and hydrophobic effects.[1] However, the high fidelity observed in pairing of complementary DNA sequences is largely due to nucleobases *via* Watson-Crick pairing and hydrogen-bonding interactions.[2] Related interactions also play a critical role in stabilizing higher-order RNA structures, such as hairpin loops, whereas Hoogsteen base-pairing is important in the formation of triple helix DNA and so-called G-quartets. Thus, in the broadest sense, hydrogen-bonding interactions involving base-pairs must be considered as playing a pivotal role in such critical areas as genetic coding, biological information storage, and protein synthesis.

One of the core goals of many chemists has been to overcome the natural realm and to use complementary nucleobase-pairing to construct novel

---

* This work has been carried out at the University of Maryland in the group of Prof. Jeffery T. Davis.

† This chapter is based on: L. Ma, M. Melegari, M.Colombini, J.T. Davis, *J. Am. Chem. Soc.* **2008**, in press.

supramolecular assemblies. Molecular self-assembly is central to many processes in both biology and supramolecular chemistry.

The synthetic G-quartet motif, a hydrogen-bonded macrocycle formed by cation templated assembly of guanosine, was first identified in 1962 as the basis for the aggregation of 5'-guanosine monophosphate. We now know that many nucleosides, oligonucleosides, and synthetic derivatives form a rich array of functional G-quartets.

Davis' group[3] and others,[4] have proposed the G-quartet motif as a scaffold for building synthetic transmembrane ion channels which may ultimately provide new sensors and antimicrobical agents.[5]

In this chapter we report three different ditopic lithocholate molecules, as a case study to pinpoint the main interactions responsible of ion channels self-assembly in phospholipid membranes. The specific interactions involved in solution are analyzed and their potentials for the generation of large and stable pores in planar lipid bilayer are explored.

6.2 The G-Quadruplex

In the presence of templating cation, guanosine derivatives, form a lipophilic G-quadruplex that is stable in non-polar solvents. The G-quadruplex, with chiral twisted supramolecular architecture, represents a nice example of a dynamic supramolecular system built from the vertical stacking of multiple G-quartets, $[G]_4$. To better understand how individual $[G]_4$ organize within G-quadruplex, $[G]_{16}$, the Gottarelli and Davis groups solved the NMR structure of the octamer$[G]_8$·KI in $CDCl_3$.[6] This study showed that the $[G]_8$·KI existed as single diastereomer with the templating K^+ sandwiched between an all-*anti* G-quartet and an all-*syn* G-quartet. Figure 6.1 illustrates the synthetic potential of self-assembly from guanosine to G-quadruplex.

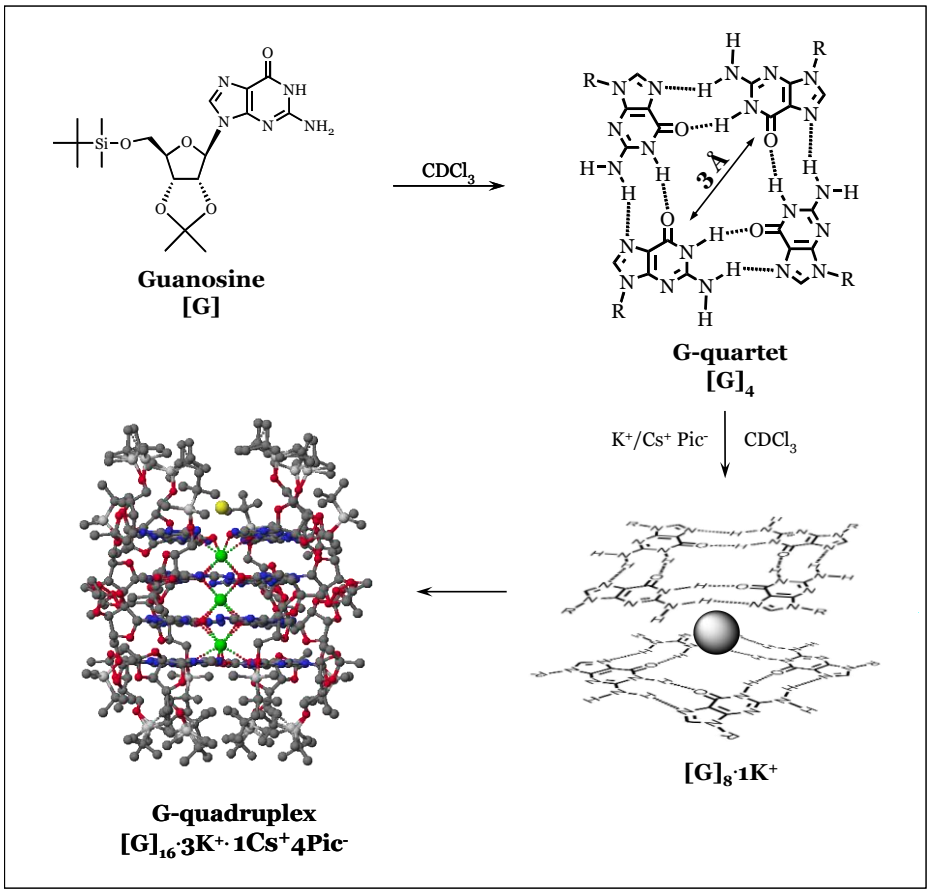

Figure 6.1. From Guanosine to G-quadruplex**.**

While the non-covalent interactions that enable formation of a G-quadruplex are certainly interconnected, the structure can be dissected into three organizational levels. At the first level, four molecules of guanosine, [G], use self-complementary hydrogen bonds to form a planar G-quartet. At the second level, an octacoordinate cation, such as K^+, forms cation-dipole interactions with eight separate molecules of [G], placing between two G-quartets. The result is two G-quartets stack with a separation of 3.3 Å between individual layers. Indeed the cation-dipole interactions stabilize hydrogen-bonded quartets and enhance base-stacking interactions to provide a C_4-symmetric $G_8{\cdot}K^+$ octamer. At the third level, the counter ions, such as picrate anions, hydrogen bond to amino groups projecting from the G-quartets. These nucleobase-anion hydrogen bonds link the two inner G-quartets in the D_4-symmetric hexadecamer

$[G]_{16}\cdot 3K^{+}\cdot Cs^{+}\cdot 4Pic^{-}$, a structure stable either in solution and in the solid state. The crystal structure obtained from chloroform has shown a single diastereomer with long-range order (24 units), with dimension of 26 x 30 x 30 Å and a molecular weight of over 8500 a.m.u.
One remarkable feature of this structure is the presence of four collinear cations, spaced 3.3 Å apart, that are arranged down a central channel. The electrostatic repulsion that might be expected between the channel cations is clearly minimized by the G-quartet oxygen atoms and aromatic rings.

6.3 Toward synthetic ion channels

In the last few decades, the supramolecular macrocycle of lipophilic G-quartets[3] and the similar folic acid quartets[7] have been proposed as powerful scaffolds for building synthetic supramolecular ion channels. NMR studies have shown that base pairs in DNA G-quadruplexes open slowly and G-quadruplex dissociation is often quite slow, taking days or weeks. Yet, K^{+} ions are bound for only milliseconds.[8] These results suggest that ions move without disruption of the G-quartet, thus making that G-quadruplex analogous to an ion channel. Indeed, Davis' group found that a non-covalent assembly of 16 guanosine monomers could be cross-linked to give a "unimolecular" G-quadruplex that can transport Na^{+} across lipid membranes.[9]
Despite the thermodynamic stability of the non-covalent G-quadruplex assembly, individual guanosine subunits are in dynamic equilibrium between "monomer" and hexadecamer when lipophilic G-quadruplexes are in solution.[10] To circumvent these problems, posed by such kinetic instability, they decided to use olefin methatesis to cross-link subunits that had been organized within a G-quadruplex.

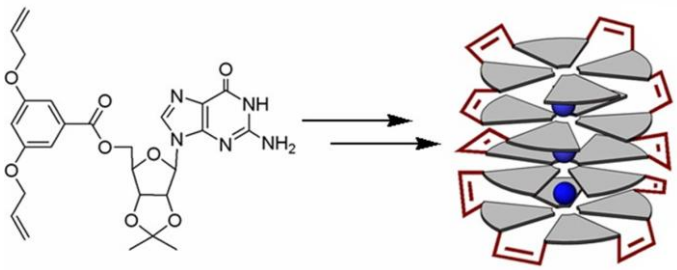

Figure 6.2. Olefin metathesis strategy that provides an unimolecular G-quadruplex.

They obtained circular dichroism and NMR evidence for the formation of the supramolecular complex shows in Figure 6.2. Moreover the unimolecular G-quadruplex obtained apparently folds into a conformation that allows it to transport Na^+ ions across phospholipid bilayer membranes.
On the other hand, the Lehn and Barboiu groups have independently shown that ditopic monomers with guanine end-groups form dynamic supramolecular polymers, in a reversible process that is templated by alkali cations. In addition to the central G-quartet channel, such structures might well stack to form pores for transmembrane transport. Of particular relevance to this present study was Barboiu's demonstration that Na^+ and K^+ ions could be transported across films made from G_4-quartet polymers.[11]
Moving from these considerations, we report a different approach to stabilize the G-quartet channels self-assembled in lipid bilayer.
To achieve this goal, a ditopic compound with hydrophilic guanosine to cap the ends of a hydrophobic bis-sterol, was designed (Figure 6.3).

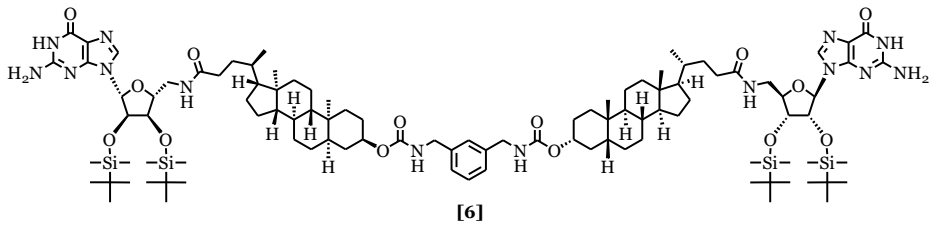

[6]

Scheme 6.3. Ditopic guanosine lithocholate **6.**

The bis-lithocholic acid spacer was inspired by Kobuke's studies that showed how bis-cholic acid derivatives are able to self-assemble and give small cation-selective channels, in planar phospholipid membrane.[12]
We have conceived compound **6** because its structure combines two different aspects:

- the hydrophilic guanosine moieties afford the self-assembly of the G-quartet and G-quadruplex, which can give transmembrane ion channels.
- the hydrophobic bis-lithocholic acid linker is able to increase the permeability of the compound in the phospholipid membrane (hydrophobic environment).

The structure of the compound **6** enables the formation of several different aggregates, as is depicted in Figure 6.4.

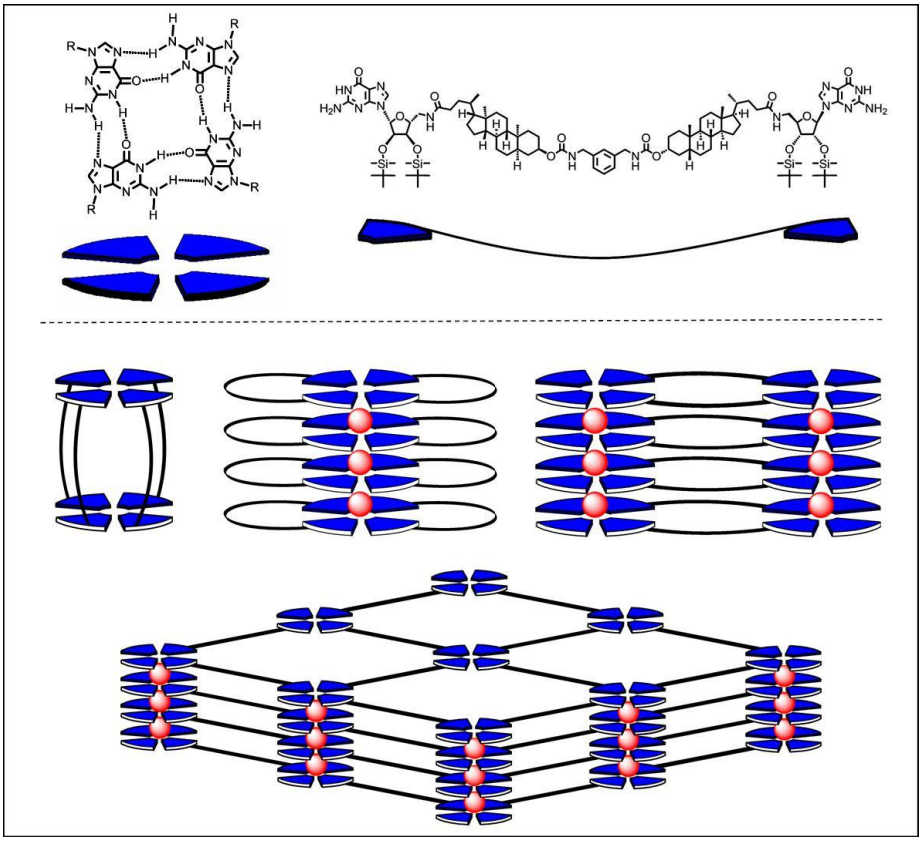

Figure 6.4. Possible G- quartet stack formed by bis-G-lithocholate **6**.

Some of these self-assembled structures are possible because the linker is sufficiently flexible to assume several conformations. As confirmed by the modelling represented in Figure 6.5, two molecules of **6** are able to fold and self-assemble together.

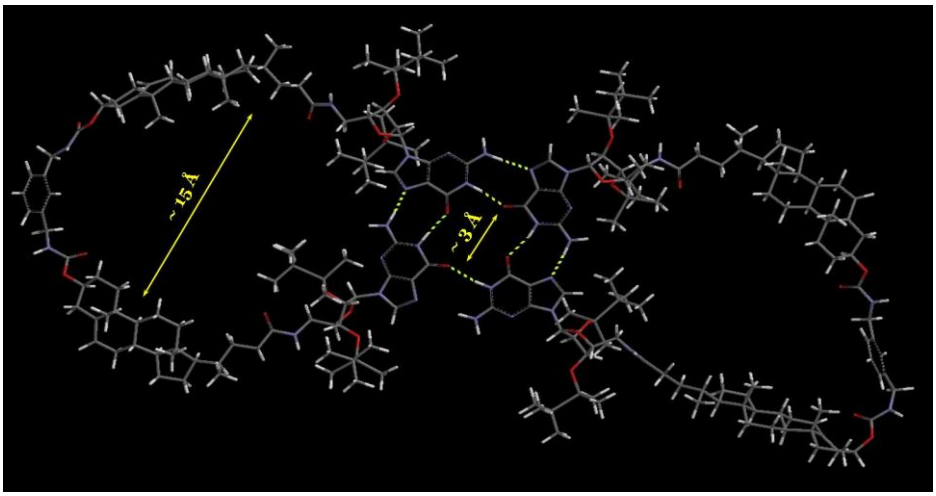

Figure 6.5. Molecular modelling of a possible self-assembling mode of two molecules of **6**.

The resulting structure shows in the middle the G-quartet motif and at the two sides the loops created by the folded linkers. Therefore we have an aggregate with three pores: a small central one (~3Å) delimited by the G-quartet and two large equivalent peripheral ones (~15Å) generated by the linkers loop. This is only an example to demonstrate the flexibility of the linker, but there are several possible structures as shown in Figure 6.4.

Since it is not easy to demonstrate *a priori* that these aggregates are possible only with guanosine end groups and that these structures are likely ion-channels, we have designed "control" compounds.

Therefore for a meaningful comparison we have synthesized also compounds **7** and **8** equipped with methyl amide and adenosine end groups, respectively (Figure 6.6).

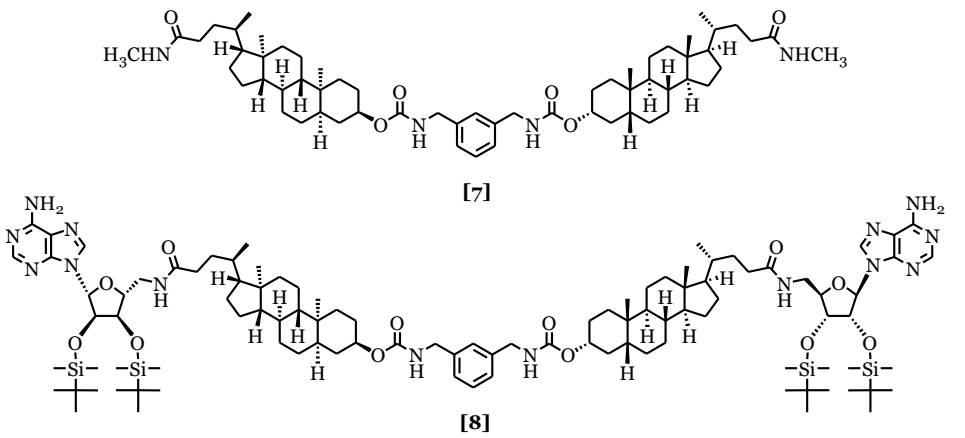

Scheme 6.6. Bis-lithocholamide **7** and bis-A-lithocholate **8** compounds**.**

In the first case, the introduction of a methyl amide, as an end-group, prevents the formation of any panoply of H-bonding interactions. Therefore compound **7** should not be able to self-assemble into any of the types of aggregates depicted in Figure 6.4. This will be a clear evidence that the guanosine presence is fundamental for the self-assembly required for the ion-channels formation.
Differently, in compound **8**, the end-groups are derivatives of adenosine, a nucleoside with different pattern of H-bonding donor and acceptor moieties than guanosine. This compound forms a different network of H-bonding interactions with respect to the guanosine. Despite the different geometry, the adenosine end group may allow the aggregation in supramolecular structures, but preclude the formation of a structure similar of the G-quartet and preventing the topology of self-assembled aggregates expected with the compound **6**. Moreover, the stability of the possible array of H-bonding interactions is smaller than the case of the G-quartet, also because the adenosine does not show the stabilizing effect by an octacoordinate cation. Finally, with the compound **8** we wanted to confirm that only with the guanosine end-groups is it possible to generate stable and extremely reproducible ion-channels.
The synthesis of the bis-lithocholate acid linker is presented in the Scheme 6.7 (see Experimental part).

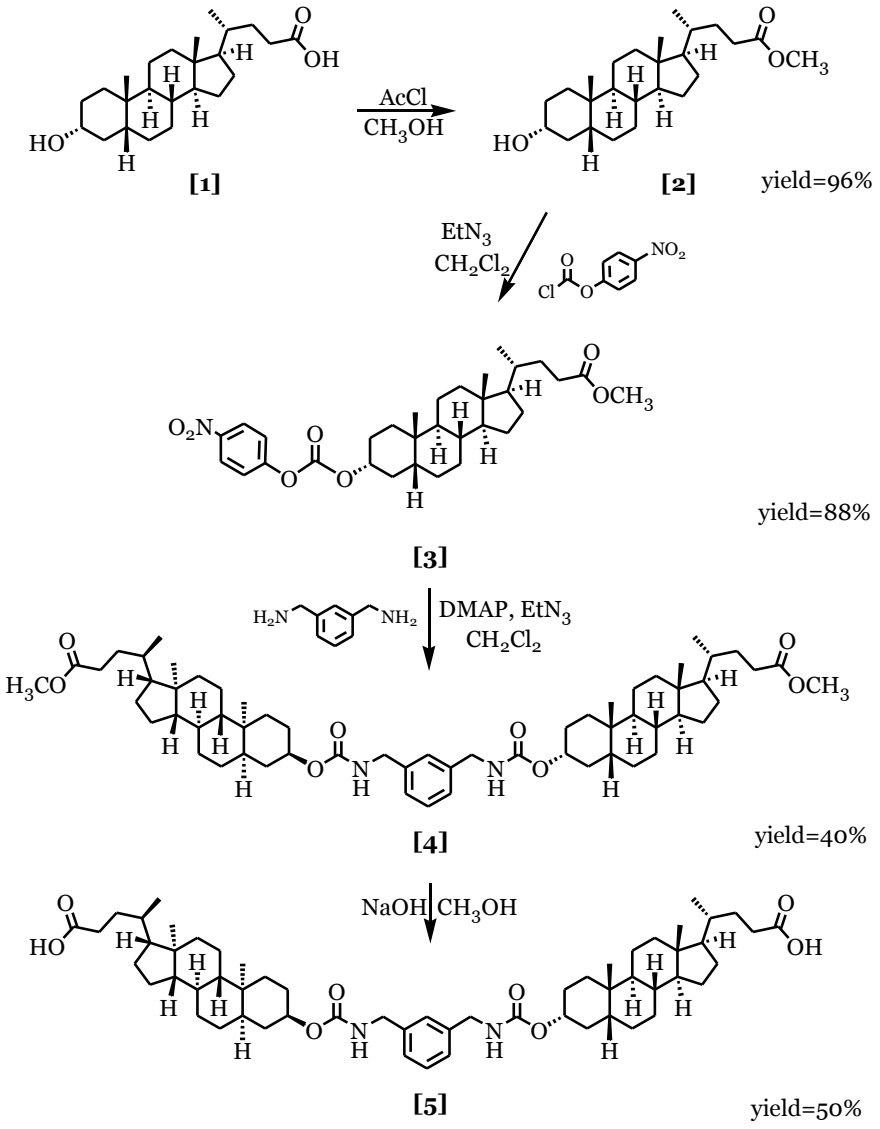

Scheme 6.7. Synthesis of bis-lithocholate linker.

The first reaction, that is the protection of the lithocholic acid carboxylic group, required for the next steps, proceeds through an anhydride intermediate giving compound **2** in high yield.

The second step involved a particular reagent, 4-nitrophenyl chloroformate, which, after reacting with the remaining alcoholic OH, introduces a good

leaving group, necessary for the next coupling reaction. With this reaction we obtained the pure compound **3** by recrystallization in high yield.
The limiting step of the entire procedure is the double coupling between two lithocholate molecules, **3,** and the m-xylylene diamine. Despite introduction of the nitrophenyl leaving group, the problem remains the double attachment to the diamine which requires long reaction times and does not proceed in high yield.
Finally, deprotection of the methoxy moieties gave compound **5**, which bears at the two ends free carboxylic acid groups.
Afterward, we performed the final coupling between the linker **5** and the three end groups: methyl, guanosine and adenosine derivatives. This final reaction is summarized in Scheme 6.8.

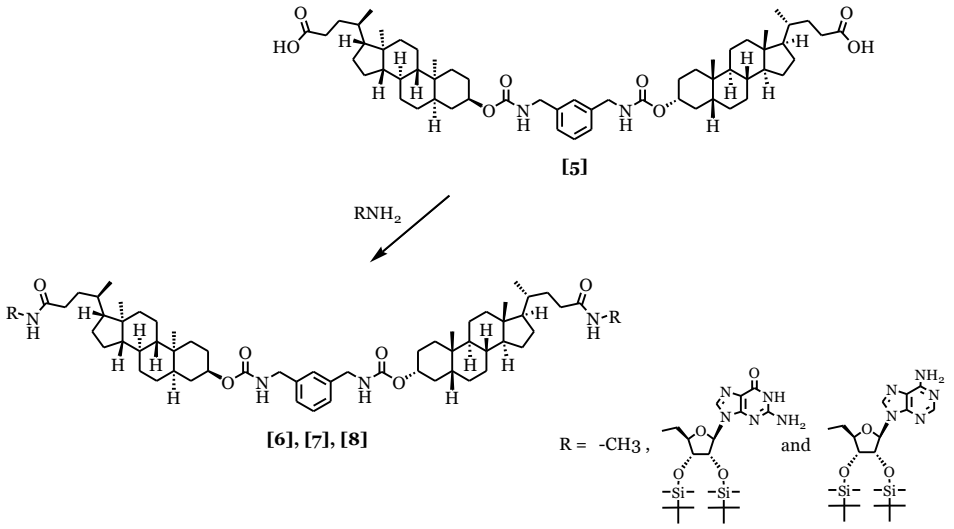

Scheme 6.8. Synthesis of bis-G-lithocholate **6**, bis-lithocholamide **7** and bis-A-lithocholate **8**.

In all three cases, the problems of this step are the same: the initial difficult activation of the carboxylic acid linker end groups, and the incomplete course of the reaction. To solve the first problem it was necessary to allow to stir the linker solution for 4-6 hours in presence of a coupling agent (such as CDI or EDC), before adding the amine derivative. Regarding the second problem, the difficulty comes in the purification step because the desired product (double coupling product) has the same R_f as the mono coupling by-product. Only with

the addition of Et_3N on the TLC plate or in the chromatographic column silica, did the complete separation of the two products becomes possible.
In this way, we have obtained and fully characterized the lithocholate compounds **6**, **7** and **8**.

6.4 Solution studies

Before testing the ability of compounds **6**, **7**, **8** to form transmembrane pores, we have investigated the behaviour of these molecules in solution. First, we have performed ^{1}H NMR analyses to study the self assembled properties in relation to the solvent polarity.
The spectrum of guanosine-lithocholate **6** gives sharp peaks in DMSO-d_6, a polar solvent that inhibits self-assembly mediated by hydrogen bonding. This showed the attribution of all resonances (Figure 6.9 a).

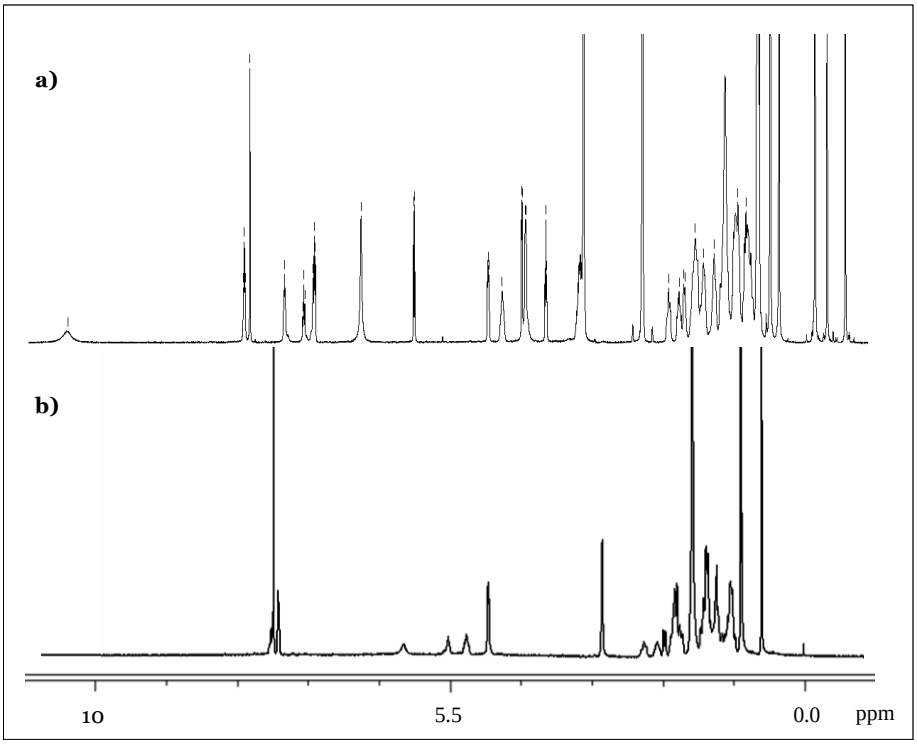

Figure 6.9. ^{1}H NMR of the bis-G-lithocholate in DMSO-d_6 (a) in $CDCl_3$ (b).

On the other hand, the ^{1}H NMR spectrum of **6** in $CDCl_3$ (Figure 6.9 b) gave very broad signals, consistent with self-association. The same behaviour is showed by the adenosine-lithocholate **8** because, as mentioned above, also this compound is able to self assemble into supramolecular structures by H-bonding interactions.

Instead, the other control compound, lithocholamide **7**, has a well-resolved spectrum also in $CDCl_3$, as expected for a molecule with little propensity to aggregation.

Since the stacking of the G-quartet led to a columnar, chiral assembly (G-quadruplex) we can confirm the formation of this structure using a solution technique able to detect the chirality of compounds.

Circular dichroism (CD) spectroscopy measures differences in the absorption of left-handed polarized light versus right-handed polarized light, due to structural asymmetry. Achiral objects are CD silent, while resolved chiral structures induce CD spectra containing both positive and negative signals.

Therefore we used CD spectroscopy to gain evidence that **6** can form chiral stacked G_4-quartets in a non-polar environment.[13]

In Figure 6.10 is shown the CD spectra for different samples of **6** in $CHCl_3$. First, the CD spectrum of **6** (blue trace) was taken after its isolation from a silica gel column. This sample showed a small amount of CD activity in the 200-280 nm region, suggesting that there might be some stacked G_4-quartets in solution.

We next added excess [2.2.2]-cryptand, a potent ionophore, to ensure that any adventitious cations bound to **6** would be removed. Indeed, the resulting CD spectrum (green trace) showed CD activity closed to zero. Further evidence of this behaviour came from the ^{1}H NMR analysis before and after the [2.2.2]-cryptand addition: the addition of [2.2.2]-cryptand induced changes in the guanosine N_1-H signals between δ 11-12 ppm, another indication that self-association of **6** was sensitive to the presence of cations.

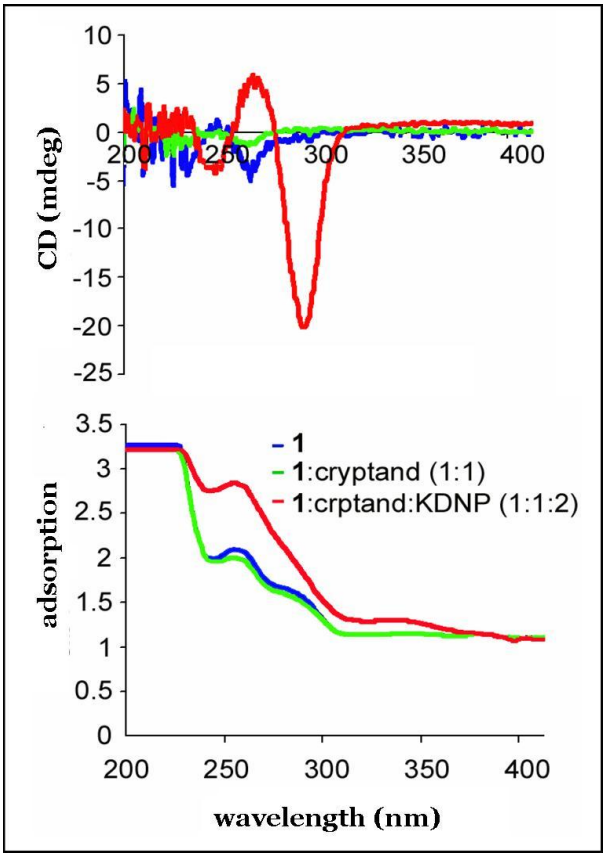

Figure 6.10. CD and absorption spectra of bis-G-lithocholate **6** (blue line); after addition of mixed 1 equiv of [2,2,2]-cryptand (green line); after solid-liquid extraction of K^+ DNP^-.

We next stirred the sample of **6** and [2.2.2]-cryptand in the presence of excess K^+ 2,6-dinitrophenolate (DNP) salt. The CD spectrum of the guanosine-lithocholate **6** was significantly different after extraction of K^+ DNP^- (red trace): this sample showed a CD signature that was diagnostic for stacked G-quartets, with a positive band at λ = 266 nm and a negative peak at λ = 240 nm.[13]
In addition, the complex formed by bis-G-lithocholate **6** and K^+ showed a strong negative band at λ = 296 nm, the same signal that has been observed for DNA G-quadruplexes.
On the other hand, as expected, the control compound, bis-lithocholamide **7**, showed no CD activity under identical conditions.

Overall, the combined ^{1}H NMR and CD data indicate that K^+ can template the formation of stacked G_4-quartets by compound **6** in a non-polar environment.

6.5 Voltage-Clamp experiments

Voltage-Clamp is used by electrophysiologists to measure the ion currents across a neuronal membrane, while holding the membrane voltage at a set level. The concept of the voltage clamp is due to Kenneth Cole[14] and George Marmount[15] in the 1940s. Cole discovered that it was possible to use two electrodes and a feedback circuit to keep the membrane potential at a level set by the apparatus.

With this technique we are able to monitor the transport rates of ions across membranes through ion channels, where the rate of transport is measured as an ionic current (units of pico ampere, pA). This phenomenon arises simply due to the fact that ions carry charges, and potential, or voltage (units of millivolts, mV) can be applied across membranes. This potential is called membrane potential, and it is either created electrically (for example by a battery with electrodes on either side of the membrane) or chemically by ionic concentration gradients.

An interesting analogy can be drawn between ion channels and electronic circuits. Here the ion channel acts as a resistor (units of Giga ohms, GΩ), or in inverse terms, as a conductor (units of pico siemens, pS), and the phospholipid bilayer membrane acts as a capacitor. In simple bilayer electrophysiology setups, the membrane capacitance is on the order of pico farads (pF).

Planar lipid bilayers (BLM) are used for functional studies of ion channel using electrophysiological techniques. Two chambers (*cis* & *trans*) are separated by a thin, but non-conducting partition with a small hole which is punched or drilled. A lipid solution is then formed into a planar bilayer membrane in the hole. Ion channels can then be incorporated into the BLM by several methods. A voltage-clamp amplifier, that can deal with the large capacitances of these membranes, can then measure the ionic current through inserted channels.

BLM electrophysiology provides several distinct advantages, including control of the constituents on either side of the membrane, manipulation of lipid composition, and the ability to study rare or challenging channels inaccessible to patch-clamp methods.

In this work, we used this voltage-clamp technique to demonstrate that **6** forms single ion-channels in planar membranes. We tested also the compounds **7** and **8** as control experiments, as already mentioned above.
Before moving to the results, it is necessary to explain the method used to incorporate the compounds in the membrane, once formed in the hole. Usually the compound is added to the aqueous solution of the *cis* side of the chamber. Since this solution is stirred, the compound is able to reach the partition and insert in the membrane.
Since our compounds are not soluble in water, this procedure is not easy to use, therefore we have performed a premixed method. With this different procedure we mixed the compound with the phospholipid solution before the membrane formation, in order to preclude the solubility problem.
In detail, all experiments are carried out applying a voltage of -10 mV in 1M KCl (*trans*)/KCl (*cis*) solution, which is buffered a pH 7.0 (see Appendix D for more experimental details).
After the formation of the membrane, with the guanosine-lithocholate **6** already inside, each experiment showed conductance states of different magnitudes appearing and disappearing over a 2-3 hours period, which corresponds to be the mean life of the membrane.
The representative records of conductance, after application of the guanosine-lithocholate **6** to the planar bilayer is reported in Figure 6.11.
This pattern of "open" and "closed" conductance is consistent with the dynamic aggregation and dissolution of self-assembled channels. Moreover, some of these channels have remarkably long lifetimes (seconds) and large conductance values (nS). This mean that the compound **6** is able to self-assemble, probably into the structures depicted in Figure 6.4, and form big and stable transmembrane pores, distinguishing them from most synthetic ion channels that conduct in the pS range with millisecond lifetimes.[1, 3, 16, 17]

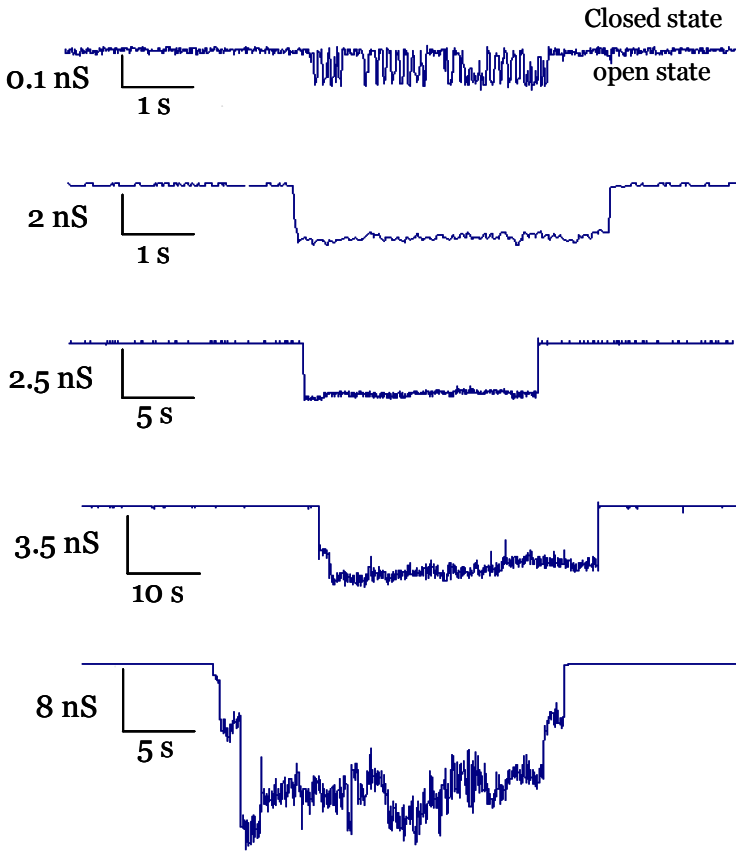

Figure 6.11. Representative "open-closed" event traces from voltage-clamp experiments in presence of **6**.

The magnitude and lifetimes of the ion conductance supported by **6** shows several values during a single experiment, the same depicted in Figure 6.11.
Channels with conductance values of 0.1-1.0 nS typically have the shortest "open" lifetimes (10-80 ms). These smaller channels always appear during initial events in any experiment.
Larger channels with conductance levels of 1-5 nS have much longer "open" lifetimes, typically lasting longer than 10 s. Moreover, the formation and disassembly of pores with 1-5 nS conductance are the most frequent events observed during any experiment.

Only occasionally we observe long periods of larger conductance (> 20 nS).
Analysis of data from 6 experiments showed comparable numbers of increments and decrements at discrete conductance values, consistent with the opening and closing of channels of the same size (Table 6.12).

Conductance (nS)	Number of open events
< 0.1	146
1-5	420
5-20	14
> 20	2

Table 6.12. Number of "open" events counted from a total of 6 experiments, regarding the insertion of guanosine-lithocholate **6** in BLM.

To prove that the presence of the guanosine end groups is fundamental for the formation of stable ion-channels we tested the two control compounds, **7** and **8**. At first, the addition of the lithocholamide control **7** to planar bilayer membranes never resulted in measurable conductance. This negative result is due to the inability of this compound to form H-bonding interactions, already explained above. On the other hand, the adenosine-lithocholate **8** after insertion in the membrane has shown several "open-close" events similar to those depicted in Figure 6.11. We have already discussed that this compound enables the self-assembly by H-bonding interactions, but with different geometry and stability with respect to the guanosine-lithocholate compound. The difference between this two compounds is clear by looking at the results obtained in these planar bilayer membrane studies. While in the case of the guanosine-lithocholate **6** the conductance values are reproducible, that is in each experiment the magnitudes of the events are always the same, in the case of the adenosine-lithocholate **8** the "open-closed" events present always different conductance values.
Indeed the analysis of data from 5 experiments shows several numbers of increments and decrements, consistent with the random opening and closing of the channels (Table 6.13).

Conductance (nS)	Number of open events
< 0.1	31
0.2-0.9	30
1-2	11
2-4	4

Table 7.13. Number of "open" events counted from a total of 5 experiments, regarding the insertion of adenosine-lithocholate **8** in BLM.

These results show that the adenosine end-groups can self-assembled in ion-channels, but only the guanosine end-groups are capable to form stable, discrete and reproducible transmembrane pores.

The reversal potential (or Nernst potential) is another information that can be obtained from the membrane experiments. Reversal potential of a particular ion is the membrane voltage at which there is no net flow of ions from one side of the membrane to the other. When a channel type that is selective to one species of ion dominates within the membrane, then the voltage inside the membrane will equilibrate to the reversal potential for that ion (i.e. assuming the outside of the membrane is at 0 volts). For example, the resting potential of most cells is close to the potassium reversal potential because at rest, potassium conductance dominates. During a stereotypical action potential, the small resting conductance mediated by potassium channels is overwhelmed by the opening of a large number of sodium channels, which brings the membrane potential close to the reversal potential of sodium. When a membrane has significant permeabilities to more than one ion, its potential can be calculated from the Goldman-Hodgkin-Katz equation[18] rather than the Nernst equation.

In this work the reversal potentials, recorded in the presence of a 10-fold KCl gradient, were measured to determine the ion selectivity of the guanosine-lithocholate channels (see Appendix D for more experimental details). The reversal potential, E_{rev}, is essentially constant for the 1-5 nS channels, suggesting no significant enlargement or contracture of these pores during an experiment. The ion selectivity of the 1-5 nS channels, calculated from the Goldman-Hodgkin-Katz equation, revealed a cation selective pore ($P_{K+}/P_{Cl-} = 6.38 \pm 0.30$).

The K^+ selectivity of these type of ion-channels confirms the central role of this cation in the self-assembly of the compound **6**.

An important parameter, that can be extrapolated from the conductance values, is the dimension of the pore. In this way, we can verify if the hypothetical suggested structures are consistent with the real aggregates formed in the membrane. To estimate the ion-channel diameter, we used the Hille equation which approximates the channel as a cylinder filled with a bulk-like electrolyte and flanked by access resistances of the adjacent buffer.[15]

In the case of 0.1 nS of conductance (at 1 M KCl), we can estimate a diameter equal to ~2.6-2.7 Å, a value that is quite close to the diameter of the G_4-quartet's central cavity. If the smallest conductance value is consistent with the G-quartet pore, the channels which conduct in the 1-20 nS range must be due to different and much larger pores. For instance, the Hille diameter for a single channel of 2.5 nS was estimated to be about 12 Å. Such a single channel is significantly larger than a the diameter of a G_4-quartet, suggesting that ion transport likely proceeds through larger pore(s) that forms upon self-assembly of guanosine-lithocholate **6**, as emphasized in the Figure 6.5.

We envision that the bis-lithocholate linker provides the walls for the transmembrane pore, and the cation-filled G-quadruplex, formed upon hydrogen-bond self-assembly, serves as a structural pillar that anchors the assembly within the membrane.

6.6. Conclusions

In summary, in this chapter we have demonstrated that the properties of compounds **6**, **7** and **8** in solution, can be hold true also in phospholipid membranes. The guanosine-lithocholate **6** forms large (nS conductance) and stable pores, with "open" times of seconds, distinguishing them from most synthetic ion channels that conduct in the pS range with millisecond lifetimes. The smaller conductance values near 0.1 nS, may arise as ions are moved through the central channel of a G-quadruplex. However, pores that conduct on the 1-20 nS scale must necessarily have diameters that are significantly larger than that provided by a G-quartet. It is tempting to suggest that the self-assembled structures proposed to explain formation of G-quartet polymers, are responsible for the function of **6**. On the other hand, we have confirmed the importance of the guanosine end-groups with the two control experiments. Indeed, compound **7** did not show any activity, and compound **8** formed ion-channels but without reproducible transmembrane conductivity, indicating that the self-assembled pores are not so stable. Moreover in this last case a correlation between ion channel structure and size is not accessible.
Regardless of the actual membrane-active structures, the demonstration that **6** forms large and stable transmembrane channels suggests that this nucleoside-sterol may well be able to allow larger biomolecules to move in and out of liposomes and/or cells. Davis' group are currently pursuing such studies.

6.7. Acknowledgments

Special thanks to Prof. Jeffery T. Davis for this opportunity, to Ling Ma for her collaboration and precious help in each part of this work. Moreover, I would like to thank Will, Paul, Yomi and Sofya, the other members of Davis' group, for their precious support.

6.8. Experimental section

Adenosine derivative (2', 3'-bis-TBDMS, 5'-amino adenosine) and guanosine derivative (2', 3'-bis-TBDMS, 5'-amino guanosine) were prepared following published methods.[‡]

Methyl lithocholate (2).

To a suspension of lithocholic acid **1** (5 g, 13.3 mmol) in MeOH (50 mL), acetyl chloride (472 μL, 6.6 mmol) was added dropwise. The obtained solution was stirred for 24 h at room temperature. Then water (50 mL) was added to the solution and the white precipitate was collected by filtration and dried *in vacuo*. The crude product was recrystallized from acetonitrile to give **2** as white solid (4.98 g, 96%). ^{1}H NMR ($CDCl_3$, 400 MHz) δ = 3.64 (s, 3 H, -CO_2CH_3), 3.60 (m, 1 H, -*CH*-OH), 2.35-2.21 (m, 2 H, -CH_2-CO_2CH_3), 1.94-0.89 (m, 36 H), 0.62 (s, 3 H, -CH_3). ESI-MS: m/z 391.1 $[M+H]^+$.

Methyl 3α-(4-nitrophenylchloroformate) lithocholate (3).

A solution of **2** (2.5 g, 6.4 mmol) in CH_2Cl_2 (100 mL), 4-nitrophenylchloroformate (2.3 g, 11.5 mmol) and Et_3N (2.7 mL, 19.2 mmol) was stirred at room temperature for 3 h. The mixture solution was washed with 3x15 ml Na_2CO_3 saturated solution, then 3x15 ml H_2O. The organic layer was dried over $MgSO_4$ and the solvent was evaporated under reduce pressure. Then the crude mixture was recrystallized from acetone to give **3** as white solid (3.13 g, 88%).^{1}H NMR ($CDCl_3$, 400 MHz) δ =8.27 (d, 2 H, Ar), 7.37 (d, 2 H, Ar), 4.70 (m, 1 H, -*CH*-O-CO_2Ar), 3.65 (s, 3 H, -CO_2CH_3), 2.34-2.21 (m, 2 H, -CH_2-CO_2CH_3), 1.94-0.89 (m, 36 H), 0.63 (s, 3 H, -CH_3). ESI-MS: m/z 556.4. $[M+H]^+$.

[‡] F.W. Kotch, V. Sidorov, Y.F. Lam, K.J. Kayser, H. Li, M.S. Kaucher, J.T. Davis, *J. Am. Chem. Soc.* **2003**, *125*, 15140-15150.

Bis [(24 - methoxycarbonyl) - 3 - lithocholanyl] - N', N xylylene Dicarbamate (4).

To a mixture of **3** (2 g, 3.6 mmol) and m-xylylene diamine (0.2 mL, 1.4 mmol) in CH_2Cl_2 (90 mL) was added Et_3N (2 mL, 1.4 mmol) and DMAP (0.017 g, 0.14 mmol). The reaction mixture was allowed to stir at reflux for 48 h, after which time TLC analysis indicated the reaction was complete. The crude mixture was concentrated, dissolved in CH_2Cl_2 and washed sequentially with saturated $NaHCO_3$ until the aqueous phase was no longer yellow. Then solvent of the organic layer was evaporated under reduce pressure and the remaining solid was purified by column chromatography (SiO_2, 2:1 EtOAc:hexane) to give **4** as a white solid (1.4 g, 40%). ^{1}H NMR ($CDCl_3$, 400 MHz) δ = 7.28 (t, 1 H, Ar), 7.18-7.16 (m, 3 H, Ar), 4.87 (m, 2 H, -N*H*-CH_2Ar), 4.63 (m, 2 H, -*CH*-O-CONH), 4.33 (d, 4 H, -NH-C*H*$_2$Ar), 3.64 (s, 3 H, -CO_2C*H*$_3$), 2.34-2.21 (m, 2 H, -C*H*$_2$-CO_2CH_3), 1.94-0.89 (m, 36 H), 0.62 (s, 3 H, -CH_3). ESI-MS: m/z 986.6 $[M+NH_4]^+$.

Bis[(24-carboxyl)-3-lithocholanyl]-N',N-xylylene Dicarbamate (5).

A mixture of **4** (0.35 g, 0.36 mmol) in MeOH (100 mL) was stirred at 70˚C until complete dissolution. Then 18 mL of 1N NaOH solution were added. The reaction mixture was allowed to stir for 4 h at 70˚C. After concentration of the solvent, a solution of 1N HCl was added to adjust the pH at 2-3. The mixture was extracted with CH_2Cl_2 and the organic solution was washed with water. Solvent was removed under reduced pressure and the residue was recrystallized with MeOH to give **5** as white solid (0.17 g, 50%).^{1}H NMR ($CDCl_3$, 400 MHz) δ = 7.28 (t, 1 H, Ar), 7.17 (bm, 3 H, Ar), 4.96 (bm, 2 H, -N*H*-CH_2Ar), 4.62 (m, 2 H, -*CH*-O-CONH), 4.32 (bd, 4 H, -NH-C*H*$_2$Ar), 2.34-2.21 (m, 2 H, -C*H*$_2$-CO_2CH_3), 1.94-0.89 (m, 36 H). ESI-MS: m/z 958.7 $[M+NH_4]^+$.

Bis [24-(2',3'-bis-TBDMS,5'-amino guanosine)-3-lithocholanyl]-N',N-xylylene dicarbamate (6).

A suspension of **5** (0.1 g, 0.11 mmol) and CDI (0.04 g, 0.27 mmol) in CH_2Cl_2 (20 mL) was stirred for 4 h at reflux. Then 2',3'-bis-TBDMS,5'-amino guanosine (0.14 g, 0.28 mmol) was added and the reaction mixture was allowed to stir at reflux for 24h. Solvent was removed under reduced pressure and the crude

product was purified by column chromatography (SiO_2, 1:0.05 CH_2Cl_2:MeOH) to give **6** as a white solid (0.12 g, 59%). ^{1}H NMR (DMSO-d_6, 400 MHz) δ = 10.71 (bs, 2 H, N*H*), 8.07 (t, 2 H, N*H*-$COCH_2$), 7.97 (s, 2 H, *H*$_8$), 7.50 (t, 2 H, N*H*-CO_2), 7.23 (t, 1 H, Ar), 7.08 (m, 3 H, Ar), 6.48 (s, 4 H, N*H*$_2$), 5.69 (d, 2 H, *J* = 7.6 Hz, *H*$_{1'}$), 4.66 (dd, 2 H, *J* = 7.6 Hz, 4.4 Hz, *H*$_{2'}$), 4.45 (m, 2 H, -*CH*-O-CONH), 4.19 (d, 2 H, *J* = 4.4 Hz, *H*$_{3'}$), 4.13 (bd, 4 H, -NH-C*H*$_2$Ar), 3.84 (t, 2 H, *J* = Hz, *H*$_{4'}$), 3.41-3.33 (m, 4 H, *H*$_{5'}$, *H*$_{5''}$), 2.21-0.88 (m, 38 H), 0.66 (s, 9 H, C*H*$_3$), 0.57 (s, 3 H, C*H*$_3$), 0.07(d, 12 H, -C*H*$_3$), -0.06 (s, 6 H, SiC*H*$_3$), -0.31 (s, 6 H, SiC*H*$_3$). ESI-MS: m/z 1926.3 $[M+H]^+$.

Bis[(24-N-methylamide)-3-lithocholanyl]-N',N-xylylene Dicarbamate (7).

To a mixture of **5** (150 mg, 0.27 mmol) and EDC (0.13 g, 0.81 mmol) in CH_2Cl_2 (20 mL) was added Et_3N (0.038 mL, 2.2 mmol) and DMAP (6.6 mg, 0.012 mmol). The reaction mixture was allowed to stir at reflux for 6 h, after which time TLC analysis indicated the reaction was complete. Then a solution of 2.0 M CH_3NH_2 in THF (0.41 mL, 0.81 mmol) was added and the reaction mixture was allowed to stir at reflux for 24h. The crude mixture was concentrated and the remaining solid was purified by column chromatography (SiO_2, 2:1 EtOAc:benzene) to give **7** as a white solid (100 mg, 39%). ^{1}H NMR ($CDCl_3$, 400 MHz,) δ = 7.28 (t, 1 H, Ar), 7.18-7.16 (m, 3 H, Ar), 5.38 (bs, 1H, -N*H*CH_3), 4.87 (m, 2 H, -N*H*-CH_2Ar), 4.63 (m, 2 H, -*CH*-O-CONH), 4.33 (d, 4 H, -NH-C*H*$_2$Ar), 2.79 (d, 3 H, -NHC*H*$_3$), 2.34-0.89 (m, 38 H), 0.62 (s, 3 H, -CH_3). ESI-MS: m/z 967.7 $[M+H]^+$.

Bis[24-(2',3'-bis-TBDMS,5'-amino adenosine)-3-lithocholanyl]-N',N-xylylene Dicarbamate (8).

A solution of **5** (0.25 g, 0.27 mmol) and CDI (0.13 g, 0.81 mmol) in anhydrous THF (20 mL) was stirred for 4 h at 70˚C, after which time TLC analysis indicated the reaction was complete. Then 2',3'-bis-TBDMS,5'-amino adenosine (0.4 g, 0.81 mmol) was added and the reaction mixture was allowed to stir at reflux for 24h. Solvent was removed under reduced pressure and the crude product was purified by column chromatography (SiO_2, 1:0.04 CH_2Cl_2:MeOH) to give **8** as a white solid (0.21 g, 40%). ^{1}H NMR (DMSO-d_6, 400 MHz) δ = 8.41 (s, 2 H, *H*$_3$), 8.29 (t, 2 H, N*H*-$COCH_2$), 8.15 (s, 2 H, *H*$_8$), 7.49 (t, 2 H, N*H*-CO_2),

7.33 (s, 4 H, NH_2), 7.23 (t, 1 H, Ar), 7.09 (m, 3 H, Ar), 5.87 (d, 2 H, J = 7.6 Hz, $H_{1'}$), 4.98 (dd, 2 H, J = 7.6 Hz, 4.4 Hz $H_{2'}$), 4.45 (m, 2 H, -CH-O-CONH), 4.19 (d, 2 H, J = 4.4 Hz, $H_{3'}$), 4.13 (bd, 4 H, -NH-CH_2Ar), 3.94 (t, 2 H, J = 5.6 Hz, $H_{4'}$), 3.51-3.31 (m, 4 H, $H_{5'}$, $H_{5''}$), 2.21-0.88 (m, 38 H), 0.66 (s, 9 H, CH_3), 0.57 (s, 3 H, CH_3), 0.08 (d, 12 H, -CH_3), -0.15 (s, 6 H, SiCH_3), -0.51 (s, 6 H, SiCH_3). ESI-MS m/z 1895.1 $[M+H]^+$.

6.9. References

[1] G.A. Jeffrey, W. Saenger *in Hydrogen Bonding in Biological Structures*, (ED.: Springer), Berlin, **1991**.

[2] J.D. Watson, F.H. Crick, *Nature*, **1953**, *171*, 737.

[3] a) J.T. Davis, *Angew. Chem. Int. Ed. Engl.* **2004,** *43*, 668-698; b) J.T. Davis, G.P. Spada, *Chem. Soc.Rev.* **2007,** *36*, 296-313.

[4] a) L. Chen, N. Sakai, S.T. Moshiri, S. Matile, *Tetrahedron Lett.* **1998**, *39*, 3627; b) B. Datta, M.E. Bier, S. Roy, B.A. Armitage, *J. Am. Chem. Soc.* **2005**, *127*, 4199; c) Y. Krishnan-Ghosh, E. Stephens, S. Balasubramanian, *J. Am. Chem. Soc.* **2004**, *126*, 13895.

[5] S. Matile, A. Som, N. Sorde, *Tetrahedron* **2004**, *60*, 6405.

[6] A.L. Merlow, E. Mezzina, G.P. Spada, S. Masiero, J.T. Davis, G. Gottarelli, *J. Org. Chem.* **1999,** *64*, 5116.

[7] N. Sakai, Y. Kamikava, M. Nishii, T. Matsuoka, T. Kato, S. Matile, *J. Am. Chem. Soc.* **2006**, *128*, 2218.

[8] Q.W. Xu, H. Deng, W.H. Braunlin, *Biochemistry* **1993**, *32*, 130.

[9] M.S. Kaucher, W.A. Harrel, J.T. Davis, *J. Am. Chem. Soc.* **2006**, *128*, 38.

[10] M.S. Kaucher, Y.F. Lam, S. Pieraccini, G. Gottarelli, J.T. Davis, *Chem. Eur. J.* **2005**, *11*, 164.

[11] C. Arnel-Herault, A. Pasc, M. Michau, D. Cot, E. Petit, M. Barboiu, *Angew. Chem. Int. Ed. Engl.* **2007**, *46*, 8409.

[12] a) M. Yoshii, M. Yamamura, A. Satake, Y. Kobuke, *Org. Biomol. Chem.* **2004**, *2*, 2619; b) Y. Kobuke, T. Nagatani, *J. Org. Chem.* **2001**, *66*, 5094-; c) C. Goto, M. Yamamura, A. Satake, Y. Kobuke, *J. Am. Chem. Soc.* **2002**, *123*, 2152.

[13] For a review on the CD spectroscopy of G-quadruplexes: G. Gottarelli, S. Masiero, G.P. Spada, *Enantiomer* **1999**, *3*, 429.

[14] M.F. Bear, B.W. Connors, M.A. Paradiso *in Neuroscience: Exploring the Brain*, (ED.: Lippincott Williams & Wilkins), Baltimore, **1996**,Chapter 4.

[15] K.S. Cole *in A Brief history of Computational Neuroscience*, Duke University.

[16] a) T.M. Fyles, *Chem. Soc. Rev.* **2007**, *36*, 335; b) N. Sakai, J. Mareda, S. Matile, *Mol. BioSystems* **2007**, *3*, 658.

[17] For exceptional synthetic channels that show nS conductance, see: a) B. Baumeister, N. Sakai, S. Matile, *Angew. Chem. Int. Ed. Engl.* **2000**, *39*, 1955; b) P.H. Schlesinger, R. Ferdani, J. Liu, J. Pajewska, R. Pajewki, M. Saito, H. Shabany, G.W. Gokel, *J. Am. Chem. Soc.* **2002**, *124*, 1848-; c) T.C. Fyles, C.C. Tong, *New J. Chem.* **2007**, *31*, 655.

[18] B. Hille, *Ionic Channels of Excitable Membranes*, 3rd ed., Sunderland, MA, **2001**.

Appendix A. *Reagents, chemicals and instruments used*

All commercial reagent were ACS reagent grade and used as received. For the synthesis all solvents were dried over 3 Å and 4 Å molecular sieves.

- Chromatography was performed using 70-230 mesh silica purchased from Merck and 40-120 μ Sephadex G-10 purchased from Pharmacia Fine Chemicals. Thin layer chromatography was performed on Kieselgel 60 F254 and Uniplate^{tm} Silica Gel GF silica-coated glass plates and visualized by UV and I_2.

- ^{1}H NMR spectra were recorded on Bruker Avance 300 (300 MHz), Bruker DRX-400 and Varian INOVA 600 (600 MHz) spectrometers and all chemical shifts (δ) were reported in parts per million (ppm) relative to proton resonances resulting from incomplete deuteration of NMR solvents. ^{31}P NMR spectra were recorded on AMX-400 (162 MHz) and all chemical shifts were reported to external 85% H_3PO_3 at 0 ppm.

- ESI-MS characterization experiments were performed on a Waters ACQUILITY SQD Detector equipped with a ESCi® multi mode ionization (APCI/ESI).

- Circular dichroism (CD) spectra were recorded on a JASCO-810 spectropolarimeter with a 1 cm and 1 mm path length quartz cuvette.

- The surface morphology characterization was performed in air by no contact mode atomic force microscope (AFM) model C-21 produced by Danish Micro Engineering, mounting a DualScope Probe Scanner 95-50.

Appendix B. *ESI-MS Studies*

Mass spectrometry experiments were performed with the BioApex 47e Fourier transform ion cyclotron resonance mass spectrometer equipped with an Infinity™ cell, a passively shielded 4.7 tesla 160 mm bore superconducting magnet, and an external Apollo™ electrospray ionization source. The sample was introduced to a 70˚ off-axis sprayer (stainless steel metal capillary) through a syringe infusion pump at a flow rate of 1.5 μL/min. Room temperature nitrogen (N_2) was used as a nebulizing and counter-current drying gas. The measurements and data handling were accomplished with Bruker XMASS software, version 6.0.2.

Samples for alcohol complexation contained 0.5-1.0% (*v/v*) trifluoroacetic acid, 30–100% (*v/v*) suitable alcohol, and, correspondingly, 0-70% (*v/v*) acetonitrile (ACN). Cavitand concentration in samples was 2.0-4.0 μM. The samples for water complexation contained cavitand (2 μM), 1-20 % (*v/v*) H_2O, 0.5 % (*v/v*) acetic acid and ACN as a solvent.

Competition experiments with cavitands were performed with a $cavitand_1$/$cavitand_2$ ratio of 1:1 in the presence of ethanol. Each experiment was carried out on five different samples and each sample was measured five times. The overall variance was calculated from the standard deviation of sampling and the standard deviation of the measurement ($s_{tot}^2 = s_1^2 + s_2^2$).

In collision induced dissociation (CID) experiments, collisionally cooled precursor ions were isolated by the CHEF procedure (10). Isolated ions were thermalized during 3.0 s delay, translationally activated by an on-resonance radio frequency (RF) pulse, and allowed to collide with pulsed argon background gas. Each spectrum was a collection of 32 scans.

Appendix C. *Sensors Measurements*

Sensing measurements were performed using a 10 MHz AT-cut quartz. Cavitands films were deposited on gold electrode areas on both sides of the quartz transducers by spin coating, VE (Vacuum Evaporation) or GDS (Glow discharge-induced sublimation) deposition technique (see detailed description in Chapter 4). Each microbalance is coated with the same amount of cavitand (44 μg) which is verified by measuring the frequency shift of Δf=20±0.5 kHz on the final coated QCM. The measurement system (Gaslab 20.1; IFAK, Magdeburg) is equipped with a flow chamber, containing four coated quartz crystals, a reference quartz crystal and a thermocouple. The temperature of the chamber was thermostated at 20±0.1°C. The QCM chamber is connected with two mass flow controllers (Brooks 5850S): one allows to control the flow rate of alcohol mixture between 2 and 50 mL/min and the other controls the flow rate of pure nitrogen from 150 to 200 mL/min. The starting stream of N_2 (200±2 mL/min) was then replaced by a N_2+alcohol mixture (200±2 mL/min); the N_2/alcohol ratio is imposed by the desired final alcohol concentration considering that the total amount of the stream must be 200±2 mL/min. After reaching of the flat characteristic plateau (equilibrium of partition coefficient) the chamber was flushed with pure N_2 to restore the starting conditions. During the whole process the coated quartz crystal frequency was measured as a function of the time every 1 second. All measurements were repeated at least four times, with variations in response of less than 3%. All alcohols used, have been supplied by SAPIO S.r.l. in gas cylinders with a certified concentration of in ppm. The graduated cylinders have been prepared following the standard gravimetric procedure of the normative ISO 6142.
In case of comparison between different alcohols a correction factor *A* was applied to all experimental data to take account of the different molecular weights (MW):

$$f_{norm} = f_{exp} A \qquad \text{where} \qquad A = MW_{methanol} / MW_{analyte}$$

Appendix D. *Planar bilayer conductance experiments*

Planar phospholipid membranes were prepared by the monolayer method,* across a 100-μm-diameter hole in a Saran partition. Monolayers were produced using a solution of 0.5% w/v asolectin, 0.5% w/v DiPhyPC, 0.1% w/v cholesterol in hexane. This technique produces solvent-free phospholipid membranes whose lipid composition (focusing on the polar head-groups) is similar to that found in the mitochondrial outer membrane. It differs from the natural membrane in lacking proteins.

The aqueous solution contained 1.0 M KCl, 1 mM MgCl2, and 5mM PIPES (pH 7.0). 20 μL of the compound **6**, **7** or **8** (0.5 mg/mL of CH_2Cl_2) were premixed with the phospholipids solution in hexane.

The transmembrane voltage was electronically clamped and the current through the membrane was recorded. The voltage values indicated are the voltage differences across the membrane *cis* side minus *trans* side.

Salt gradient was applied to determine charge and metal ion selectivity. Potassium *versus* cloride permeability ratio was calculated from reversal potential V_r obtain under KCl concentration gradient (1M/0.1M, *cis*/*trans*) using the equation derived from Goldman-Hodgin-Katz voltage equation:

$$P_{K^+}/P_{Cl^-} = \left[a_{Cl^-_{cis}} \exp(-V_r F/RT) - a_{Cl^-_{trans}}\right] / \left[a_{K^+_{cis}} - a_{K^+_{trans}} \exp(-V_r F/RT)\right]$$

where $a_{Cl^-_{trans}}$, $a_{Cl^-_{cis}}$, $a_{K^+_{trans}}$ and $a_{K^+_{cis}}$ are the activities of Cl^- and K^+ in *cis* and *trans* side, *F* the Faraday constant, *R* gas constat and *T* the absolute temperature.

* M. Colombini, Characterization of channels isolated from plant mitochondria, *Methods Enzymol.* **1987,** *148*, 465–475.

Appendix E. *X-Ray Crystallographic Studies*

The crystal structure of complexes Tiiii[H,CH_3,CH_3]·MeOH, Tiiii[H,CH_3,CH_3]·2CF_3CH_2OH·2H_2O, MeCav[H,CH_3], Tiiii[H,CH_3, CH_3]·4H_2O, AB 2POii2PSii[H,CH_3,Ph]·H_2O, AB 2POii2PSii[H, CH_3, Ph]·CH_3OH·CH_2Cl_2, AC 2POii2PSii[H,CH_3,Ph]·4CH_3OH·4H_2O·CH_2Cl_2 were determined by single crystal X-ray diffraction methods. Crystallographic and experimental details for the structures are summarized in Table Z. Intensity data and cell parameters were recorded at room temperature (with the exception of AB 2POii2PSii[H,CH_3,Ph] ·CH_3OH·CH_2Cl_2 and AC 2POii2PSii[H,CH_3,Ph]·4CH_3OH·4H_2O·CH_2Cl_2, which were collected at 173 K) on a Bruker AXS Smart 1000 single-crystal diffractometer, equipped with a CCD area detector using graphite monochromated $Mo_{k\alpha}$ radiation.

The structures were solved by direct methods using the SIR97 program[†] and refined on F_o^2 by full-matrix least-squares procedures, using the SHELXL-97 program.[‡] Both programs were used in the WinGX suite.[§]

The data reductions were performed using the SAINT[**] and SADABS[††] programs.

All the non-hydrogen atoms were refined with anisotropic atomic displacements, with the exclusion of the methanol guest in Tiiii[H,CH_3,CH_3] ·MeOH, the trifluoroethanol and water molecules in 4POiiii[H,CH_3,CH_3] ·2CF_3CH_2OH·2H_2O, the water molecule in AB 2POii2PSii[H,CH_3,Ph] ·H_2O and one water molecule and two methanol molecules in AC 2POii2PSii[H, CH_3, Ph] ·4CH_3OH·4H_2O·CH_2Cl_2. The hydrogen atoms were included in the refinement at idealized geometries (C–H 0.95 Å) and refined "riding" on the corresponding

---

† A. Altomare, M.C. Burla, M. Camalli, G.L. Cascarano, C. Giacovazzo, A. Guagliardi, A.G.G. Moliterni, G. Polidori, R. Spagna, *J. Appl. Crystallogr.* **1999**, *32*, 115-119.

‡ G.M. Sheldrick, *SHELXL97. Program for Crystal Structure Refinement*, University of Göttingen: Göttingen, Germany, **1997**.

§ G.X. Win, L.J. Farrugia, *J. Appl. Crystallogr.*, **1999**, *32*, 837-838.

** *SAINT, Software Users Guide*, 6.0; Bruker Analytical X-ray Systems: **1999.**

†† G.M. Sheldrick, *SADABS Area-Detector Absorption Correction*, 2.03; University of Göttingen: Göttingen, Germany, **1999**.

parent atoms. The weighting scheme used in the last cycle of refinement was $w = 1/[\sigma^2 F_o^2 + (0.1305P)^2]$, $w = 1/[\sigma^2 F_o^2 + (0.2181P)^2]$, $w = 1/[\sigma^2 F_o^2 + (0.1321P)^2]$, $w = 1/[\sigma^2 F_o^2 + (0.0180P)^2]$, $w = 1/[\sigma^2 F_o^2 + (0.0429P)^2]$, $w = 1/[\sigma^2 F_o^2 + (0.1102P)^2]$, $w = 1/[\sigma^2 F_o^2 + (0.1834P)^2 + 1.3736P]$, where $P = (F_o^2 + 2F_c^2)/3$ for Tiiii[H,CH_3,CH_3]·MeOH, Tiiii[H,CH_3,CH_3] ·2CF_3CH_2OH·2H_2O, MeCav[H,CH_3], Tiiii[H,CH_3,CH_3]·4H_2O, AB 2POii2PSii[H,CH_3,Ph]·H_2O, AB 2POii2PSii[H,CH_3, Ph]·CH_3OH·CH_2Cl_2, AC 2POii2PSii[H,CH_3,Ph]·4CH_3OH·4H_2O·CH_2Cl_2.
Geometric calculations were performed with the PARST97 program.[‡‡]
Drawings were obtained with the DS ViewerPro 6.0 and Mercury 1.4.2 program.[§§]

‡‡ M. Nardelli, *J. Appl. Crystallogr.* **1996**, *29*, 296-300.

§§ http://www.ccdc.cam.ac.uk/mercury/

Table Z1. Crystallographic data and refinement details for:

	Tiiii[H,CH_3,CH_3]·MeOH	**Tiiii[H,CH_3,CH_3]·2H_2O·2CF_3CH_2OH**
Formula	$C_{37}H_{40}O_{13}P_4$	$C_{40}H_{46}F_6O_{16}P_4$
Formula weight	816.61	1020.65
Crystal system	Tetragonal	Monoclinic
Space group	*P4/n*	*P21/n*
a/Å	15.496(3)	12.431(2)
b/Å	15.496(3)	22.447(3)
c/Å	7.854(2)	17.852(3)
β/°		106.159(3)
V/Å^3	1886.0(7)	4784.6(1)
Z	2	4
D_c/g cm^{-3}	1.438	1.417
F(000)	852	2112
μ/mm^{-1}	0.266	0.247
Crystal dimensions	0.15 x 0.12 x 0.10	0.18 x 0.11 x 0.10
$\theta_{min,max}$/°	3.72, 23.27	1.49, 22.56
Index ranges	-17≤ *h*≤15 ; -17≤ *k* ≤14 ; -8≤ *l* ≤8	-13≤ h ≤13; -24≤ k ≤24; -19≤ l ≤19
Reflections collected	6695	35910
Independent reflections	1340 (*R*int = 0.0604)	6253 (*R*int = 0.0871)
Observed reflections	622	3552
Data/restr./param.	1340 / 1 / 130	6253 / 17/ 536
R [Fo>4σ(Fo)][a]	0.0652	0.0971
wR_2[a]	0.1769	0.2731
$\Delta\rho_{min,max}$/e Å^{-3}	−0.472, 0.500	−0.587, 0.854
S[b]	1.000	1.002

[a]$R_1 = \Sigma \parallel Fo|-|Fc||/\Sigma|Fo|$, $wR_2 = [\Sigma w(Fo^2-Fc^2)^2/ \Sigma wFo^4]^{1/2}$. [b]Goodness-of-fit S = $[\Sigma w(Fo^2-Fc^2)^2/ (n-p)]^{1/2}$, where *n* is the number of reflections and *p* the number of parameters.

Table Z2. Crystallographic data and refinement details for:

	MeCav[H, CH_3]	**Tiiii[H,CH_3,CH_3]·4H_2O**
Formula	$C_{36}H_{32}O_8$	$C_{36}H_{44}O_{16}P_4$
Formula weight	592.62	856.59
Crystal system	Orthorhombic	Tetragonal
Space group	*Pnma*	*P4/n*
a/Å	10.479(1)	14.396(8)
b/Å	19.209(2)	14.396(8)
c/Å	14.767(1)	9.799(5)
V/Å^3	2972.5(5)	2031(1)
Z	4	2
D_c/g cm^{-3}	1.324	1.401
F(000)	1248	896
μ/mm^{-1}	0.093	0.256
Crystal dimensions	0.16 x 0.14 x 0.10	0.16 x 0.13 x 0.12
$\theta_{min,max}$/°	1.74, 24.06	1.41, 27.57
Index ranges	-12≤ *h*≤12; -22≤ *k* ≤22; -16≤ *l* ≤16	-15≤ h ≤18; -18≤ k ≤16; -12≤ l ≤7
Reflections collected	20726	11151
Independent reflections	2413 (*R*int = 0.0427)	2354 (*R*int = 0.0994)
Observed reflections	1663	1187
Data/restr./param.	2413 / 0 / 214	2354 / 3/ 140
R [Fo>4σ(Fo)][a]	0.0594	0.0481
wR_2[a]	0.1865	0.0765
$\Delta\rho_{min,max}$/e Å^{-3}	−0.170, 0.610	−0.288, 0.423
S[b]	1.026	1.006

[a]R_1 = Σ || Fo|-|Fc||/Σ|Fo|, wR_2 = [Σ w(Fo^2-Fc^2)^2/ ΣwFo^4]$^{1/2}$. [b]Goodness-of-fit S = [Σw(Fo^2-Fc^2)^2/ (*n*-*p*)]$^{1/2}$, where *n* is the number of reflections and *p* the number of parameters.

Table Z3. Crystallographic data and refinement details for:

	AB 2POii2PSii[H,CH_3,Ph] ·H_2O	**AB 2POii2PSii[H,CH_3,Ph] ·CH_3OH·CH_2Cl_2**
Formula	$C_{56}H_{46}O_{11}P_4S_2$	$C_{58}H_{50}O_{11}P_4S_2Cl_2$
Formula weight	1082.93	1181.88
Crystal system	Monoclinic	Monoclinic
Space group	*P21/n*	*P21/n*
a/Å	7.956(1)	7.829(1)
b/Å	24.294(4)	24.652(2)
c/Å	27.425(4)	28.303(3)
β/°	93.268(2)	91.966(2)
V/Å^3	5292(1)	5459.2
Z	4	4
D_c/g cm^{-3}	1.359	1.438
F(000)	2248	2448
μ/mm^{-1}	0.282	0.375
Crystal dimensions mm	0.16 x 0.13 x 0.10	0.14 x 0.12 x 0.09
$\theta_{min,max}$/°	1.49, 23.29	1.44, 25.01
Index ranges	-8≤*h*≤8; -26≤ *k* ≤26; -24≤ *l* ≤30	-9≤ h ≤8; -23≤ k ≤29; -33≤ l ≤33
Reflections collected	22310	26977
Independent reflections	7582 (*R*int = 0.0983)	9597 (*R*int = 0.1068)
Observed reflections	2676	4178
Data/restr./param.	7582 / 2 / 659	9597 / 1/ 700
R [Fo>4σ(Fo)][a]	0.0702	0.0878
wR_2[a]	0.1334	0.2118
$\Delta\rho_{min,max}$/e Å^{-3}	−0.310, 0.610	−0.740, 0.791
S[b]	1.009	1.012

[a]R_1 = Σ || Fo|-|Fc||/Σ|Fo|, wR_2 = [Σ w(Fo^2-Fc^2)^2/ ΣwFo^4]$^{1/2}$. [b]Goodness-of-fit S = [Σw(Fo^2-Fc^2)^2/ (*n*-*p*)]$^{1/2}$, where *n* is the number of reflections and *p* the number of parameters.

Table Z4. Crystallographic data and refinement details for:

	AC 2POii2PSii[H,CH_3,Ph]·4CH_3OH·4H_2O·CH_2Cl_2
Formula	$C_{117}H_{114}Cl_2O_{28}P_8S_4$
Formula weight	2414.98
Crystal system	Triclinic
Space group	*P-1*
a/Å	19.035(1)
b/Å	19.286(1)
c/Å	19.837(1)
α/°	109.381(1)
β/°	111.105(1)
γ/°	104.099(1)
V/Å^3	5837.9(5)
Z	2
D_c/g cm^{-3}	1.374
F(000)	2516
μ/mm^{-1}	0.311
Crystal dimensions mm	0.18 x 0.11 x 0.10
$\theta_{min,max}$/°	1.49, 22.56
Index ranges	-26≤ h ≤26; -26≤ k ≤25; -27≤ l ≤27
Reflections collected	73938
Independent reflections	28803 (*R*int = 0.0393)
Observed reflections	16390
Data/restr./param.	28803 / 2/ 1441
R [Fo>4σ(Fo)][a]	0.0792
wR_2[a]	0.2541
$\Delta\rho_{min,max}$/e Å^{-3}	−0.811, 2.426
S[b]	1.032

[a]$R_1 = \Sigma \parallel Fo|-|Fc||/\Sigma|Fo|$, $wR_2 = [\Sigma\, w(Fo^2-Fc^2)^2/\, \Sigma wFo^4]^{1/2}$. [b]Goodness-of-fit S = $[\Sigma w(Fo^2-Fc^2)^2/\,(n-p)]^{1/2}$, where *n* is the number of reflections and *p* the number of parameters.

The author

Monica Melegari was born in Reggio Emilia (Italy) on the 19th of June 1980. In 1999 she obtained her diploma at the Liceo Scientifico "A. Moro" in Reggio Emilia. In November 2004, she graduated in Industrial Chemistry, at the Department of Organic and Industrial Chemistry of the University of Parma, under the supervision of Prof. Enrico Dalcanale with a thesis entitled "Self-assembly of coordination cages bearing peripheral hydrophilic moieties".

In January 2005, she started a three years Ph.D. research project at the Department of Organic and Industrial Chemistry of the University of Parma, under the supervision of Prof. Enrico Dalcanale. During this period, she joined for six months the group of Prof. Jeffery T. Davis at the Department of Chemistry and Biochemistry of the University of Maryland, as Ph.D. Visiting student.

The results of the research conducted during the period 2005-2007 are described in this thesis.